THESIS

EVALUATION OF WIND TURBINE TOWERS UNDER THE SIMULTANEOUS APPLICATION OF SEISMIC, OPERATION AND WIND LOADS

Submitted by

Vanessa Smith

Department of Civil and Environmental Engineering

In partial fulfillment of the requirements

For the Degree of Master of Science

Colorado State University

Fort Collins, Colorado

Summer 2013

Master's Committee:

Advisor: Hussam Mahmoud

Bogusz Bienkiewicz
Mitchell Stansloski

ABSTRACT

EVALUATION OF WIND TURBINE TOWERS UNDER THE SIMULTANEOUS APPLICATION OF SEISMIC, OPERATION AND WIND LOADS

Wind turbines are widely recognized as a renewable energy resource and as such, their safety and reliability must be ensured. Many studies have been completed on the blade rotor and nacelle components of wind turbines under wind and operation loads. While several studies have focused on idealized wind turbine models, significant advancements on the global and local performance of these models under seismic loads in combination with other loads has been lacking. A study on the evaluation and performance of realistic wind turbine models under wind, operation and seismic loads is proposed and successfully completed. First, the geometry and loading for three wind turbine models are developed. A series of finite element analyses is conducted for each model under a variety of load combinations and earthquake records. Both global results and localized behavior were obtained for each analysis in order to identify areas of improvement within the wind turbine structure. Global results include drift ratios, normalized base shear and fast Fourier transformations to evaluate the stability of the wind turbine during operation. Localized performance focused on the welded connection at the base of the turbine and included Von Mises stresses as well as low-cycle fatigue analyses to determine the number of cycles to failure (initiation of through-thickness crack). These results show that certain turbine models are more susceptible to these loads than others. Several analyses indicate yielding at the turbine base and resonant conditions. The results from these analyses identify several critical issues within the wind turbine design and operation protocol.

ACKNOWLEDGEMENTS

I would like to thank first and foremost my advisor, Dr. Hussam Mahmoud for his continuous guidance and support throughout the completion of this thesis. I would also like to thank Dr. Bogusz Bienkiewicz and Dr. Mitchell Stansloski for participating as members of my thesis committee. Paul Veers and Scott Hughes from the National Renewable Energy Laboratory's Wind Technology Center provided valuable information throughout the early stages of this research. Roark Lanning of RES Americas, Inc. provided technical information regarding specific wind turbine geometry for this project as well.

I would also like to thank my family for their continuous support throughout my schooling. Without their encouragement, I would not be where I am today.

TABLE OF CONTENTS

LIST OF TABLES

LIST OF FIGURES

1 INTRODUCTION

1.1 Statement of the Problem

As the need for renewable energy sources increases, the methods of design and analysis for the structures servicing these sources must continue to advance to become more resilient when subjected to various loading conditions. The different sources of renewable energies include solar, geothermal, hydropower, ocean, hydrogen and wind. The advantage of utilizing wind turbines for energy harvesting is that wind is free and can be easily captured without adding any greenhouse gases or other pollutants. Wind farms can vary in size, which allows them to be used throughout residential and commercial sectors. Wind farms are also located in areas where farming and agricultural development can still take place. These turbines have the potential to aid in the economic development of many countries and allow energy to be provided to remote areas that are not served by current electric grids. Most research conducted on wind turbines has focused on the effects of wind and operation loading as it pertains to the blade rotor and nacelle of the turbine. However, very little progress has been made in understanding the effects of these loads in combination with seismic loading as well as the effect of seismic loading alone on a turbine tower by itself. The importance of understanding the response of wind turbine towers to seismic loads or the combination of seismic, wind and operation loads stems from the fact that many wind farms are located in high seismic regions. As seen in Figure 1-1 below, there are several wind farms in California that produce a large amount of energy. Because this region is at a higher risk of earthquake activity, it is especially important to ensure that these turbines are designed for seismic loads in combination with wind and operation loads.

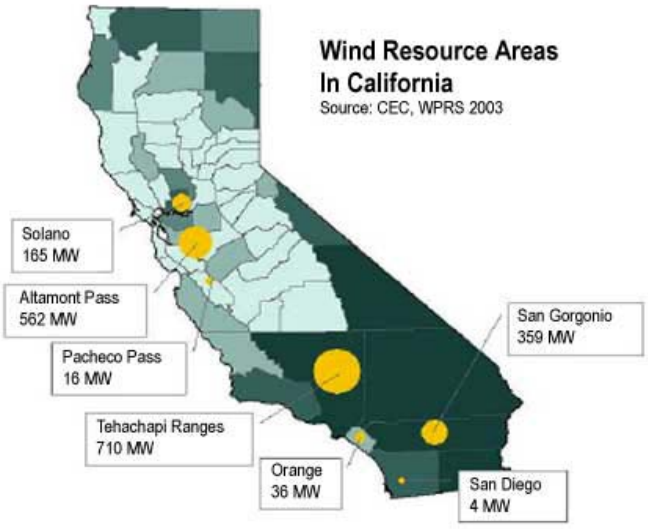

Figure 1-1: Wind Farms in California
(True Wind Solutions, 2007)

Codes have also failed to address this area and need advancement as the world becomes more dependent on this type of energy. As evidenced by Figure 1-2, it is important to understand how wind turbines might respond under these types of loading.

Figure 1-2: Collapse of Wind Turbine Near Arlington, Wyoming
(Brome, 2010)

Recently, there has been more interest in the scientific community to study the effects of seismic loading on wind turbines and wind turbine blades. An example of one such study has been completed at the University of California in San Diego (UCSD) (I Prowell, Veletzos, Elgamal, & Restrepo, 2008). The study included shake table testing that simulated a real earthquake on a full-scale wind turbine. Throughout this study, it was noted that many wind turbine seismic studies rely on existing codes and guidelines intended for simple building structures. Modeling of wind turbines under seismic loading utilizing these codes and guidelines has not been reliable because it fails to accurately depict the dynamic behavior of wind turbines, which is significantly different than the dynamic behavior of other structures.

Some of the areas of concern that have been found include the use of dated codes to analyze and design wind turbines for seismic load and the lack of information regarding seismic loading specifically for wind turbine design. The information that these codes do provide for determining seismic loads or combined loading is oftentimes vague when applied to wind turbine design and analysis. Many designers use the 1997 Uniform Building Code (UBC) or the 2006 International Building Code (IBC). These codes are not intended for use in wind turbine design and in the case of the UBC, are dated. These codes also do not require evaluating structures under combined seismic and wind loading, but rather evaluating a worst case situation by choosing either wind or seismic loading. Agbayani (2010) emphasized the lack of design codes for wind turbines by pointing out that both the IBC and the American Society of Civil Engineer's *Minimum Design Loads for Buildings and Other Structures* ASCE 7 provide guidelines for determining seismic loads for structures, which are far less complex than wind turbines. He adds that neither of these codes addresses simultaneous load situations for structures, which would be necessary in the case of combined wind, operation and seismic loads on wind turbines. In the

Guidelines for Design of Wind Turbines by DNV/Riso, it is stated that earthquakes should be considered, but gives no regulation or recommendation as to how the response to earthquakes should be evaluated (Riso National Laboratory, 2001). The International Electrotechnical Commission's (IEC) current code requires a conservative simplified seismic analysis in order for a wind turbine to be certified (IEC, 2009). Lastly, a study completed in Greece (Bazeos et al., 2002) noted the requirements of the *Guideline for Certification of Wind Turbines* from Germanischer Lloyd. This code requires that all structures must remain linear elastic during their life cycle and further states that inertial and gravitational loads caused by seismic activity should be considered (GL, 2010). The lack of information that these codes and guidelines provide demonstrates the need for more advanced research in this area.

The above background clearly shows the need for analytical or numerical models that are capable of capturing the response of wind turbines under different and combined loading conditions. The advantage of such models is that they can provide more clear insight on the true behavior of the system under these load combinations. Available research shows that seismic loading must be considered when designing and analyzing wind turbines, but that the seismic load must be accurate so that the wind turbine shows the correct response. Current research also demonstrates that there is a lack of knowledge in design codes and guidelines regarding seismic activity that must be addressed. By creating a numerical model that can be used to study the effects of these loads, significant advancement in the development of these codes and guidelines can be made. Designers can utilize resources that are created specifically for wind turbines rather than trying to manipulate codes that are in some cases decades old to fit a wind turbine design. This research can address the unique deformation and dynamic behavior of wind turbines and use that information to create better guidelines. This model will provide a global

response of the whole system and also local behavior so that stresses can be seen in critical areas of the turbine.

This research presents a new modeling approach that incorporates seismic and operation loading and combined seismic, operation and wind loading onto realistic wind turbines structures. By evaluating real earthquake records in regions of high seismic activity where wind turbines are actually located, the true response of these wind turbines can be analyzed. This work will aid in the development of codes that address wind turbine behavior and will aid designers in designing and analyzing wind turbines for realistic seismic and combined loading.

1.2 Objectives and Scope of Research

As previously discussed, prior research has indicated that seismic loading is an important consideration in designing and analyzing wind turbines. The study conducted at UCSD provides an introduction on the impacts that seismic events have on the structural integrity of wind turbines. It also shows the dire need for development of more accurate codes and guidelines for wind turbines in this area. The following chapter will highlight more studies that demonstrate the need for improvements to wind turbine design codes in regards to combined loading effects from seismic, wind and operation loads.

The research conducted through this study will incorporate examples of real wind turbines and all of their components under seismic and operation loading and also under combined seismic, wind and operation loading. The seismic events will reflect real earthquakes in areas where wind farms are located in the state of California. This ensures that the response predicted by the models will provide an accurate representation of what really happens during an earthquake. These models will also capture the localized behavior of the base flange, welds and bottom portion of the tower under seismic loads.

Significant background research had to be conducted before any models could be developed. Because of the proprietary nature of most wind turbine designs, it was crucial to make sure that the correct geometry, mass properties and loading data was used. This information was provided by various resources including the National Renewable Energy Laboratory (NREL) and RES-Americas. Upon completion of this work, three models were created simulating a 60-meter, 90-meter and 120-meter turbine. Each of these models used corresponding geometric, mass and loading data. These models were then evaluated under various loading conditions to determine the global and local performance of each tower under these cases. The global response includes tower drift, base shear and turbine operational stability. The local behavior includes stress concentrations at the weld toe and localized buckling of the tower, if any. The results allowed for an understanding of how the wind turbine responds under the given loading situations.

For the purposes of this research, it is important to note that while several studies have been completed on fatigue life issues for wind turbines, only low-cycle fatigue that develops as a result of seismic loading will be evaluated. Most turbine designs are limited by the fatigue life of individual components including the blades and other mechanical components. Studies in this area therefore focus on the high-cycle fatigue of these individual components, which is caused by wind loading. It is important, however, to understand how this high-cycle fatigue influences a wind turbines performance throughout its lifetime. Furthermore, it is important to understand how wind loading in combination with seismic loading could impact the fatigue life of a wind turbine.

In order to achieve these objectives, the following tasks and subtasks were accomplished:

1. Comprehensive Literature Review

a. Review work completed by NREL and other agencies to determine loading, geometry and component masses
b. Identify previous work from other studies and the results that pertain to this research

2. Develop Geometric Models
    a. Create detailed geometrical drawings of three wind turbines including 60-meter, 90-meter and 120-meter turbines based on the results of the literature review and discussion with engineers at RES-Americas
    b. Create equivalent blade geometric sections to simplify blade geometry
3. Develop Finite Element Models
    a. Create finite element models that allow both global and local deformations to be identified
    b. Complete frequency analyses for each turbine model and compare to values obtained during literature review
    c. Perform non-linear time-history analysis under seismic and operation loads, which will include 10 real earthquake records
    d. Perform non-linear time-history analysis under seismic, operation and wind loads using the same 10 earthquake records
4. Interpret Results
    a. Determine areas of high stress and deformation within the turbine model
    b. Compare seismic and operation loading against combined seismic, operation and wind loading
    c. Compare differences in stresses and deformations between the three models

1.3 Organization of Thesis

This research presents a new model for understanding the structural response of wind turbines on seismic and operation loading and combined seismic, operation and wind loading. The models developed in the finite element software, ABAQUS, will allow for depiction of the global response of the system and moreover, a better representation of the localized behavior at

the base region of the turbine. These results provide valuable information for a better understanding of how to design and analyze wind turbines for these loading conditions.

This thesis includes five chapters. Chapter 1 discusses the problem statement, objectives and scope of this research and the organization of this thesis. It will outline the current status of studies completed on wind turbines under seismic loading and highlight areas of necessary improvement. Chapter 2 discusses the detailed background and literature review conducted throughout the course of this research. Most of this information comes directly from NREL and several universities involved in the study of seismic loading on wind turbines. This chapter also shows the limitations of previous work and existing codes, and reinforces the need for this research to be completed. Chapter 3 outlines the finite element formulations for completion of this research. This includes the discussion of the three geometric models, how those geometries were chosen and the corresponding masses for various components of each turbine. It also includes a detailed explanation of how the models were created in ABAQUS and how each model was tested and analyzed. Chapter 4 discusses the results from the testing completed in ABAQUS. These results are divided into two categories: seismic and operation loads and seismic, operation and wind loads. Chapter 5 compares results between the three turbine models and the various load combinations applied to each model. These results provide a clear insight into which turbines are most impacted by the various combinations of loads. Chapter 6 summarizes the results of this research and discusses future research needs in this field.

2 BACKGROUND AND LITERATURE REVIEW

2.1 Introduction

As wind turbine technology improves, it is necessary for the design of these structures to accurately account for the various types of loading that could be experienced during a turbine's lifetime. Numerous studies have been made into the failure and fatigue issues with turbine blades and mechanical equipment (Fitzwater, 2004; Holmes, 2002; Nijssen, 2006; Sutherland & Veers, 1995; Sutherland, 1999). Studies into the actual response of wind turbines under combined loads, however, are lacking. Furthermore, a wind turbine design code, which could dictate combined seismic and operation loads as well as seismic, wind and operation loads, has not been developed in the United States, which leaves design up to individual companies. This code could also include the methods for analyzing turbines under these load combinations to ensure that the global response and local behavior are accurate. The need for improved design for these types of loads is growing as the world becomes more dependent on these sources of energy.

The literature review presented in this paper provides an understanding on the current state of research into the study of seismic loading on wind turbines. Firstly, a discussion of current knowledge a discussion of relevant previous studies related to wind turbines and earthquakes will be given. In addition to this discussion, a summary of any relevant mathematical expressions or developments will be provided. Finally, an introduction into any codes and guidelines that dictate current design and analysis of wind turbines and how these codes and guidelines lack sufficient information for this field will be discussed.

This literature review will not present any research involving the impact of seismic loading on a wind turbines blade rotor or nacelle region. While some studies have been

conducted in this area, the focus of this research is to understand the impact of combined loading on the structure of the tower rather than the various mechanical components of the turbine. Another research area that will not be a main focus point in this literature review is the results obtained from studies done on experimental testing. Some results from preliminary wind turbine shake table experimental tests from UCSD will be discussed. In large part, however, there has not been significant progress on experimental testing of wind turbines under seismic loading. This is a developing field and most research focuses on wind turbine responses to seismic loads developed in finite element models.

2.2 Preliminary Wind Turbine Studies under Various Loads

While there is a significant lack of knowledge in the area of seismic loading on wind turbines, there has been noteworthy progress made towards understanding wind turbine response under wind loads and operation loads. Most studies have focused on fatigue and failure issues that occur with the blade assembly and nacelle. Some studies have been completed, however, on the possible fatigue and extreme loads that wind turbines may experience during their lifetimes (Fitzwater, 2004; Huskey & Prascher, 2005; Ritschel, Warnke, Kirchner, & Meussen, 2003). These studies have been completed over the last 15 – 20 years and continue to advance. The target economical lifetime of a wind turbine is 20 years (Nijssen, 2006) and is most often governed by wind turbine components, specifically the blades. Most fatigue centered studies therefore focus on the lifetime of these components under high-cycle fatigue due to wind loading.

As mentioned previously, most of the research conducted on wind loading has focused on the rotor and nacelle. These studies have been vital to the improvement of blade geometry and material design, but have not given any information for improvements to the design of the wind

turbine overall structure. Studies on the rotor and nacelle components of a wind turbine are necessary because they aim to lower the cost of energy and loading on the wind turbine. Many designs have been formulated with this in mind. Manufacturers, however, have found it difficult to create new designs in a market where current demand is high and the future limit on the size of wind turbines is uncertain. To address these issues, the U.S. Department of Energy along with the National Renewable Energy Laboratory formulated the Wind Partnership for Advanced Component Technologies (WindPACT) project in 2000. As a result, Global Energy Concepts, LLC (GEC) was awarded one contract for this project (Griffin, 2001). The following summarizes the results and impacts of this study.

The most significant outcome of this work was the study of the effects of alternative blade designs and configurations on the wind turbine. This research evaluated several blade designs and configurations and how they would impact the overall cost of energy and loads experienced by the turbine. Preliminary results indicated that by combining tower feedback and the reduction of the solidity of the blades, there was a "substantial reduction in the tower section and in the tower flexural stiffness" (Malcolm & Hansen, 2006). These results also indicated that the natural frequency of the system was reduced. This led to a reduction in hub height of the tower from 84 meters to 80 meters. Upon completion of this study, results indicated that there was no single blade configuration that significantly reduced cost of energy or overall loading on the turbine. This is important because they indicate that while most research focuses on the blade component of a wind turbine, the loading on the overall system is still an important and potentially critical issue.

In 1999, a study conducted by NREL and Riso National Laboratory in Denmark focused on predicting ultimate loads for the design of wind turbines (Madsen, Pierce, & Buhl, 1999).

Most turbines at that point were designed with a focus on fatigue loads and ultimate loads, with ultimate loads limiting the design in most cases. The ultimate loads evaluated in this research only considered wind loading in cases such as extreme wind speeds in parked rotor situations, lower wind speeds with wind gusts, start-up, shut-down and yawing. Two load cases were considered and were obtained from the Danish wind turbine design standards developed at Riso. These cases included wind turbine loading during power production and loading under a parked condition. The results indicated that these predicted loads must be combined with statistical methods in order to obtain better results. The results also showed that the predicted ultimate loads under parked conditions with an extreme wind speed were under-predicted and needed further evaluation (Madsen et al., 1999). The study demonstrates the need for development of research and guidelines that accurately predict the response of wind turbines under these types of loading. It also shows that wind loading alone can play a significant role in the overall high-cycle fatigue of a wind turbine and may imply that wind loading combined with seismic loading could lead to significant damage.

In 1995, Sandia National Laboratory completed research using a cumulative damage technique to evaluate wind turbine components under wind loading and develop fatigue analysis for such components using the LIFE2 Fatigue Analysis code. LIFE2 analyzed the high-cycle fatigue of these components due to wind loading. This research also included the completion of a reliability analysis to account for the uncertainties and randomness of wind loading. They concluded that because wind loading is random, it is difficult to determine service life of wind turbine components (Sutherland & Veers, 1995). By combining experimental results from wind loading on wind turbines and wind speed data from various locations, extreme loads for high-cycle fatigue damage can be calculated.

A 1999 study completed at Sandia National Laboratories evaluated the best practices available at the time for the high-cycle fatigue analysis of wind turbine components (blades and blade joints) (Sutherland, 1999). This study was completed because of observations within the wind turbine community regarding the overdesign of wind turbines and the early failure of wind turbine components at wind farms in California. Because of these observations, most of the research completed on wind turbines during this time focused on high-cycle fatigue issues. This study focused on technology within the U.S. but also referenced European sources because of the vast amount of information they provided that the U.S. did not. The results of this study stated that wind turbines "require detailed analyses to ensure survival under normal operating conditions in a turbulent environment" (Sutherland, 1999). The study also indicates that designers can "address design problems with a high degree of confidence" using the information available through this study. While this study provided valuable information at the time, it was unable to make up for the lack of codes and guidelines in the U.S. regarding wind loading and seismic loading. It also demonstrates that there is a need to understand the response of wind turbines under seismic loading since these early turbines had fatigue problems under normal operating conditions.

Research conducted at Stanford University (Fitzwater, 2004) combined these two research efforts in an attempt to determine extreme loads on wind turbines. Two cases were identified, which included turbine specific design independent of the site, and a site-specific case. Models were then built to identify short term loads on wind turbines and then used to predict potential long term loading. These loading cases were then used to estimate the extreme load and fatigue ranges for wind turbines. This research did not, however, include seismic

events as an extreme load case and rather focused on the extreme situations arising from wind loading alone.

In 2005, NREL completed more research on wind turbine tower design loads, which included various operation loads (Huskey & Prascher, 2005). Six different variations of operation loads were considered in conjunction with various load cases such as maximum speed, maximum exposure and wind. Testing was completed to determine ultimate loads on wind turbines due to the six combinations of operation loads. It was determined that the loads calculated were not conservative enough when comparing them to the loads seen during testing.

These research studies highlight the importance of understanding how extreme wind and operation loading can impact the response of a wind turbine. They show that extreme loads can and do occur under normal operation and that the addition of a seismic event may lead to far more serious damage. Many researchers have recognized that seismic loading is an important aspect to consider and that codes and guidelines in the U.S. and Europe fail to provide accurate analysis and design techniques for seismic loading. While this section discusses the wind and operation loading aspects, the next section will discuss the preliminary studies completed on seismic loading and wind turbines and also show why further research into this topic is necessary.

2.3 Preliminary Studies on Seismic Loads

The effects of seismic loading on wind turbines have gained attention in the last decade. Because this is still an advancing topic, early studies generally provide a simplified finite element analysis and only small-scale turbine experiments. These early simulations and experiments provide insight to a turbines global response and show a better understanding of how these systems deform under earthquakes. What these studies fail to provide, however, is an

understanding of local deformations throughout the tower and the base. As turbines become larger, it is important to have accurate numerical models that can predict a turbines response under a variety of loads.

The previously mentioned study completed by the University of Patras in Greece (Bazeos et al., 2002) offers a look at the effects of seismic loading on a wind turbine from a simplified finite element modeling approach. This prototype turbine consists of a 38-meter tower under gravitational, wind, operation and seismic loads.

The static loading for this model includes the gravitational loads and the operation and survival aerodynamic (wind and operation) loads. The gravitational load is applied in the finite element model as a point mass on the top of the tower representative of the nacelle, blade assembly and other mechanical equipment. The operation aerodynamic loading represents the resistance of the turbine to normal wind loading and the loading created by operation of the turbine. The survival aerodynamic loading is representative of the 50-year wind loading that the turbine would experience in a parked condition.

For the purposes of the seismic analysis, two finite element models were created. The first one depicts a much more realistic model of the turbine while the second uses a simplified model including line elements to depict the tower. The results from these analyses indicated nearly identical turbine responses. The results also demonstrated that the seismic analysis did not produce any critical response. This does not indicate, however, that other turbine sizes would not have a critical response under seismic loading. Because this turbine model is small compared to most wind turbines, it is necessary to further study the response of larger turbines under this type of loading. The models were also evaluated using existing codes and guidelines, which are more applicable to simpler structures. This preliminary research shows that the global

response of a wind turbine system may be captured when using a simplified model, but local behavior is not. Critical areas of high stress at the base of a tower cannot be seen when using this type of simplified model.

In 2003 at the 2nd World Wind Energy Conference in Cape Town, South Africa, results from a study were presented that demonstrated the growing need for a better understanding of seismic loading on wind turbines. Work conducted by various researchers indicated that the methods of designing wind turbines were based on civil engineering guidelines that were not suitable for the dynamic response that occurs during an earthquake (Ritschel et al., 2003). This study used a simplified approach to modeling a real wind turbine. This included the use of line elements along with bending stiffness and lumped masses throughout the turbine height (see Figure 2-1 for an illustration of this model).

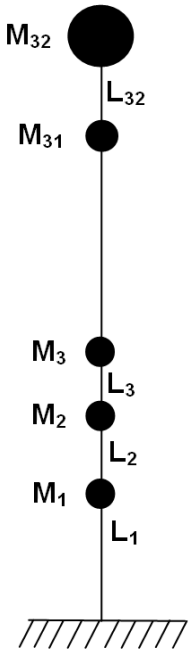

Figure 2-1: Simplified Finite Element Model
(Ritschel et al., 2003)

The results from this analysis show that this method provides reliable results for designing or improving wind turbines in earthquake prone regions. It does state, however, that a peak acceleration of only 0.3g was used, which is less than what may actually be experienced during an earthquake in high seismic regions.

Another study completed in 2006 (Ritschel, Warnke, & Haenler, 2006) aimed to develop a computer simulation code that could capture all structural loads on wind turbines. This would allow for both pre- and post-processing and was to include all relevant dynamic effects on wind turbine models. These dynamic effects included every load experienced within the turbine starting from the soil and foundation interaction and ending with the losses seen in the blade tips.

The majority of the motivation for the development of this software was because current codes used for other building structures do not include provisions for wind turbine structures. This includes the lack of information regarding design for seismic loading. As such, this research included the development of a model to determine the response of a wind turbine under seismic loads. The model created for this study is similar to the simplified finite element structure described in Figure 2-1. Tower modes and frequencies were obtained in order to identify estimates for earthquake loads. During the study, however, it was determined that "the disadvantage of this approach is that the vibration modes of the turbine are oversimplified and loads on certain components of the turbine as for example blade loads are neglected" (Ritschel et al., 2006). The recommendation from this observation was to create a more realistic finite element model to more accurately represent the response of a wind turbine under seismic loading. At the conclusion of this research, the simplified model was able to provide a general idea of the global response of a wind turbine under various dynamic effects. This also provides a good basis for what to expect in a more realistic simulation.

The majority of recent developments in seismic loading and wind turbines come from the University of California at San Diego (UCSD). Several studies were conducted that included both experimental testing on a large outdoor shake table and finite element modeling. Some of the studies also evaluated software developed by NREL in order to identify the capabilities of that software and any potential improvements that can be made.

In 2004, an experimental study and finite element simulations were completed at UCSD. The study utilized the NEES Large High Performance Outdoor Shake Table, which is the world's largest capacity and first outdoor shake table of its kind (I Prowell et al., 2008). Most methods of estimating seismic forces on wind turbines up to this point included either conducting finite element simulations or using building codes intended for simpler structures. Because wind turbines are considered to behave very differently than other structures, it is necessary to adhere to different guidelines for design. One of these guidelines is provided by Germanischer Lloyd, which requires that wind turbines must remain elastic and sustain no damage during an earthquake (GL, 2010). This is contrary to conventional performance-based earthquake design where the structure is designed such that the earthquake energy is dissipated in certain areas of the structure through large inelastic deformation. Research in this field is therefore necessary in order to facilitate future wind turbine designs. It is important to note that the UCSD research focused on investigating the seismic demand for wind turbines in a parked state.

The experimental turbine had a height of 23 meters, which is much smaller than most commercially used wind turbines. Five high-intensity earthquakes were used for the seismic loading in the model. Figure 2-2 and Figure 2-3 depict the setup and accelerometer locations for the testing completed at UCSD.

Figure 2-2: Experimental Setup at UCSD
(I Prowell et al., 2008)

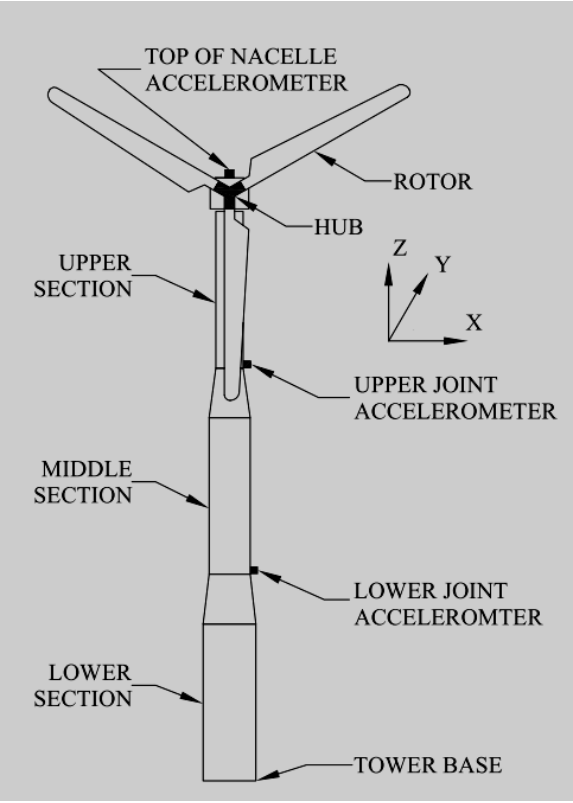

Figure 2-3: Accelerometer Location for Experimental Testing
(I Prowell et al., 2008)

The experimental testing was completed first in order to use the results for calibration of the finite element model. The finite element model was then analyzed for various seismic events. The finite element model was developed using OpenSees and included five types of elements. The tower and blades were represented by elastic line elements and the nacelle was represented as a rigid line element connected to the top of the tower. The results of a frequency analysis on this configuration agreed with the experimental results, which indicated that this simplified model was "capable of adequately capturing the complexity of the dynamic behavior for the first mode" (I Prowell et al., 2008). The results of the finite element analyses focused on maximum bending moments seen throughout the tower. Some of these results showed that some of the bending moments seen approached levels allowed by various codes such as the AISC Steel Construction Manual (AISC, 2005).

These results were instrumental in the beginning of experimental testing of wind turbines under seismic loading. They allowed for verification of finite element modeling by using the experimental setup as a comparison for mode shapes and geometry. Two important conclusions were drawn from this research. First, bending moments within the tower were mostly within the allowances given by codes and guidelines. Second, the available codes and guidelines do not provide accurate assessments for seismic loading for wind turbine design. As a result, further studies must be completed to address these issues.

A follow-up study from this same testing completed in 2008 (Ian Prowell, Veletzos, & Elgamal, 2008) also included some conclusions and recommendations about this research. One observation was that the experimental and computer modeling tests did not evaluate a turbine during operation. The combination of operation and seismic loads could be significant and produce higher bending moments than seismic loading alone. Another important observation

was that the 2006 International Building Code did not require the evaluation of simultaneous wind and seismic loading. As a result, the testing completed did not evaluate either test under simultaneous wind and seismic loads. Again, the combination of these two could produce significantly higher moments and stresses throughout the turbine.

In 2009, UCSD in collaboration with NREL conducted a study into the efficiency and potential updates to the NREL software FAST (I Prowell, Elgamal, & Jonkman, 2009). FAST allows users to evaluate the dynamic behavior of a wind turbine under various types of loading in the time domain. This study was completed to update FAST so that it could better represent the more realistic wind turbine models being developed. Up to this point, most models were simplified and did not truly represent the actual structure of a wind turbine. Also dictating previous research were the requirements from various codes and guidelines. Although many studies had been completed, most did not provide a publically available tool for evaluating wind turbines under simultaneous loads.

The updated FAST software includes most of the same elements used in previous research at UCSD. The five elastic elements include the three blades, tower and drive shaft. The nacelle is again modeled as a rigid element. The updates provided by UCSD enable FAST to be the first publicly available software to capture the dynamic behavior of wind turbines under combined loading. While this software provides advanced capabilities for loading evaluation, it lacks the ability to accurately represent the structure of a wind turbine. By incorporating a more realistic model, studies can be completed that evaluate the local deformations and stresses throughout a wind turbine rather than just a global response from the whole system.

Another study completed in 2010 by UCSD and NREL focused on the response of wind turbines in parked and operating conditions to simultaneous wind and seismic loads (I Prowell,

Elgamal, Romanowitz, Duggan, & Jonkman, 2010). This study focused on both the parked and operating states because of certain code requirements such as the International Electrotechnical Commission and Germanischer Lloyd requirements that designers must consider a turbine in operation during an earthquake in order for a turbine to be certified (GL, 2010; IEC, 2009). Most designers adhere to this requirement by analyzing both situations and combining results. This is not only inefficient, but may produce overly conservative results leading to higher costs. The goal of this research was to develop a method for applying these loads simultaneously to have a better understanding of the response. Figure 2-4 depicts the experimental setup for this study.

Figure 2-4: Experimental Turbine for UCSD and NREL Study
(I Prowell, Elgamal, Romanowitz, et al., 2010)

Several computer programs developed by NREL were utilized to simulate wind loads on the turbine. The simulations were separated into two categories including combined wind and seismic loading and seismic loading alone. A 6.9 magnitude earthquake record from California was used. Wind loading was applied over 10 minutes and the earthquake was applied for approximately one minute. Several simulations were conducted, which represented the various operation states for the wind turbine. The results of this study indicated that bending moment varied throughout the model depending on the loading and operational state. It also showed that aerodynamic damping of the wind turbine could significantly impact the response of the wind turbine. Moment demands may be higher for seismic loading alone but lower for combined wind and seismic loads. The study then states that "such implications could clearly affect the economic viability of wind energy in regions with a high seismic hazard" (I Prowell, Elgamal, Romanowitz, et al., 2010). Because of this conclusion, it is necessary to further evaluate seismic loads and the effects on the response of wind turbines under these situations. As many of these turbines are constructed in high seismic regions, the risk becomes greater as turbines become larger.

Further testing was completed at UCSD for a larger wind turbine under 132 total simulations (Ian Prowell, Elgamal, Jonkman, & Uang, 2010). These simulations included the updates made to FAST, 22 total earthquake records, three operational states and two horizontal components for each earthquake. The three states included parked, operating and emergency shutdown (I Prowell, Elgamal, & Uang, 2010). Results were similar to those presented above. They demonstrate that FAST provides an accurate global response of wind turbines under various loading situations. These results also demonstrate how larger wind turbines might respond under various earthquakes and earthquake directions in several operational states.

While research has advanced in the field of seismic loads on wind turbines, more studies must be completed that focus on a realistic finite element model under simultaneous loads. Experimental testing has allowed for some finite element model validation, but fails to demonstrate how much larger turbines respond under combined loads. Furthermore, publicly available software such as FAST provides a good basis for simultaneous loads but represents the structure of a wind turbine in a very simplified form. It demonstrates how the whole system responds but lacks the ability to provide stresses and deformations at the local level. Codes and guidelines in place today have evolved in some of their requirements, but they have not yet provided designers with a set of tools to accurately design wind turbines for load situations that must be considered. It is imperative that the methods to study these load effects and the codes that dictate wind turbine design evolve.

2.4 Mathematical Expressions

Although many studies have been done that relate to wind turbines, there have not been as many expressions derived that characterize turbine response under various types of loading. Several existing expressions for dynamics of structures and other tall, slender structures have been applied to this field. For example, the response and loading for high-mast lighting towers has characteristics similar to wind turbines. Several expressions have also been developed for ultimate and fatigue loads for wind turbines. Several codes have their own expressions for seismic loads, wind loads and building responses under these types of loads. Each of these will be discussed further in this section.

As mentioned, many studies on tall, slender structures have produced results and mathematical expressions, which can be applicable to wind turbines. In 2006, a study was completed at Colorado State University for the Colorado Department of Transportation on a

reliability-based procedure for the design of high-mast lighting structures (Goode & van de Lindt, 2006). The analysis methods for this study included fatigue, reliability, dynamic motion, wind models and a finite element model. As expected, the dynamic response of the system was governed by the equation of motion as follows:

$$[M]\{\ddot{x}\} + [C]\{\dot{x}\} + [K]\{x\} = \{F(t)\} \quad \text{Equation 2-1}$$

Where [*M*] is the mass matrix, $\{\ddot{x}\}$ is the acceleration, *[C]* represents the damping matrix, $\{\dot{x}\}$ is the velocity, *[K]* is the stiffness matrix, *{x}* is the displacement and *{F(t)}* is the forcing function. Both the mass and stiffness matrices must be obtained as well as the damping matrix, which can be expressed as Rayleigh damping:

$$[C] = \alpha[M] + \beta[K] \quad \text{Equation 2-2}$$

Where *[C]* is the damping matrix, α is a predefined constant, *[M]* is the mass matrix, β is another predefined constant and *[K]* is the stiffness matrix.

The predefined constants, α and β are determined as,

$$\alpha = \xi\left[\frac{2\omega_1\omega_2}{\omega_1+\omega_2}\right] \quad \text{Equation 2-3}$$

$$\beta = \xi\left[\frac{2}{\omega_1+\omega_2}\right] \quad \text{Equation 2-4}$$

Where ω_1 and ω_2 are the circular natural frequencies and ξ represents the damping ratio, which is also used to calculate the parameters for Rayleigh damping. The combination of these expressions can thus be used for the basic understanding of a turbines dynamic response. These expressions also aid in the development of damping parameters for use in any analytical and computer modeling.

Another development from this study that is applicable to wind turbines is the wind load model, which provides expressions for determining the wind velocity and wind velocity profiles. First, the wind velocity power spectrum, S(z,n) is provided as,

$$\frac{nS(z,n)}{u_*^2} = \frac{200f}{(1+50f)^{5/3}} \qquad \text{Equation 2-5}$$

Where n is frequency, u_* is shear velocity, S is the wind velocity power spectrum, z is the reference height and f is given through the following:

$$f = \frac{nz}{u(z)} \qquad \text{Equation 2-6}$$

Where z is the height above ground, $u(z)$ is the wind velocity at that height and n is the frequency. Ultimately, the wind velocity time series is expressed as,

$$u(t) = \bar{u} + \sum_{All\ \Delta n} \sqrt{2S_{mid}\,\Delta n}\cos(2\pi n_{mid}\,t - \varphi) \qquad \text{Equation 2-7}$$

Where $\bar{u}$ is the mean wind velocity, S_{mid} is the power spectrum at the mid-point of the frequency interval, Δn is the frequency interval, n_{mid} is the mid-point frequency, t is the time and φ is a random phase angle.

A wind velocity profile was then developed in order to determine the forcing expression for the structure. For this study, a logarithmic profile was created using the following expressions from Simiu's *Wind Effects on Structures* (as cited in Goode & Van de Lindt, 2006):

$$u(z) = \frac{u_*}{k}\ln\frac{z}{z_0} \qquad \text{Equation 2-8}$$

Where $u(z)$ is the wind velocity at height z, k is the von Karman constant, u_* is the shear velocity, z is the reference height and z_0 is the roughness coefficient. Once obtaining the profile,

Morison's equation (as provided by Goode & Van de Lindt, 2006) can be used to relate the wind velocity to wind force. This equation is as follows:

$$F = \frac{1}{2}\rho_{air} A C_d u_{wind} |u_{wind}| \quad \text{Equation 2-9}$$

Where, F is the wind force, ρ_{air} is the mass density of the air, A is the tributary area for the nodal force, C_d is the drag coefficient and u_{wind} is the nodal wind velocity. These wind velocity and force expressions can be valuable in determining similar forces for wind turbines.

In regards to fatigue and ultimate loads for wind turbines, there have been several studies that have produced useful mathematical expressions for this field. These expressions provide a basic understanding of the types and magnitudes of potential loads that would cause damage or failure of a wind turbine. In 2002, an Australian university study was completed on the closed-form solutions of fatigue life of wind turbines under wind loading (Holmes, 2002). The goal of this study was to develop both lower and upper fatigue limits for narrow band resonant and wide band background responses. The author first introduces a fatigue failure model along with Miner's rule as follows:

$$Ns^m = K \quad \text{Equation 2-10}$$

$$\sum \left(\frac{n_i}{N_i}\right) = 1 \quad \text{Equation 2-11}$$

Here, the fatigue failure expression is developed by observing constant amplitude fatigue tests that can usually be expressed as an s-N curve where s represents the stress amplitude and N is the number of cycles to failure. For many materials, this can be expressed as a linear approximation if log s and log N are plotted. For this expression, m varies between five and 20 and K is a constant. Miner's rule is then introduced as a criterion for failure for a range of amplitudes under repetitive loading. N_i represents the number of cycles required to cause failure while n_i

represents the number of stress cycles for a given amplitude. When this is equal to one, failure is expected. After evaluating the narrow band and wide band responses, the application to wind loading was developed.

First, the probability distribution for the mean wind speed, *U*, is best approximated by a Weibull distribution and given as,

$$f_U(\bar{U}) = \frac{k\bar{U}^{k-1}}{c^k}\exp\left[-\left(\frac{\bar{U}}{c}\right)^k\right] \quad \text{Equation 2-12}$$

Where $\bar{U}$ is the mean wind velocity, *k* represents the shape factor and *c* represents the scale factor. Combining this expression with expressions developed for the narrow band and wide band responses will lead to expressions for total damage during specific time periods for wind turbines. These estimates provide a useful tool for approximating the high-cycle fatigue life of wind turbines under wind loads.

The 2002 University of Patras study on the static, seismic and stability analysis of wind turbines provides some analytical expressions for the elastic design spectrum for horizontal acceleration (Bazeos et al., 2002). These expressions were based on the Greek Seismic Code where the design has a 10% exceedance likelihood over a 50-year period. Three expressions are given as,

$$R_e(T) = A\gamma_1\left[1 + (\eta\beta_0 - 1)\frac{T}{T_1}\right], 0 \le T \le T_1 \quad \text{Equation 2-13}$$

$$R_e(T) = A\gamma_1\eta\beta_0, T_1 \le T \le T_2 \quad \text{Equation 2-14}$$

$$R_e(T) = A\gamma_1\eta\beta_0\frac{T_2}{T}, T_2 \le T \quad \text{Equation 2-15}$$

Here, *A* is the site specific maximum acceleration, γ_1 is the significance factor, η is the correction factor for damping ratios other than 5%, β_0 is the design spectra multiplier, *T* is the period in

seconds and T_1 and T_2 are the cut-off periods for different soil conditions. These expressions were used in the development of the finite element model for this study. This model was discussed in Section 2.3.

Finally, two codes provide more mathematical basis for understanding loads on wind turbines and the response of these structures. The Riso *Guidelines for Design of Wind Turbines* (Riso National Laboratory, 2001) includes the same equation of motion as shown above. Along with this equation are applications of Morison's equation for off-shore turbines and design damage equations. The equation of motion is accompanied by a finite element representation for analysis similar to Figure 2-5 below.

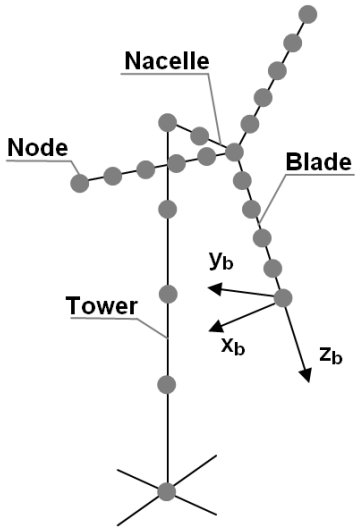

Figure 2-5: Finite Element Representation for Wind Turbine Model
(Riso National Laboratory, 2001)

ASCE 7 (ASCE, 2005) also provides several expressions that can be utilized in the design and analysis of wind turbines. Specifically, the chapter on wind loads is especially applicable. The velocity pressure, q_z, can be calculated using the following expression:

$$q_z = 0.613 K_z K_{zt} K_d V^2 I \ (N/m^2) \qquad \text{Equation 2-16}$$

Where K_z is the velocity pressure exposure coefficient, K_{zt} is the topographic factor, K_d is the wind directionality factor, V is the wind velocity in m/s and I is the importance factor.

These expressions provide a good basis for understanding wind turbine loading and response, but lack the ability to give a complete set of tools for wind turbine design and analysis. The previous sections discussed pertinent studies and research efforts in the analytical and finite element modeling fields, which can aid in the future development of codes and guidelines.

2.5 Current Codes and Guidelines

Current design practices for wind turbines rely on codes and guidelines that are mostly intended for typical building structures. In the past decade or so, several updates have been made to these codes and guidelines to aid designers in addressing seismic loads. Some of the studies previously discussed demonstrate the results of research conducted on wind turbines to account for these new requirements. This section will discuss both the lack of accurate seismic load modeling for designers and the lack of a standard design code for wind turbines in the United States. Several codes available in the U.S. and Europe will also be discussed including the 2006 International Building Code, ASCE 7-05, Riso *Guidelines for Design of Wind Turbines*, International Electrotechnical Commission (IEC) *Wind Turbine Design Requirements* and the Germanischer Lloyd *Guideline for the Certification of Wind Turbines*.

2.5.1 Current Design Code Challenges

As the world's largest renewable energy consultant, GL Garrad Hassan has been widely recognized as the leader in technical advances regarding wind turbine development (GL Garrad Hassan, 2013). They provide technical information and software for the design of wind farms and are currently working on ways to improve off-

shore wind energy. In 2009, a paper on seismic loading on wind turbines by Garrad Hassan was presented at the American Wind Energy Association Windpower Conference (Ntambakwa & Rogers, 2009). This paper discussed the seismic load limitations of current codes and previous research completed by several institutions. The purpose of this study was to provide recommendations for improvements that can be made to the current codes and guidelines.

As mentioned above, many of the codes used in current wind turbine design were not developed explicitly for wind turbines, but rather for simpler building structures. Most of these codes currently call for the separate evaluation of wind turbines under operation loads and seismic loads. These loads are then superimposed to provide designers with a combined load situation. Because this analysis is more applicable to a simple structure, designs can become too conservative. By further understanding the actual behavior and response of wind turbines, more accurate codes can be developed, which will aid designers in creating more optimized wind turbine systems.

Most codes within the U.S. are based on the 2006 International Building Code. The seismic load requirements within the IBC are based on ASCE 7-05 (ICC, 2006). The main issue is, once again, the lack of explicit requirements for wind turbines. Two available design procedures in ASCE 7 include the Equivalent Lateral Force Procedure and the Modal Response Spectrum Analysis (ASCE, 2005). The Equivalent Lateral Force (ELF) Procedure analysis is based on structural characteristics, occupancy category and site characteristics. Site characteristics including soil site class and mapped ground motion values provide designers with a response spectrum. The designer then determines the period of the structure. In ASCE 7-05, values are provided based on the structure

type. None of these predetermined values, however, are directly applicable for wind turbines. Various other factors are calculated including the Response Modification Factor (R), which accounts for the ductility, overstrength and damping of the structure. Also evaluated is the importance factor, which is based on the occupancy category. Again, it is difficult to determine both of these factors because wind turbines do not fall into any of the available categories for simple buildings. The Modal Response Spectrum Analysis involves the determination of the natural modes of a structural system. This procedure is less common than the ELF procedure and much less literature is available for this procedure in ASCE 7.

Other available analysis tools include numerical modeling programs. For instance, the Garrad Hassan program GH Bladed is used in the design and certification of many wind turbines. This program incorporates an iterative process of computing the response spectrum, calibrating it to a target spectrum, scaling it and then repeating until results are adequate. This software is also based on available codes and guidelines including the GL *Guideline for the Certification of Wind Turbines*. Results of this software indicate that codes must take into account aeroelastic damping, which occurs during operation of the wind turbine. Damping under these conditions is typically around 5%, but drops significantly when the turbine is in a parked state. "If aeroelastic damping is not present (i.e. a parked condition), standard building code procedures do not allow for an adjustment in damping ratios different from those observed in conventional building systems, and therefore cannot take the low level of damping of a parked turbine into consideration" (Ntambakwa & Rogers, 2009). Further analyses have to be considered because current codes do not provide any provisions for this case.

In 2010, another paper was presented at the 2010 Structures Congress, which highlighted the lack of design guidelines for wind turbines in the U.S. (Agbayani, 2010). This lack of guidelines presents challenges when attempting to obtain certification for wind farms. Wind turbine certification from European agencies requires compliance with various European standards. Any designs for wind turbines in the U.S. must meet the standards presented by these European codes in order to meet the requirements for certification by these agencies. Furthermore, wind turbine design incorporates challenges not faced by simpler structures. These include local buckling of the tower, fatigue of the system and resonance under seismic and operation loading. Any code must be able to provide designers with a standard that adequately represents a wind turbine structure.

Various agencies within the U.S. are currently working on the development of wind turbine design standards. These agencies include NREL, the Department of Energy, the American Wind Energy Association (AWEA) and the American Society of Civil Engineers (ASCE). They aim to create a standard for design and safety of wind turbines, provide designers with one set of code requirements and give criteria for the accurate review of wind turbine design plans. These will address a variety problems faced by designers in the U.S including permitting, wind loading, fatigue and local buckling.

One of the major problems in the United States is that many wind turbines are not permitted or reviewed by a professional engineer. This stems from several factors including a lack of understanding of the U.S. permitting process and moreover, the overall thought that as long as wind turbines meet European certification requirements, additional reviews are unnecessary. This becomes problematic because there are no

provisions in current codes that exclude wind turbines from the permitting and review process. Ultimately, the design provisions found in ASCE 7-05 "imply that wind farm towers may be treated like any other nonbuilding structure type whose engineering design is subject to building code requirements and the permitting process" (Agbayani, 2010). It is therefore necessary that any new code or guideline includes this requirement unless sufficient evidence can be provided that would indicate that wind turbines do not need additional permitting or reviewing.

Another issue that will need to be addressed in codes and guidelines is the discrepancy in wind loads between the ASCE 7-05 provisions and the provisions given by the IEC code. While the discrepancy may not be enormous, it will be necessary to identify whether designers can use either guideline or if they must use one over the other.

Fatigue design is a challenge of wind turbine design that is not always present in the design of other structures. Currently, the 2006 IBC does not explicitly require fatigue design for structures. Many designers, however, find it necessary to design these structures for high-cycle fatigue based on wind loads and low-cycle fatigue based on seismic loads. European codes currently require fatigue design for their wind turbines. When reviewing codes within the U.S., it is noted that "AISC specifications require consideration of fatigue" (Agbayani, 2010). While the IBC may not mention fatigue design as a requirement, it does reference AISC specifications for design, which implies that fatigue must be considered. Furthermore, fatigue may govern the design of wind turbines in certain cases.

Lastly, the U.S. codes do not provide any provision for local buckling for the thin-walled, tubular steel wind turbine towers. There is existing literature regarding these

types of towers, which could be incorporated into new codes for wind turbine design. The AISC manual, for instance, would provide detailed information on the behavior of steel for these situations.

These studies highlight the need for new codes in the United States to address design and analysis issues in the wind turbine industry. These studies also show the significance of seismic loads in wind turbine design. While several codes have included seismic loading, updates must be made to both the modeling procedures and the design requirements to ensure accurate designs. It is important that as this field grows, the safety and reliability of these structures is maintained.

2.5.2 Current Seismic Provisions in Codes and Guidelines

As previously mentioned, there are several codes available to aid designers in the U.S. and Europe. In general, European codes are more advanced because wind turbine technology evolved much more rapidly there than it did in the U.S. The codes in the U.S. do not explicitly apply to wind turbine designs, and are therefore much less suitable for that application. All of these codes will be discussed with an emphasis on the seismic load provisions provided in each.

Within the U.S., the most prominent building code is the 2006 International Building Code. This code serves as the design guide for most structures and lists several other codes for reference such as ASCE 7-05 and AISC. The structural design provisions in this code reference various load cases and combinations to be used for structural design. None of these consider both earthquake and wind simultaneously, which can and will occur for structures like these. For seismic loading specifically, it states that “every structure, and portion thereof, including nonstructural components that are permanently

attached to structures and their supports and attachments, shall be designed and constructed to resist the effects of earthquake motions in accordance with ASCE 7" (ICC, 2006). Exceptions to this include structures that may behave and respond differently under seismic loads than simpler structures. If wind turbines were included in this exception, it would then be expected that they would be designed according to their own design code. The ELF process required by ASCE 7 is as described in Section 2.5.1. While these two codes allow for accurate and adequate building designs in most situations, they are not suitable for the design of wind turbines. Wind turbines behave very differently than other structures, and a code that accounts for these major differences is necessary to ensure safe and quality designs.

In 2001, the second edition of the *Guidelines for Design of Wind Turbines* from Det Norske Veritas (DNV) and Riso National Laboratory was released. Because this publication was released before most seismic considerations were included in any wind turbine design standards, the code lacks valuable information in regard to seismic design. For example, it states that the "effects of earthquakes should be considered for wind turbines to be located in areas that are considered seismically active based on previous records of earthquake activity" (Riso National Laboratory, 2001). It also states that designs should use any available seismic data or, if no data is readily available, a study of the soil conditions and seismicity of the region should be completed. The design of these wind turbines must then be able to withstand any earthquake loads. This set of guidelines recognizes the need to design turbines for earthquakes but does not give designers the necessary information on how to accurately analyze their designs. Furthermore, this

guideline allows designers to decide how they want to design for earthquakes rather than referencing a uniform guideline that directly addresses seismic loads on wind turbines.

In 2005, the International Electrotechnical Commission released its International Standard for wind turbine design requirements. Since 2005, several amendments and updates have been made, which include provisions for seismic loading (IEC, 2009). This guideline is the most widely recognized set of standards for the design of wind turbines in Europe and the U.S. Because of this, it is important that it include provisions for seismic loads as well as methods of evaluating wind turbine designs for seismic loads. Currently, this code requires that simultaneous earthquake and seismic loads must be considered in designs. This is a requirement that also becomes necessary for certification of turbines. Other requirements include loads triggered by emergency shutdown situations. As with various other codes, it is common for designers to evaluate turbines under each of these loads separately and then superimpose them to determine the final design. This is oftentimes too conservative and involves seismic analysis techniques that are not appropriate for these structures.

Finally, Germanischer Lloyd (GL) introduced a set of guidelines that enables designers to use the standards provided in order to obtain certification of wind turbines (GL, 2010). This code includes seismic activity within the inertial and gravitational loads experienced by the turbine. It also includes earthquakes in the group of environmental conditions, which must be considered for design. These requirements, however, only apply to regions where seismic activity is possible. Several design load cases are provided for this situation. They include DLC 9.5, which assumes seismic loads during tower operation, DLC 9.6, which assumes a superposition of shut-down of the turbine

with seismic loads and lastly, DLC 9.7, which includes a superposition of the seismic load with a previous grid loss. It further states that seismic loads can be calculated in either the time domain or frequency domain and must include a sufficient number of modes for the analysis. Wind turbines should be designed to remain ductile for an earthquake with a return period of 475 years (GL, 2010). Again, this code fails to provide users with the methods for seismic analysis of turbines. It also states that seismic risk must be evaluated only in regions where earthquakes could occur. Many wind farms are located in regions that are not at immediate risk for earthquakes, but could sustain significant damage if an earthquake were to occur.

2.6 Summary and Conclusion

This chapter presents the previous work and applicable codes and guidelines that pertain to wind turbines. While there has been significant work done on understanding the effects of wind and operation loads on wind turbine blades, there has not been a comparable amount of research done on the effects of these types of loading along with seismic loading on the actual turbine structure. Some experimental testing has been completed in the last decade that demonstrates the ability of simplified finite element models to identify the global response of wind turbines under seismic loads. This research has proved to be valuable for the development of codes and guidelines, which include seismic loads in their design standards. Further research is needed, however, to ensure that the methods of analysis are correct. These methods must provide designers with an accurate turbine response for any possible modes of vibration as well as an accurate method of evaluating the local behavior of turbines under seismic loads and combined loads.

3 FINITE ELEMENT FORMULATION

3.1 Introduction

In order to create several finite element models that can be used to analyze the combined loading effects on wind turbines, it is necessary to identify the potential sites, geometry of the turbine, loading and critical load combinations. Once optimum wind and earthquake sites are identified, the potential wind and seismic loads from these locations are characterized. Three turbine models are created using AutoCAD and their geometry exported into ABAQUS for analysis under various loads. The development of these models will be discussed in this chapter along with the modeling and simulation approach.

3.2 Site Identification and Description

A preliminary investigation into potential wind turbine sites is necessary in order to identify the proper wind turbine sizes and loads to be applied in the simulations. The site characteristics that are most critical include wind speeds and seismic risk. For wind speed, valuable information is obtained from NREL. As seen in Figure 3-1 below, NREL provides a wind resource map that identifies wind speeds, wind power density and wind power potential for locations throughout the United States. USGS provides a seismic hazard map for a 2% in 50-year return period probability of exceedance that details the risk for seismic activity throughout the U.S. This map can be seen in Figure 3-2. By evaluating these two maps together, ideal sites can be identified. For the purposes of this research, it is decided that wind turbine sites in southern California provide the most combined risk from wind and seismic loading.

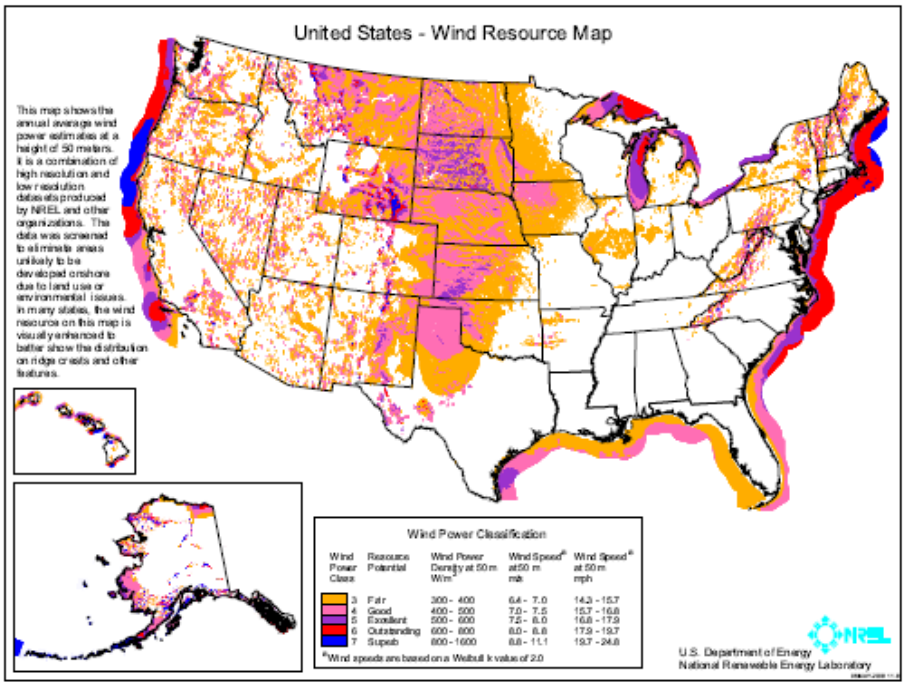

Figure 3-1: Wind Resource Map from NREL
(NREL, 2009)

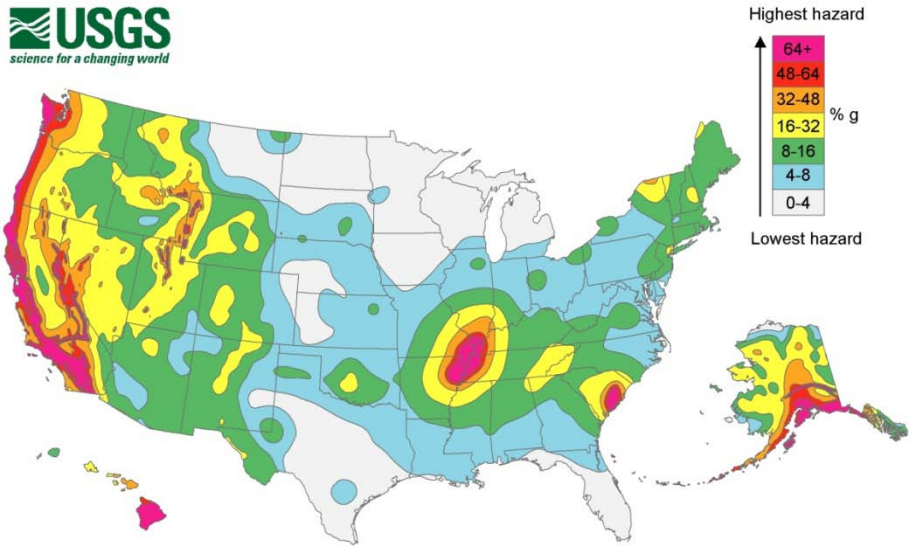

Figure 3-2: Seismic Hazard Map from USGS
(USGS, 2008)

After deciding to look at locations in southern California, the focus is then placed on determining which current wind farm is the most ideal for this research. As there are many wind farms in this region, it is important to identify wind farms with site conditions that are similar to the ones chosen for this study. To that end, wind farms located near or on the San Andreas Fault are chosen because of their high seismic risk.

Figure 3-3 shows cities with respect to the fault. Three major wind farms are in operation in California including Altamont, Tehachapi and San Gorgonio ("Overview of Wind Energy in California," 2013). Both Altamont and Tehachapi are located further north than desired, so the wind farm chosen is San Gorgonio located near Palm Springs. Because this wind farm was commissioned in the early 1980's, some turbines are smaller and more dated than others. Hub heights range from 50 meters to 120 meters, making this wind farm appropriate for analysis in this research.

Figure 3-3: San Andreas Fault
(Lynch, 2006)

The San Andreas Fault lies between the North American and Pacific plates and is of particular interest because of the large number of high-intensity earthquakes throughout history that have occurred along that fault line. Because these plates are constantly moving, the areas around the fault are highly susceptible to earthquake activity.

3.3 Geometric Development

In order to make sure that the results of this research are realistic, it is important to accurately develop the geometry for the models. Three models are created to identify the response of wind turbines under combined loading and how it varies between turbine heights. These models included a 60-meter, 90-meter and 120-meter model. As most geometrical information regarding wind turbines is proprietary, it is somewhat difficult to obtain consistent and necessary information. Two sources, however, provide an adequate basis for the development of geometry. These include information provided through a phone conversation and email exchanges with RES Americas, Inc., which is a renewable energy company that constructs wind farms throughout the United States, as well as information from a 2006 report by NREL.

RES Americas, Inc. provided information for an 80-meter tower manufactured by Vestas (personal communication, August 8, 2012). This information indicates that the towers are comprised of tapered, tubular steel that vary in thickness throughout the height and are built in several sections connected by flanges. The base consists of a base flange with two concentric bolt circles, each with 80 total holes. The bolts are 48 millimeters in diameter and connect the base flange to the foundation. A web is also welded to the base flange and extended into the foundation. This information provides a basis for the geometric configuration for both the base flange and tower sections.As mentioned, a report compiled in 2006 by NREL provides sufficient

information for the geometry and weights of various turbine sizes (Malcolm & Hansen, 2006). The data from this NREL report is shown in Table 3-1 below.

Table 3-1: NREL Final Baseline Configurations
(Malcolm & Hansen, 2006)

	Units	**750 kW**	**1.5 MW**	**3.0 MW**	**5.0 MW**
File Name		.75A08C01 V00c	1.5A08C01 V03c Adm	3.0A08C01 V02c	5.0A04C01 V00c
Rotor diameter	m	50	70	99	128
Max rotor speed	rpm	28.6	20.5	14.5	11.2
Max tip speed	m/s	75	75	75	75
Rotor tilt	degree	5	5	5	5
Blade coning	degree	0	0	0	0
Max blade chord	m	8% of radius	8% of radius	8% of radius	8% of radius
Radius to blade root	m	5% of radius	5% of radius	5% of radius	5% of radius
Blade mass	kg	1818	4230	12936	27239
Rotor solidity		0.05	0.05	0.05	0.05
Hub mass	kg	5086	15104	50124	101014
Total rotor mass	kg	12,381	32,016	101,319	209,407
Hub overhang	m	2.33	3.3	4.65	6
Shaft length x diam	m	1.398 x 0.424	1.98 x 0.56	2.79 x 0.792	3.6 x 1.024
Gearbox mass	kg	4723	10603	23500	42259
Generator mass	kg	2946	5421	10371	16971
Mainframe mass	kg	5048	15057	45203	102030
Total nacelle mass	kg	20,905	52,839	132,598	270,669
Hub height	m	60	84	119	154
Tower base diam x t.	mm	4013 x 12.9	5663 x 17.4	8081 x 25.5	10,373 x 33.2
Tower top diam x t.	mm	2000 x 6.7	2823 x 8.7	4070 x 13	4851 x 17.6
Tower mass	kg	46,440	122,522	367,610	784,101

After analyzing these two sets of information and interpolating for various turbine heights, it is clear that the turbine geometry data from NREL aligns with that provided by RES Americas. Therefore, three different tower model configurations are developed based on these sets of data. Table 3-2 below shows the specifications for these models.

Table 3-2: Tower and Base Specifications for Finite Element Modeling

TOWER SPECIFICATIONS			
Hub Height (m)	60	90	120
Rotor Diam. (m)	50	75	100
Base Diam. (m)	4	6	8
Top Diam. (m)	2	3	4
Base Tower Thickness (m)	0.02730	0.03600	0.05400
Top Tower Thickness (m)	0.01675	0.02300	0.03300
Section Numbers	3.0	4.0	5.0
Tower Section Height (m)	20.0	22.5	24.0
Section Thickness			
Section 1 (m)	0.02730	0.03600	0.05400
Section 2 (m)	0.02203	0.031333	0.04875
Section 3 (m)	0.01675	0.02667	0.04350
Section 4 (m)	N/A	0.02200	0.03825
Section 5 (m)	N/A	N/A	0.033
Blade Mass (kg)	1818	5553	12846
Hub Mass (kg)	5086	18382	46393
Rotor Mass (kg)	12381	41500	99652
Nacelle Mass (kg)	20905	62609	136411
Tower Mass (kg)	105252	307943	816533
Total (kg)	**138538**	**412052**	**1052596**
TURBINE BASE AND BOLT SPECIFICATIONS			
Base Flange Outer D (m)	4.310	6.310	8.370
Base Flange Inner D (m)	3.590	5.590	7.650
Outer Hole Diam. (m)	4.166	6.166	8.226
Inner Hole Diam. (m)	3.734	5.734	7.794
Flange Width (m)	0.720	0.720	0.720
Flange Thickness (m)	0.060	0.060	0.060
Web Height (m)	0.038	0.038	0.038
Web Thickness (m)	0.02730	0.03600	0.05400
Bolt Specifications	M48 Grade 8.8		
Bolt Diameter (m)	0.048		
Nut Diameter (m)	0.075		
Nut Thickness (m)	0.038		
Clearance Distance (m)	0.06		
Edge Distance (m)	0.072		
Length (m)	0.098		

It is important to note several items for each turbine. Firstly, each model is generated in AutoCAD using these dimensions. The 60-meter model has a tower that is created in three sections, while the 90-meter has four and the 120-meter has five. Section thicknesses are therefore listed accordingly. For these models, the section thickness varies linearly throughout the turbine height. The rotor and nacelle masses are left unchanged from the data provided by NREL. The tower mass, however, is based on the geometric configuration of the models that are developed. This mass is larger than the mass given by NREL, but reflects the appropriate mass for the size of the tower, mass of the base and density of steel at 7850 kg/m^3. Finally, the base flange specifications are derived solely from the information given by RES Americas, as NREL does not provide data for this region. It is assumed that the bolt size, flange thickness, web thickness and web height do not vary throughout the three models.

Upon determining the tower configurations, it is then necessary to identify how the blades and nacelle would be modeled. Because wind turbine blade geometry changes throughout the length, it is important to determine how complex the blades in these three models would be. NREL provides valuable information regarding blade geometry from a study on active aerodynamic flow for wind turbine blades in 2007 (Schreck & Robinson, 2007). Figure 3-4 and Figure 3-5 below depict both a typical blade cross-section and plan view for wind turbine blades. Another important feature of wind turbine blades is the curvature throughout the length of the blade. Figure 3-6 shows how these blades are curved.

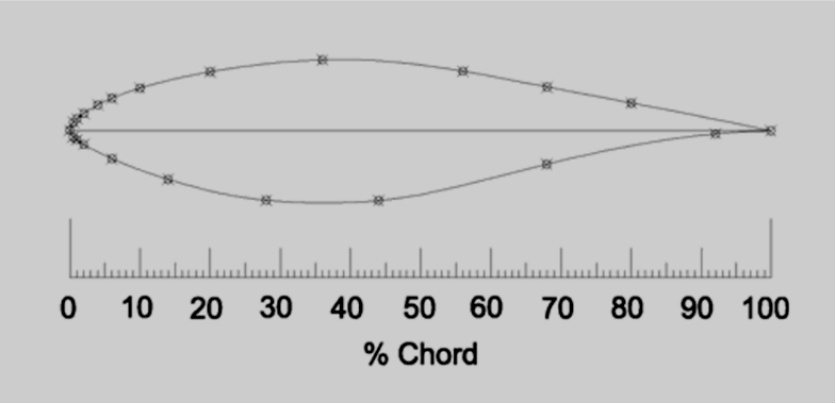

Figure 3-4: NREL Wind Turbine Blade Cross-Section
(Schreck & Robinson, 2007)

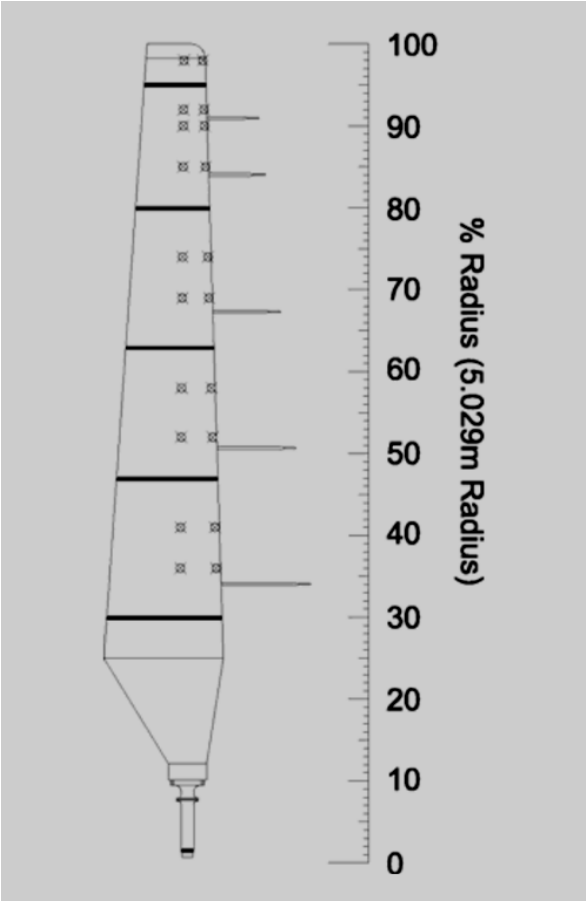

Figure 3-5: NREL Wind Turbine Blade Plan View
(Schreck & Robinson, 2007)

Figure 3-6: Depiction of Wind Turbine Blade Curvature from GE Blades at NREL (Verrengia, 2009)

After reviewing the blade geometry data, it is determined that a simplified blade configuration could be used in the finite element models because the simulations are not focused on the response of the blades, but rather on the tower as a whole. It is important, however, to mention that the length of the blades and the distribution of the mass along the length of each blade are accurately modeled. This ensures that the system dynamics are well represented. In order to create this simplified model, the above cross-section and plan views are copied into AutoCAD and three blade configurations are modeled, which correspond to the three different turbine heights. For the purposes of this research, the curvature of the blades is not included. The blades are modeled as line elements with a length based on a hub height equal to 1.2 times the rotor diameter as specified by NREL (Malcolm & Hansen, 2006).

The geometry of the nacelle can vary through different manufacturers. Most are comprised of long sections with rounded or rectangular ends. The nacelle holds various mechanical components including the gear box, generator and shaft. The rotor, which includes the blades and hub, is then attached to the shaft inside the nacelle. Because this study does not

evaluate any mechanical performance of the wind turbine, the nacelle is modeled as a line element with a rectangular cross-section in all three models.

Once all of the components of the wind turbine are developed, each configuration is assembled in AutoCAD. Each configuration consists of three blades, a blade rotator that connects the blades to the nacelle, the nacelle, tower sections, a base flange, a base web, bolts, the tower-to-base welds and the base flange-to-base web welds. Figure 3-7 shows the tower, blade and nacelle configurations and dimensions developed in AutoCAD. Figure 3-8 shows the tower base configuration for the 60-meter tower from AutoCAD.

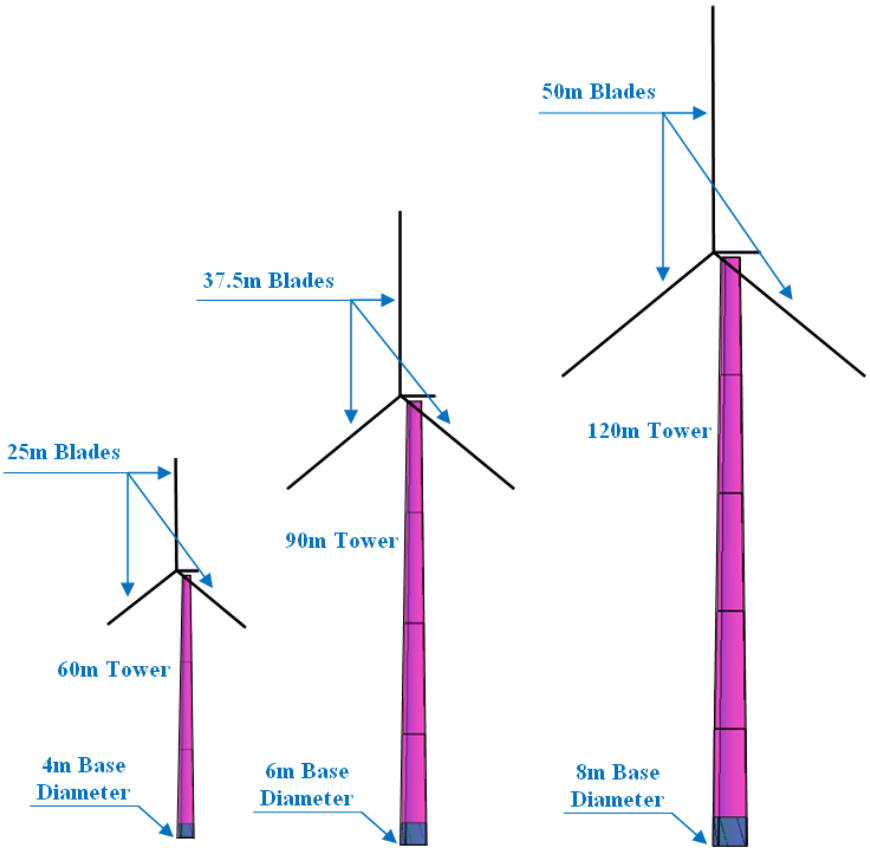

Figure 3-7: Tower Configurations from AutoCAD

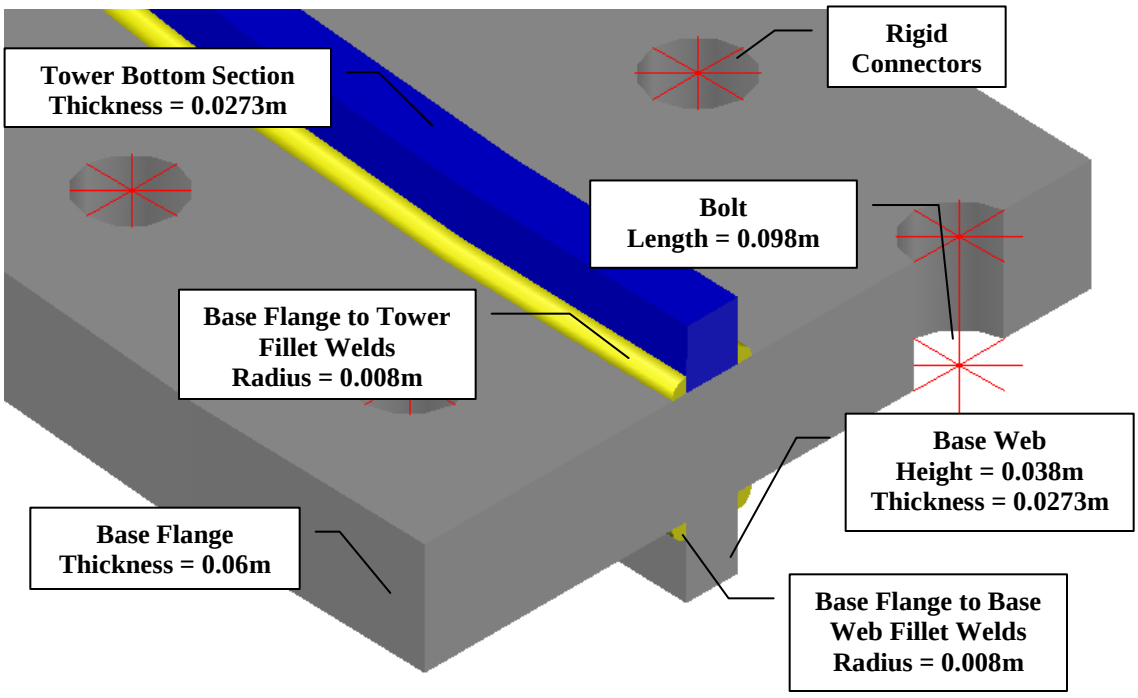

Figure 3-8: Tower Base Configuration from AutoCAD for 60-meter Tower

3.4 Finite Element Model Development

Once the various parts are created in AutoCAD, they are imported into ABAQUS. These parts include the base web, base flange, bolts, rigid bolt connectors, welds, tower sections, nacelle and blades. Each part contains its own material and section properties. The tower and base sections are imported as half-sections during this process for ease in meshing the cross-section. After each part is properly defined and meshed, the whole turbine is assembled and given the appropriate constraints, boundary conditions and loads.

The base flange, base web, welds and a tower bottom section are imported as half sections using solid section properties. The base section can be seen in Figure 3-9. Once these sections are assembled together, the base section is then meshed to form one part. This part consisted of the base flange, base web, fillet welds, bolts and tower bottom. The flange, base web, welds and tower bottom section are modeled using solid elements. To simplify the bolt model, the bolts are

modeled as line elements with eight rigid elements at the intersections of the base flange and bolt. These rigid elements connect the bolt to the outer edge of the bolt holes within the base flange and allow for nodal convergence between the bolts and the base. Figure 3-10 shows the complete mesh from this section.

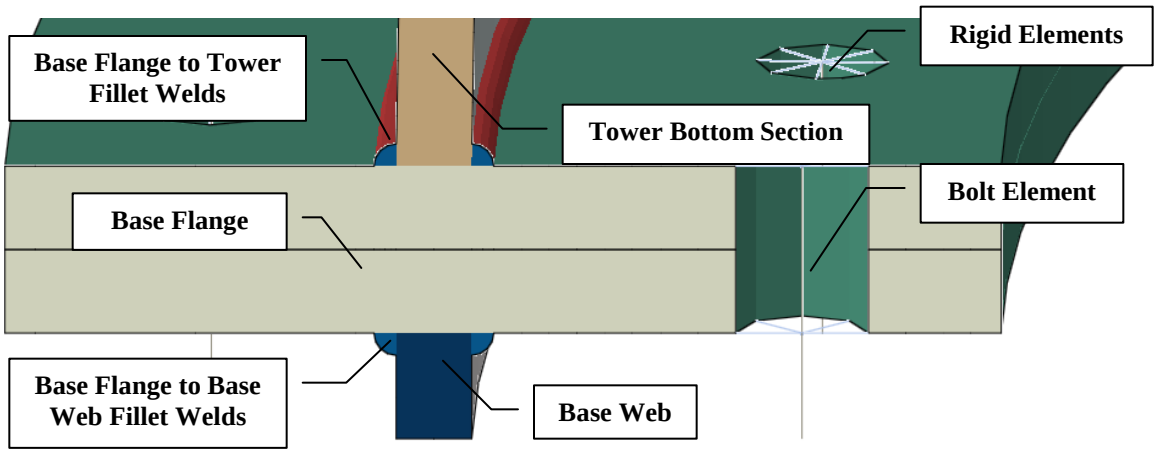

Figure 3-9: Base Section Configuration from ABAQUS

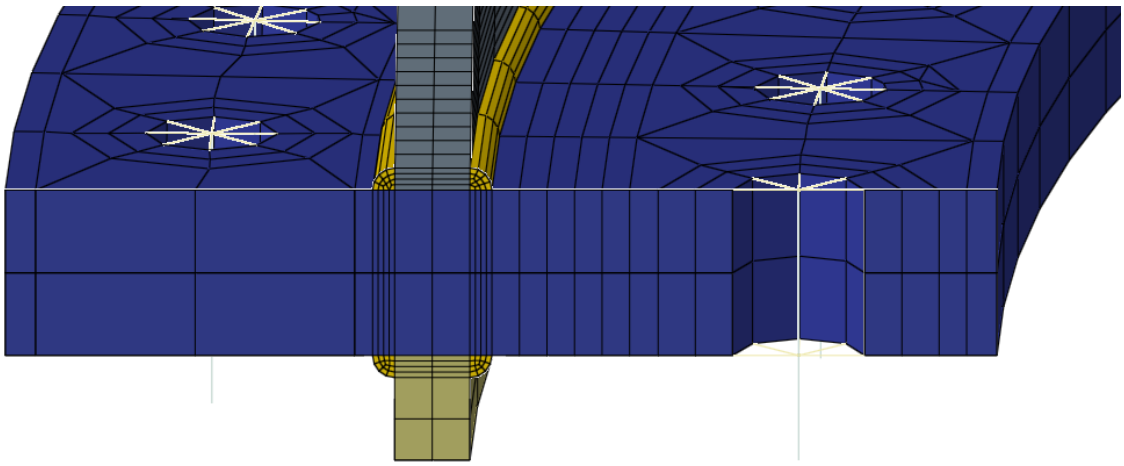

Figure 3-10: Base Section Mesh from ABAQUS

It is important to note that all of the nodes from the individual sections are aligned and that the mesh is finer at the welds and the lower sections of the tower. This allows for a better representation of stresses that develop in the tower under various types of loading.

To reduce the computational cost, the tower sections are comprised of both solid and shell elements. The tower bottom section is modeled as a solid section, as mentioned above, so that it could be successfully merged into the base section. This section is comprised of the bottom three meters of the first tower section. The other sections are developed using shell elements and the corresponding thicknesses based on the NREL literature. Figure 3-11 shows the solid tower bottom section and the first tower shell section. Figure 3-12 shows two tower shell sections and their corresponding flange sections. The tower shell and solid sections are connected using shell-to-solid coupling whereby, the edge of the tower shell section is connected to the face of the tower bottom solid section. This type of constraint allows for the motion of the shell to be coupled to the motion of the solid section. This ensures that the ground motion would accurately transfer from the solid section to the tower shell section.

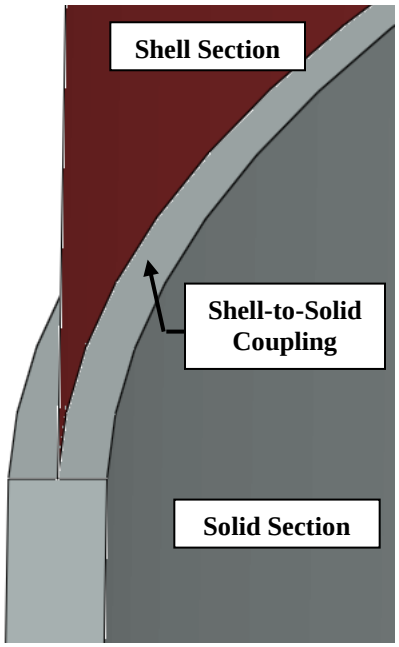

Figure 3-11: Tower Bottom to First Tower Shell Section

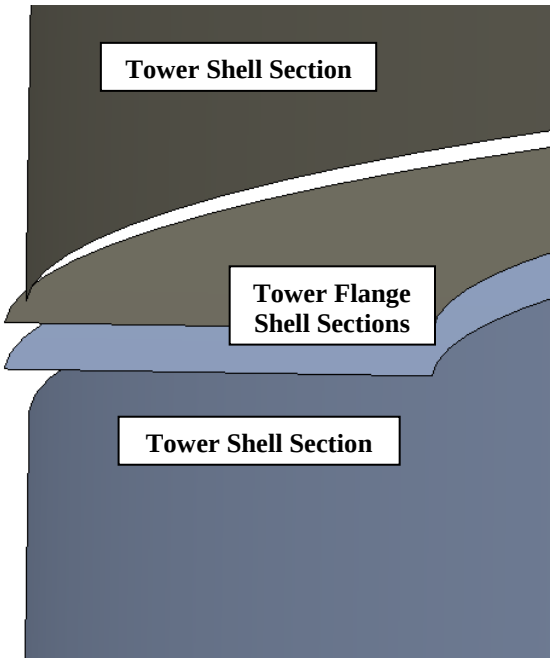

Figure 3-12: Tower and Flange Shell Sections

Finally, the blade and nacelle parts are developed. As previously stated, these use simplified geometries. The nacelle is represented as having a rectangular profile, while the blades are represented with a pipe profile. These are shown below in Figure 3-13.

The blade models are divided into several sections, and the volume, surface area, moment of inertia, radius, mass and density are found for each. For simplicity in developing the models, the blades are modeled as beam elements comprising of a constant cross-section with point masses throughout the length that are representative of the size and mass of the various sections. To accomplish this, the surface area is summed for all of the sections to find the total surface area of the blade. The radius of the pipe section is then calculated based on this value. A blade rotator element is created as the connecting point for all three blades and also as the connecting point between the nacelle and rotor.

Figure 3-13: Blade and Nacelle Beam Profiles

The pipe profile for the blades depends on the turbine model as each one has a specific radius and thickness which increases as the turbine height increases. The nacelle is assigned a material property, which has a density that corresponds to what the total mass of that component should be. The blades have point masses applied, which correspond to the geometric and mass properties of the individual sections.

After all of these sections are assembled, it is necessary to apply constraints throughout the model to ensure that each part is connected. These constraints include the following:

- Connecting the solid tower bottom section to the first tower shell section using shell-to-solid coupling as described above,
- Connecting tower section flanges to tower sections and adjacent flanges,
- Connecting the nacelle to the top of the tower using multi-point constraints (MPC),

- Connecting the small blade element (blade rotator) to the nacelle using a pin MPC to ensure that blade rotation could occur,
- Connecting the three blades to the blade rotator using a tie MPC to ensure that these blades would not rotate or move about the blade rotator, and finally,
- Applying a rigid body constraint to all three blades to ensure that they would not have excessive elongation during rotation.

This process is used for developing each of the three turbine models using the geometric configurations listed in Table 3-2. Material properties are also developed for the various sections. These properties are listed in Table 3-3 below.

Damping for the turbines is specified using Rayleigh damping. The damping factors α and β are calculated based on the first and third modes of vibration for each of the three models. For the purposes of this research, the damping ratio for the towers is set to 5% due to the high seismic demand. It is important to note that the previous research indicated that the aerodynamics of the blades in their operational state provide additional damping to the motion of the tower (Ntambakwa & Rogers, 2009). Such damping is inherently accounted for in the simulations through the rotation of the blades. The Rayleigh damping coefficients are calculated based on the frequencies of the first and third mode shapes using the following equations (Chowdhury & Dasgupta, 2003):

$$\beta = \frac{2\zeta_3\omega_3 - 2\zeta_1\omega_1}{\omega_3^2 - \omega_1^2} \qquad \text{Equation 3-1}$$

$$\alpha = 2\zeta_3\omega_3 - \beta\omega_3^2 \qquad \text{Equation 3-2}$$

Where ζ_3 is damping ratio for the third mode, ω_3 is the natural frequency for the third mode, ζ_1 is the damping ratio for the first mode and ω_1 is the natural frequency for the first mode. The

damping factors can be seen in Table 3-4 below. Lateral modes indicate a side-to-side (parallel to blades) motion of the turbine whereas fore-aft indicates a front-to-back (perpendicular to blades) motion of the turbine.

Table 3-3: Model Material Properties

Sections	Property	Value	Units
Nacelle	Density	2841	kg/m^3
	Young's Modulus	2.00E+11	N/m^2
	Poisson Ratio	0.3	
Blades	Density	0	kg/m^3
	Young's Modulus	1.40E+11	N/m^2
	Poisson Ratio	0.3	
Rotator	Density	0.5	kg/m^3
	Young's Modulus	2.00E+11	N/m^2
	Poisson Ratio	0.3	
Rigid	Density	0.001	kg/m^3
	Young's Modulus	2.00E+11	N/m^2
	Poisson Ratio	0.3	
Weld	Density	0.001	kg/m^3
	Young's Modulus	4.82E+08	N/m^2
	Poisson Ratio	0.3	
	Plastic Modulus	3.50E+08	N/m^2
Bolt	Density	7850	kg/m^3
	Young's Modulus	2.00E+11	N/m^2
	Poisson Ratio	0.3	
	Plastic Modulus	6.40E+08	N/m^2
Steel	Rayleigh Damping: α	VARIES	
	Rayleigh Damping: β	VARIES	
	Density	7850	kg/m^3
	Young's Modulus	2.00E+11	N/m^2
	Poisson Ratio	0.3	
	Plastic Modulus	3.50E+08	N/m^2

Table 3-4: Rayleigh Damping Factors

	Modes	Frequency	α	β
60-meter Tower	1- Lateral	0.6119	0.0596	0.0098
	1- Fore-Aft	0.6354		
	3- Lateral	9.3038		
	3- Fore-Aft	9.5792		
90-meter Tower	1- Lateral	0.4175	0.0402	0.0143
	1- Fore-Aft	0.4280		
	3- Lateral	6.3204		
	3- Fore-Aft	6.5677		
120-meter Tower	1- Lateral	0.3224	0.0309	0.0190
	1- Fore-Aft	0.3302		
	3- Lateral	4.7558		
	3- Fore-Aft	4.9303		

As mentioned, the blades are modeled as line elements and assigned point masses based on the individual section properties. From Table 3-2, it can be seen that the rotor diameter for the 60-meter, 90-meter and 120-meter turbines are 50m, 75m and 100m, respectively. The length of each blade is therefore half of the corresponding tower's rotor diameter. For each model, the blades are divided into several sections. The first section represents the portion of the blade that is closest to the hub and varies in length between the models. The remaining blade sections are divided equally, each being approximately four meters in length. Various geometric properties are found as previously mentioned, and the mass of each section is then determined. Because the model utilizes a uniform blade cross-section, point masses are applied throughout the blade length that reflected these section masses. The point masses are applied at the center of each section and allow for a more accurate representation of blade geometry and weight distribution than simply incorporating a constant blade density would. Table 3-5 shows the final values for section radii and point masses per turbine model.

Table 3-5: Blade Point Mass and Section Radius

	Section	Point Mass (kg)	Radius (m)
60-meter Tower	1	44.25	0.26
	2	664.64	0.79
	3	1005.10	1.19
	4	893.29	1.06
	5	663.97	0.79
	6	481.43	0.58
	7	374.31	0.45
90-meter Tower	1	148.23	0.30
	2	1423.14	0.86
	3	2133.46	1.29
	4	2268.03	1.37
	5	2067.34	1.25
	6	1737.91	1.05
	7	1414.31	0.86
	8	1113.69	0.68
	9	963.137	0.59
	10	791.095	0.49
120-meter Tower	1	355.61	0.43
	2	1860.51	0.89
	3	3487.15	1.66
	4	3999.40	1.90
	5	4086.74	1.94
	6	3794.20	1.80
	7	3391.54	1.61
	8	2897.83	1.38
	9	2443.58	1.17
	10	2044.30	0.98
	11	1829.31	0.88
	12	1613.82	0.78
	13	1396.65	0.68

3.5 Load and Boundary Condition Development

For each model, several loads and boundary conditions are identified and calculated for use in the finite element simulations. Boundary conditions include the fixed base, bolt pretension and angular velocity for rotation of the blades. Loads include operation, wind and seismic.

The first boundary condition applied to each model is the fixed condition at the base of each bolt. This simulates the location where the bolts are embedded into the reinforced concrete foundation. This boundary condition is also the location for the application of the horizontal seismic loads.

Bolt pretension is applied as a displacement boundary condition. The displacement is applied at both the top and bottom of the bolt where it intersects the base flange to simulate the pretension force. This displacement is calculated based on the material properties of the bolt. In this case, a M48 Grade 8.8 bolt is used, which has an ultimate tensile strength of 8.00E8N/m^2 and yield strength of 6.40E8N/m^2. The length of the bolts is 0.098m, and the diameter of this bolt is 0.048m which has a cross-sectional area of 0.0018m^2. The following calculations demonstrate how the displacement values are calculated.

$$P_y = \sigma_y A_{bolt} \qquad \text{Equation 3-3}$$

$$P_y = 6.40E8\,N/m^2 * 0.0018m^2 = 1.16E6N$$

$$F_{CLAMP} = 0.8 * P_y \qquad \text{Equation 3-4}$$

$$F_{CLAMP} = 0.8 * 1.16E6N = 9.26E5N$$

$$F_{CLAMP} = \frac{EA}{L}\Delta \qquad \text{Equation 3-5}$$

$$\Delta = \frac{F_{CLAMP} * L}{EA} \qquad \text{Equation 3-6}$$

$$\Delta = \frac{9.26E5N * 0.098m}{2E11N/m^2 * 0.0018m^2} = 0.00026m$$

Where σ_y is the yield stress, A_{bolt} is the cross-sectional area of the bolt, P_y is the yield force, F_{CLAMP} is the clamping force, E is Young's Modulus, L is the length of the bolt and Δ is the required displacement for clamping. The applied displacement of 0.00026m can be seen in Figure 3-14 below.

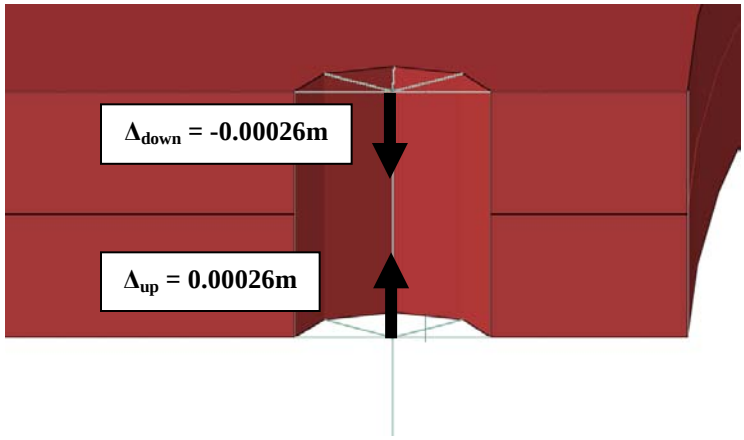

Figure 3-14: Application of Bolt Pretension as Displacement Boundary Conditions

The last applied boundary condition is the angular velocity, which depicts the speed at which the blades rotate. Information received from RES Americas indicated that the rotation of the blades was around 6 – 16 rotations per minute (rpm). This aligned with data from NREL which indicated that the maximum rotation for their systems were around 11 – 29rpm for heights between 154m and 60m, respectively. From this, it is decided that an average value would be taken from the numbers given by RES Americas. This value of 11rpm corresponds to an angular velocity around 1.15 radians per second. This boundary condition is applied to the blade rotator element in all steps of the analysis to simulate operational conditions and a constant rotational speed.

After specifying the necessary boundary conditions, several loads are identified and calculated for use in the three models. The first of these is a static gravity load which would be applied as the first step in each analysis. The bolt pretension displacement and angular velocity boundary conditions are also applied along with gravity. The next step incorporates the angular velocity boundary condition as the operation load along with the earthquake and possible wind loads. The development of these loads is based on available literature as well as software calculations for application of the loads in ABAQUS.

In order to properly identify wind loading, it is first necessary to determine the velocity at which each of these turbines would operate. If the wind velocity at the hub height is too low or too high, the rotor would not be in operation. Two reports from NREL gave good insight into the necessary wind velocities for operation. Madsen, Pierce and Buhl (1999) provided 10 minute average wind velocities for operation, cut-out and parked conditions. Table 3-6 shows the wind velocity for each along with the power law exponent, target turbulence intensity and reference height. This information indicates that 14m/s would be best suited for this research application.

Table 3-6: Design Wind Velocity for Various Operational States
(Madsen et al., 1999)

Design situation – Load case	**Wind speed (10 min aver.)**	**Power law exponent α**	**Target turb. intensity I_u**	**Reference Height**
Operation at rated wind speed	14m/s	0.2	17%	16.8m
Operation at cut-out wind speed	20m/s	0.2	17%	16.8m
Parked at extreme wind speed	45m/s	0.2	17%	16.8m

Griffin (Griffin, 2001) also provides wind velocities in a report published by NREL. This report is for four different turbine heights of different power output. The average, rated and cut-out wind velocities are provided. These values can be seen in Table 3-7 below.

Table 3-7: Design Wind Velocity for Various Turbine Heights
(Griffin, 2001)

System Rating (kW)	**V_{mean} (m/s)**	**V_{rated} (m/s)**	**$V_{cut-out}$ (m/s)**	**Rotor Diameter (m)**	**Rotor Radius (m)**	**Specific Rating (kW/m^2)**	**Tower Height (m)**
750	7.50	12.5	22.5	46.6	23.3	0.44	60.6
1500	7.89	12.5	22.5	65.9	32.9	0.44	85.6
3000	8.29	12.5	22.5	93.2	46.6	0.44	121.1
5000	7.50	12.5	22.5	120.4	60.2	0.44	156.4

From this report, it seems that the wind velocity must be at least 12.5m/s for the turbines to be operational. Based on the information provided from these two studies, it is decided that a rated wind velocity at hub height of approximately 15 m/s will be used for all three models. This ensures that the wind turbines can be operational for any height and that they will not exceed the cut-out velocity.

Once the appropriate wind velocity is determined, wind velocities, pressures and forces are calculated for the tower and blades. The wind velocities are calculated by assuming the power law model for wind distribution. The value of 15m/s is assigned as the velocity at hub height and a value of 0m/s is given at the base of the tower. The wind velocity values are obtained using the equation for the power law equation from ASCE 7-05. This equation is as follows:

$$\frac{\bar{u}(z)}{\bar{u}(z_{ref})} = \left(\frac{z}{z_{ref}}\right)^{n} \qquad \text{Equation 3-7}$$

$$\frac{\bar{u}(z)}{15m/s} = \left(\frac{1}{60m}\right)^{1/7}, \mathbf{\bar{u}(z) = 6.31 m/s}$$

Where $\bar{u}(zref)$ is the wind velocity at reference height, z_{ref} is the reference height, z is the height for the desired wind velocity, $\bar{u}$ is the desired wind velocity and n = 1/7 for Exposure C.

The velocity pressures are then calculated along the tower using the available equation from ASCE 7-05 as follows:

$$q_z = 0.613 K_z K_{zt} K_d V^2 I \ (N/m^2) \qquad \text{Equation 3-8}$$

Where K_d = 0.85 for the Main Wind Force Resisting System (MWFRS), K_{zt} = 1.0, K_z = 1.46 (60m), 1.59 (90m), 1.69 (120m) for Exposure C, I = 1 for Occupancy Category II and ρ = 1.225 kg/m^3 for air density. These pressures are then plotted against the tower height to develop a trend line that would be used in determining the wind forces on the blades. Wind velocity and

pressure values can be seen in Table 3-8 below. A plot showing the wind pressure versus tower height and its corresponding power model equation can be seen in Figure 3-15.

Table 3-8: 60-meter Turbine Wind Velocities and Pressures

60-meter Tower Rated		
Height (m)	**Velocity (m/s)**	**Pressure (N/m^2)**
1	8.35	65.01
5	10.51	103.02
10	11.61	125.60
15	12.30	141.05
20	12.82	153.14
25	13.23	163.23
30	13.58	171.97
35	13.89	179.72
40	14.16	186.72
45	14.40	193.12
50	14.61	199.02
55	14.81	204.52
60	15.00	209.68
65	15.17	214.53
70	15.33	219.13
75	15.49	223.49
80	15.63	227.66
85	15.77	231.64

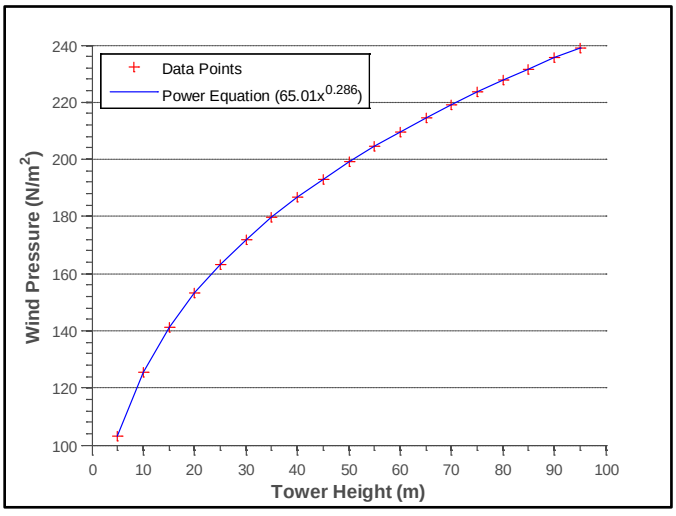

Figure 3-15: Wind Pressures versus Tower Height for 60-meter Tower

For ease in accurately simulating wind loading, the wind pressures are converted into wind forces based on the number of tower sections and the corresponding tributary area for those sections. For example, the 60-meter tower has three tower sections, so there are three regions where wind force is applied whereas the 90-meter tower had four sections, so the wind force is applied at four regions and so on. This is determined by first finding the mid-height of each tower section and then finding the surface area for one half of that tower section. This tributary area is multiplied by the average wind pressure along the height of that section which gives the corresponding total force. This total force is distributed along the nodes that are located on that half of the tower to simulate real wind loading. The total force is divided by the number of nodes, in this case 80, and then assigned a quadratic shape so that the wind is greatest at the centerline of the tower rather than uniform over the whole face. This process is completed for each tower section in each model by creating a quadratic function which represents the total force experienced by each section. This function is then used in ABAQUS to define the correct force at each node. Figure 3-16 shows the wind force applied on each tower section.

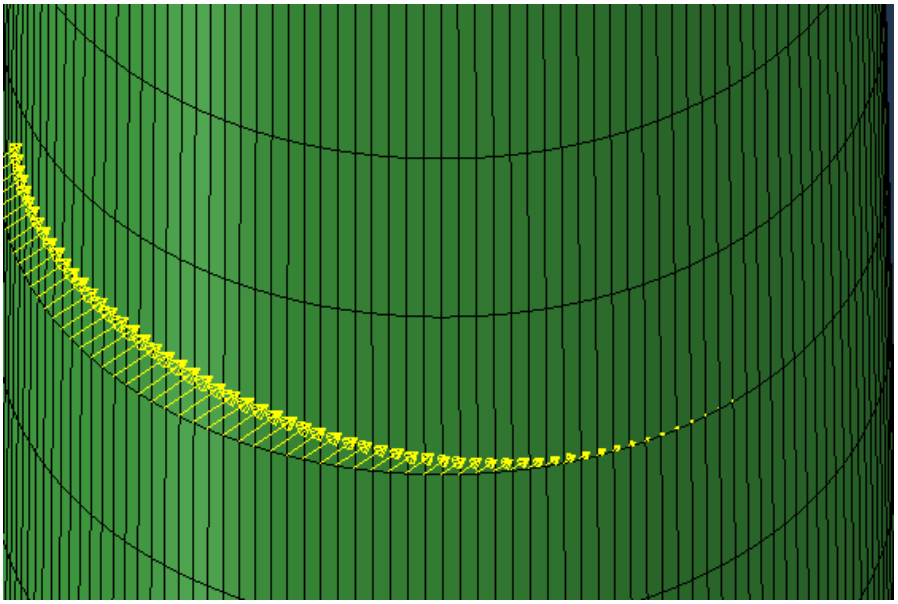

Figure 3-16: Wind Force on Tower Section

Modeling the wind force on the blades involves a different procedure as the blades rotate throughout each analysis. At each time increment during an analysis, the height, wind velocity, pressure and force change for each node on the blades. To accurately model this, an equation is developed for each blade section so that the forces on that section represent the location of the blade at any given time. The following equation demonstrates how this is accomplished:

$$\frac{(\text{Power Model Equation}) * (\text{Blade Section Area})}{(\text{Blade Section Length})} \qquad \text{Equation 3-9}$$

$$\frac{(65.01\text{Y}^{0.286}) * (20.1\text{m}^2)}{(4.0277\text{m})} \text{ (for Blade Section 2 in 60 m model)}$$

Where *Y* is the height of the blade section node at any given time, the *Power Model Equation* is the equation developed from the wind pressure curve for each turbine model, *Blade Section Area* is the area for blade section where force is applied and *Blade Section Length* is the length of blade section where force is applied. This is completed for each blade section in each model. The force is applied as a line load over the length of the blade section with the previous equation as the distribution of that force. Figure 3-17 shows how this force is applied to the blades. It is worth noting that the wind load is not specified as a time history. Because the analyses are only 10 seconds long, it is assumed that the wind load has a constant magnitude and direction. Previous studies indicated as well that wind loads could be modeled as constant or static loads (Bazeos et al., 2002). This provides a constant conservative load for the turbine throughout the entire analysis.

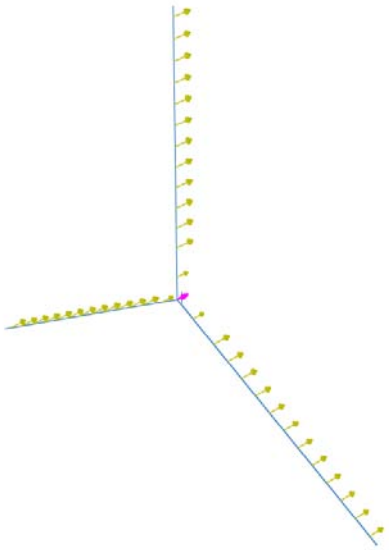

Figure 3-17: Distribution of Wind Force Along Blades

The final load that is developed for these simulations is the seismic load. This process includes identifying soil conditions for the southern California region, the number of total earthquake records needed, a magnitude range, soil conditions for these records and determining the division between near-field and far-field records. Next, the design spectrum is developed along with the response spectrum for each earthquake. The final step is to determine the scaling factors to use for the various turbine models and these earthquakes.

The first step in developing these loads is determining how many records and what type of records should be used. The Applied Technology Council provides valuable information in their ATC-63 report (FEMA P-695) on the *Quantification of Building Seismic Performance Factors* (Applied Technology Council, 2008). This report details both near- and far-field seismic records for use in modeling earthquakes. Each record also includes the earthquake year, magnitude, soil type and reporting station. For the purposes of this research, it is decided that magnitudes between 6.5 and 7.5 should be used as they represent an expected earthquake magnitude in California, for a total of 10 earthquakes. These 10 earthquakes include five near-

field and five far-field records. The next step for selecting records is to identify which soil types should be considered. After examining the region of interest in southern California, soil information is found for the Mountain View IV Wind Project near Palm Springs. The geotechnical report indicates that the site has a soil site class C and a seismic category D (Earth Systems Southwest, 2006). It is therefore decided that the soil types for the earthquake records should include mostly soil type C with some records having soil type B or D.

The 10 records are selected from FEMA P-695 based on the above criteria. In order to obtain the actual acceleration records, the Pacific Earthquake Engineering Research Center's PEER Ground Motion Database is used. This database allows the user to input record sequence numbers as specified in FEMA P-695 and obtain the horizontal acceleration records. SeismoSignal software is used to develop the response spectra for all of the earthquake records. These response spectra are used in combination with the design spectrum developed for all three models when determining the scale factor for each earthquake record. The chosen record data can be seen in Table 3-9 below. The acceleration time-history records for all earthquakes can be seen in Figure 3-18 below.

Table 3-9: Chosen Earthquake Records for Simulations

	ATC ID No.	Soil Type	Magnitude	Record Year	Record Name	Record Seq. No.
Near-Field	10	C	6.7	1994	Northridge - 01	1086
	11	B	7.5	1999	Kocaeli, Turkey	1165
	13	C	7.6	1999	Chi-Chi, Taiwan	1529
	14	D	7.1	1999	Duzce, Turkey	1605
	20	C	6.9	1989	Loma Prieta	741
Far-Field	2	D	6.7	1994	Northridge	953
	4	C	7.1	1999	Hector Mine	1787
	10	C	7.5	1999	Kocaeli, Turkey	1158
	11	D	7.3	1992	Landers	900
	22	C	6.5	1976	Friuli, Italy	125

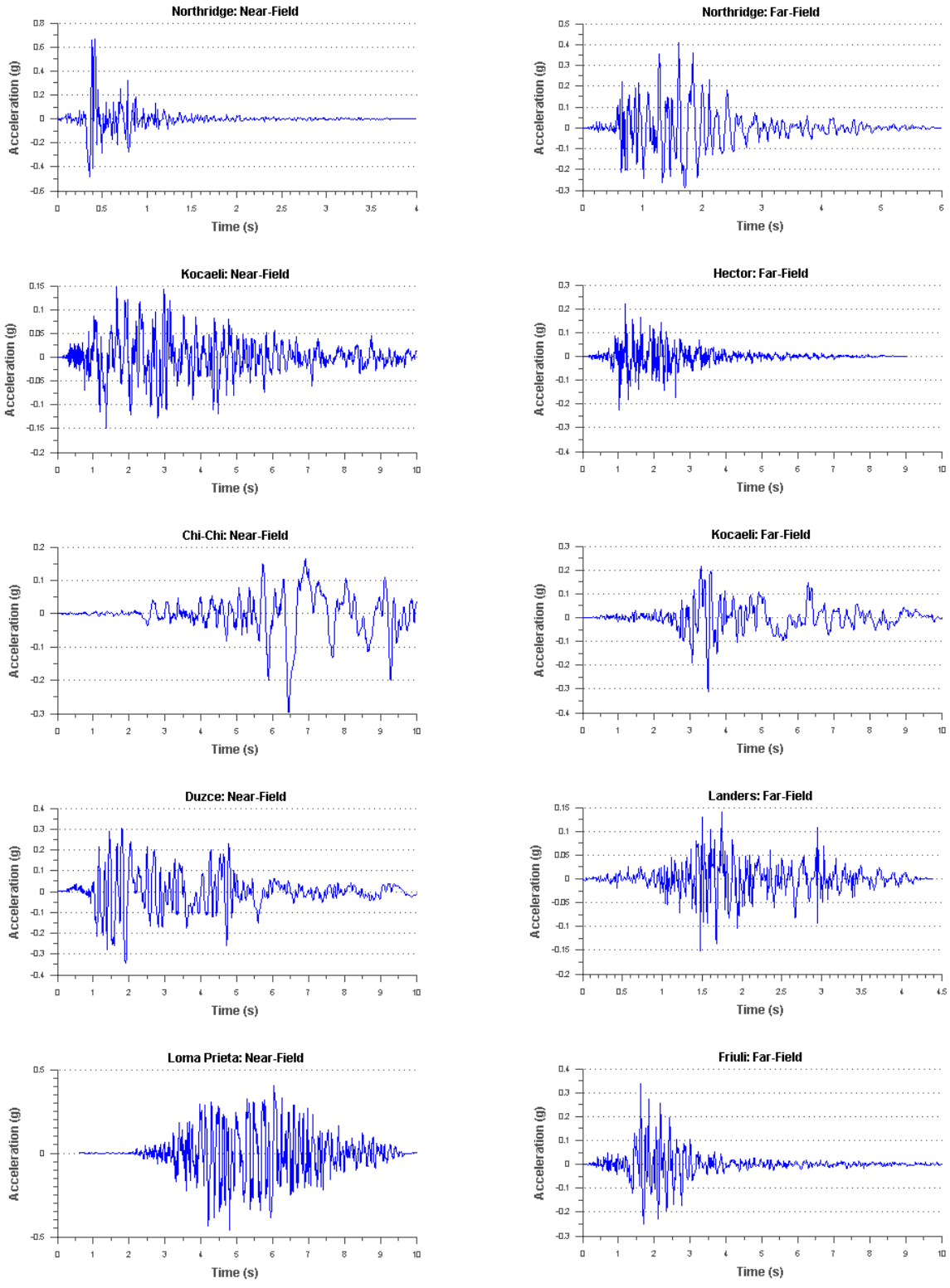

Figure 3-18: Acceleration Time-History Records for all Earthquakes

The average response spectrum is created for both the near-field and far-field record sets in order to obtain only two scale factors per turbine model. The average response spectrum for the near-field record sets can be seen in Figure 3-19 and the average response spectrum for the far-field record sets can be seen in Figure 3-20.

After the records are selected and their response spectra are created, the design spectrum is created for the turbine models. This spectrum is developed using the USGS Hazard App software used in creating seismic hazard curves and uniform hazard response spectra. ASCE 7-05 is chosen as the analysis option and the wind farm latitude and longitude are entered. Finally, the soil type is changed from B to C and the S_{DS} and S_{D1} values are calculated. The seismic induced spectral acceleration (S_a) values are then calculated and the design spectrum is created. This value represents the acceleration experienced by the structure. This spectrum can be found in Figure 3-21 below.

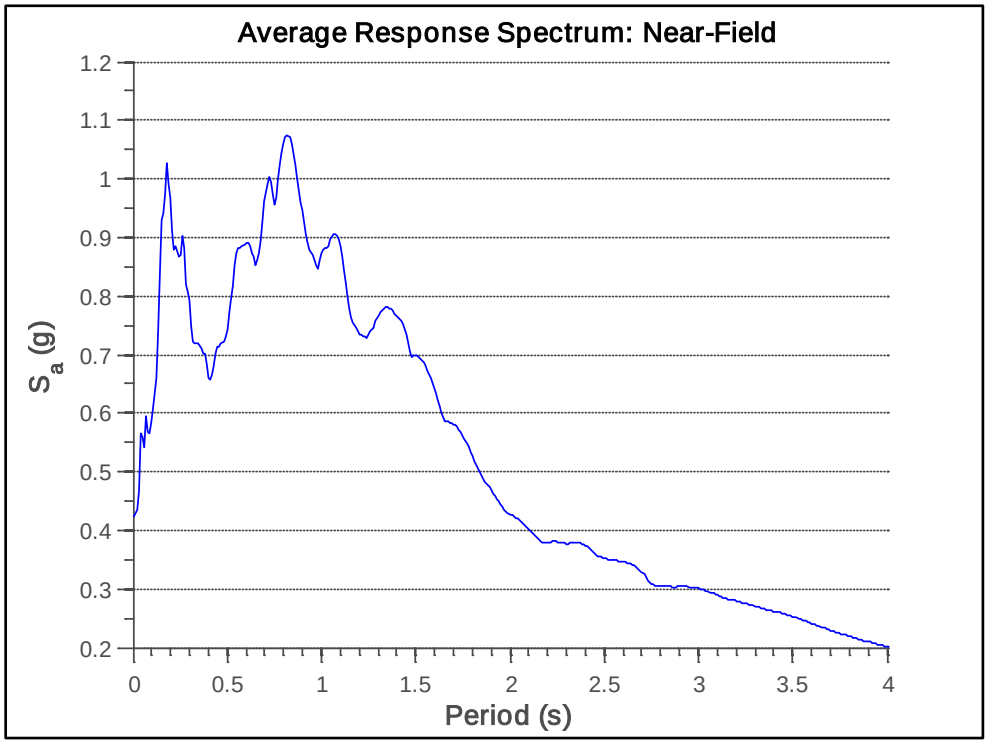

Figure 3-19: Average Response Spectrum for Near-Field Records

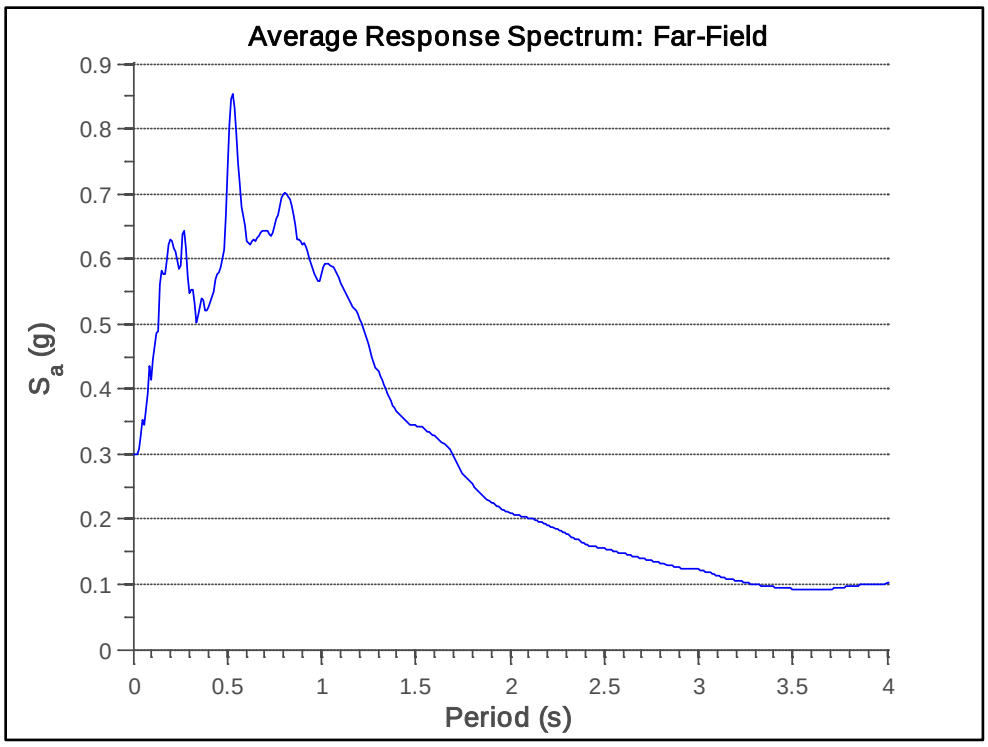

Figure 3-20: Average Response Spectrum for Far-Field Records

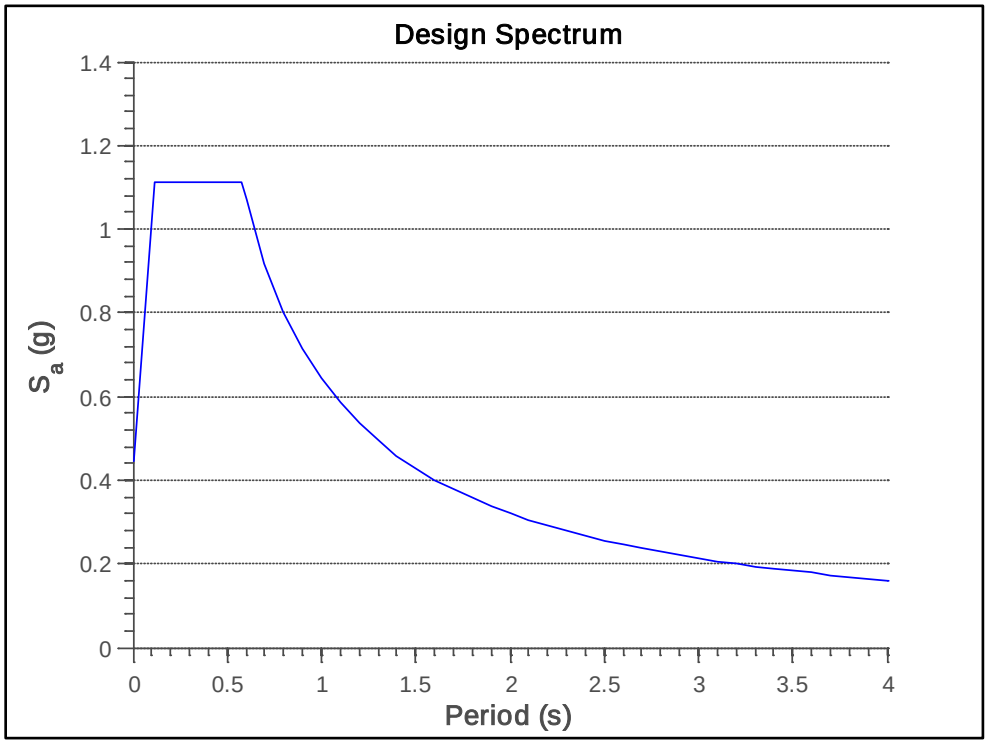

Figure 3-21: Design Spectrum for Seismic Load Application

Next, the period of each turbine has to be calculated based on the predominant frequency in each model. Figure 3-22 shows the first, second and third mode shapes for the 60-meter turbine. For each model, the first mode shape is predominant. The corresponding frequency is thus used in determining the period for all three turbines. The design spectrum is then applicable to all three models, as it incorporates the three different structure periods. Table 3-10 shows the periods for each of the three turbine models.

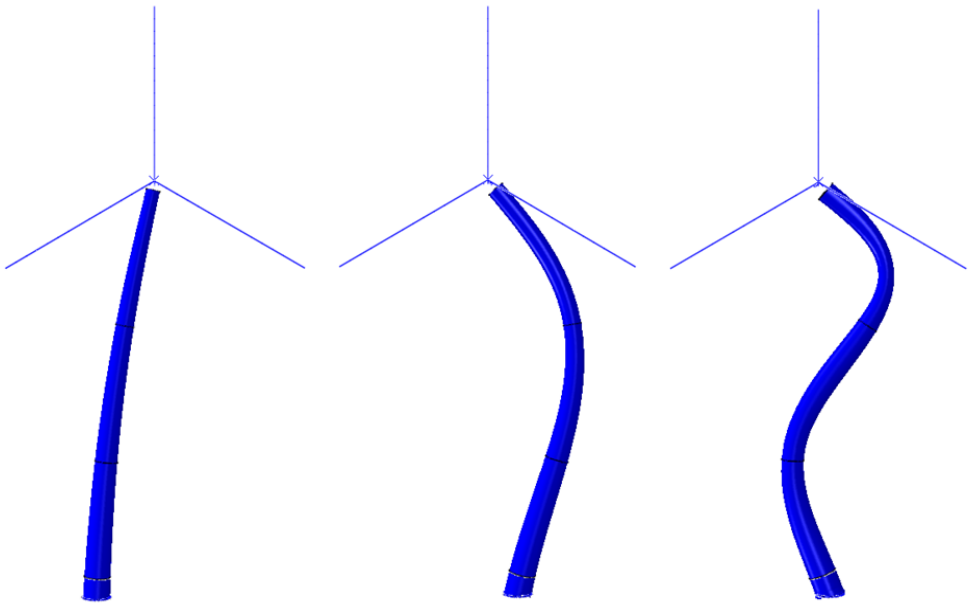

Figure 3-22: First, Second and Third Mode Shapes for 60-meter Turbine

Table 3-10: Turbine Periods

Model	1st Period (s)	2nd Period (s)	3rd Period (s)
60-meter	1.57	0.30	0.11
90-meter	2.34	0.44	0.16
120-meter	3.03	0.58	0.21

The next step is to scale the earthquake records to the design spectrum for each turbine model. The S_a values from both the design spectrum and response spectrum are obtained for the times which corresponded to the period of each turbine model. The near-field records are then

scaled down to the design spectrum while the far-field records are scaled up. The near-field scale factors for each turbine model can be seen in Table 3-11 and the far-field scale factors can be seen in Table 3-12 below.

Table 3-11: Near-Field Records Scale Factors

	1st Period (s)	Response Sa (g)	Design Sa (g)	Scale Factor
60-meter	1.57	0.5674	0.3688	0.650
90-meter	2.34	0.3744	0.2673	0.714
120-meter	3.03	0.2895	0.2070	0.715

Table 3-12: Far-Field Records Scale Factors

	1st Period (s)	Response Sa (g)	Design Sa (g)	Scale Factor
60-meter	1.57	0.2748	0.3690	1.343
90-meter	2.34	0.1618	0.2675	1.653
120-meter	3.03	0.1132	0.2071	1.829

3.6 Description of ABAQUS Analyses

Because many operational states exist for wind turbines, it is necessary to identify which load cases should be evaluated for this study. This included evaluating the wind turbine at cut-in, rated, cut-out and extreme wind velocities along with an operational velocity around 6 – 16rpm. It is also important to determine which case would be most impacted by the addition of earthquake loads.

After evaluating the various wind loads and operational states, it is decided that the wind turbine will be analyzed for a rated wind velocity and an average angular velocity for the blade rotational speed. This is decided because it represents the ideal operating state for wind turbines. The wind loading is not so high that the turbine would have to shut down, and the rotational velocity is such that the likelihood of mechanical problems in the nacelle is diminished. Finally, it is decided that the seismic loading will be evaluated in two situations: earthquake and operation, and earthquake, wind and operation. While wind turbines would not be operational if

there was no wind, it is crucial to understand the impact an earthquake would have on the turbine under operation loads only. After combining the load scenarios, it is determined that there would be 20 analyses per turbine model: 10 for the earthquake and operation and 10 for the earthquake, wind and operation. Within each set, there would be five near-field earthquake records and five far-field earthquake records.

Within the ABAQUS model, it is necessary to identify which direction the loads should be applied to obtain maximum displacements and stresses throughout the model. It is also necessary to identify how these loads should be applied for efficiency in running each analysis. Test analyses were completed that evaluated the two load combinations in a variety of directions. These directions included the perpendicular to blades and parallel to blades configurations. Specifically, analyses were conducted for the following cases:

- Parallel wind + parallel seismic
- Parallel wind + perpendicular seismic
- Perpendicular wind + parallel seismic
- Perpendicular wind + perpendicular seismic

After evaluating each of these, it is determined that the direction perpendicular to the turbine blades for the wind and seismic creates the highest stresses and displacements for the model. Therefore, each analysis has both the wind load and seismic load applied perpendicular to the blades.

In order to ensure that each analysis would run in ABAQUS, certain amplitudes and load controls are used. Each test includes a static step at which the gravity load and bolt pretension displacement are applied. The next step is a dynamic implicit step, which includes the seismic and possible wind loads. For the load case that includes only seismic loads, the step is 10

seconds long with the earthquake running throughout the whole step. For the load case including both wind and seismic loads, the step length is 15 seconds long. This allows for the wind load to be ramped up during the first five seconds of the step so that the sudden application of wind forces will not cause instability within the model. The earthquake load is then applied from five seconds to 15 seconds to last for a total of 10 seconds. This is completed for each analysis input file for a total of 60 simulations.

Upon the completion of the analyses the output of the simulations is post-processed to obtain an understanding of the global and local performance of the wind turbines. The performance parameters, discussed in the next chapter, include drift ratio and base shear for the global assessment and stresses and low-cycle fatigue at the weld toe for local assessment. In addition, a fast Fourier transform (FFT) analysis is conducted to evaluate the potential impact the earthquake frequency could have on the operational stability of the turbine. This analyzes the ground acceleration and compares that to the frequency of the first three modes of vibration and the blade rotation frequency to determine whether these values are close to or match the predominant ground motion frequency. Such condition could result in instability in the wind turbine and could result in damage to the system.

3.7 Conclusion

This chapter discusses the means by which each model was developed including the geometric and material properties of each system. Certain simplifications are made for ease in modeling using ABAQUS. A total of 60 analysis input files are generated. For each analysis, boundary conditions are applied to simulate the fixed base, bolt pretension and angular velocity for the rotational speed of the blades. The necessary wind loads and seismic loads are also applied for each of the 10 earthquakes. Two load combinations with 10 total earthquakes are

used to simulate seismic with operation and seismic, operation and wind loads. Each model therefore has 10 analyses per load combination.

4 SIMULATION RESULTS

4.1 Introduction

Upon completion of the various analyses, both global results and local behavior are obtained. The results are divided between the two load combinations for ease in comparison between the loads and turbine models. Global response includes drift ratio, base shear and turbine operational stability. Localized behavior includes the Von Mises stress and low-cycle fatigue analysis at the welded connection of the tower and base flange.

This chapter will discuss each of these for all of the simulations that were conducted. The next chapter will provide an in-depth discussion of these results and provide a comparison between the models and their load combinations.

4.2 Global Response

4.2.1 Drift Ratio

The drift ratio (DR) provides an understanding of the impact of the seismic loads on the global deformation of the wind turbine and the potential for system collapse. For each model, the drift ratio is defined as the difference between the top-of-turbine displacement and the ground displacement divided by the corresponding turbine tower height. Each value is then represented as a percentage. The maximum drift ratio is found for each turbine model under the specified load combination and earthquake record. Figure 4-1, Figure 4-2 and Figure 4-3 represent the maximum drift ratio for the 60-meter, 90-meter and 120-meter turbines, respectively, under operation and seismic loads. Figure 4-4, Figure 4-5 and Figure 4-6 represent the maximum drift ratio for the three models under wind, operation and seismic loads.

For the 60-meter turbine under operation and seismic loads, the maximum drift ratio is 1.04 for the Northridge: Far record, while the minimum drift ratio is almost zero for the Loma Prieta: Near record. The average drift ratio is 0.34.

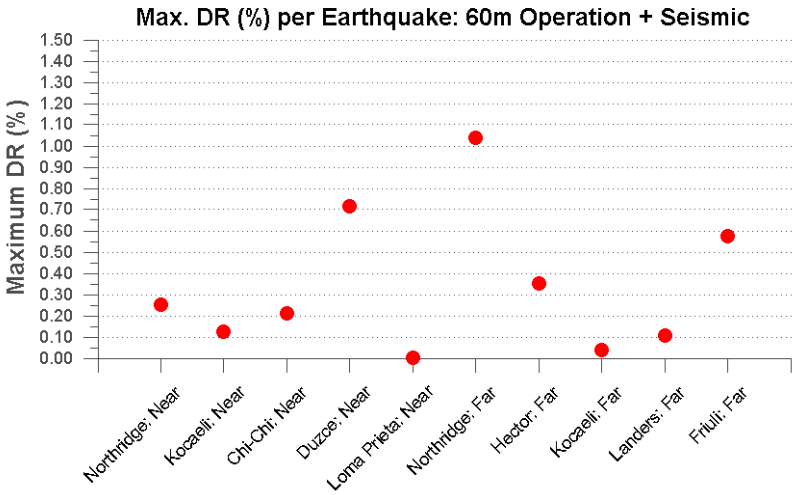

Figure 4-1: Maximum Drift Ratio (%): 60m Operation + Seismic Loading

For the 90-meter turbine under operation and seismic loads, the maximum drift ratio is 0.65 for the Friuli: Far record, while the minimum drift ratio is 0.01 for the Loma Prieta: Near record. The average drift ratio is 0.26.

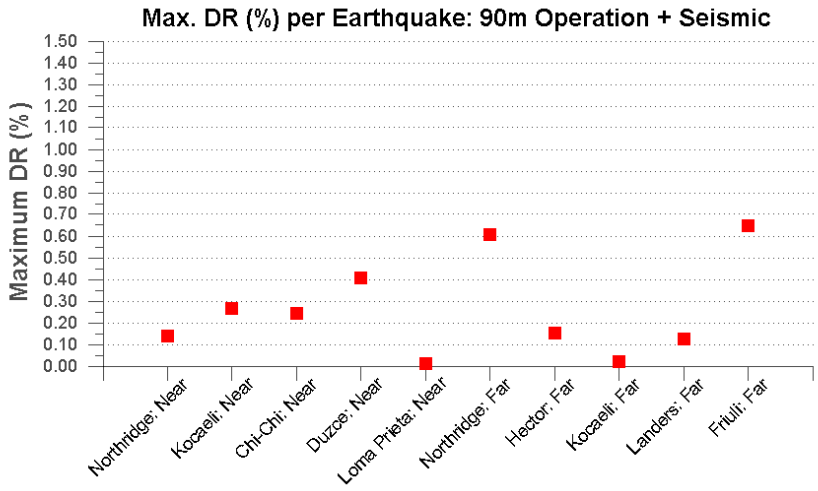

Figure 4-2: Maximum Drift Ratio (%): 90m Operation + Seismic Loading

For the 120-meter turbine under operation and seismic loads, the maximum drift ratio is 0.43 for the Northridge: Far record, while the minimum drift ratio is 0.02 for the Loma Prieta: Near record. The average drift ratio is 0.2.

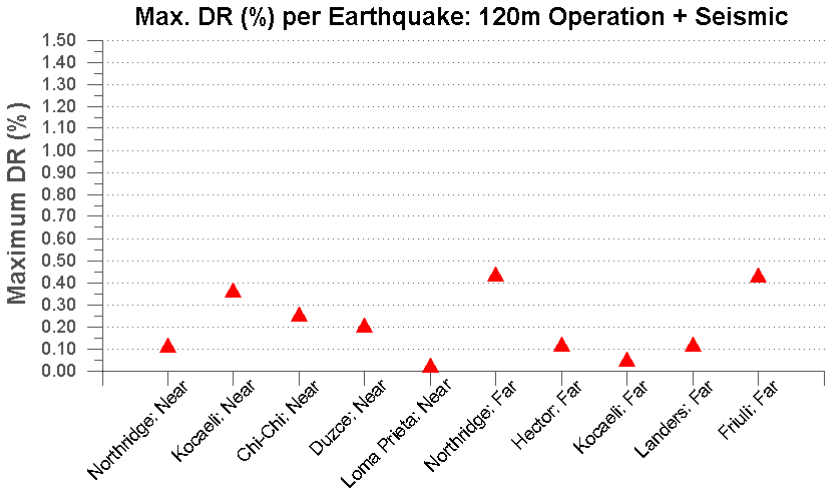

Figure 4-3: Maximum Drift Ratio (%): 120m Operation + Seismic Loading

For the 60-meter turbine under wind, operation and seismic loads, the maximum drift ratio is 1.25 for the Northridge: Far record, while the minimum drift ratio is 0.21 for the Loma Prieta: Near record. The average drift ratio is 0.49.

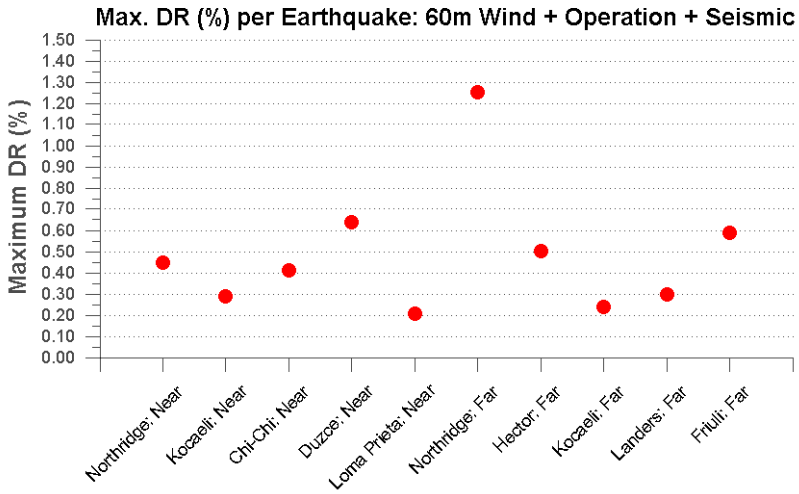

Figure 4-4: Maximum Drift Ratio (%): 60m Wind + Operation + Seismic Loading

For the 90-meter turbine under wind, operation and seismic loads, the maximum drift ratio is 0.87 for the Friuli: Far record, while the minimum drift ratio is 0.21 for the Loma Prieta: Near record. The average drift ratio is 0.42.

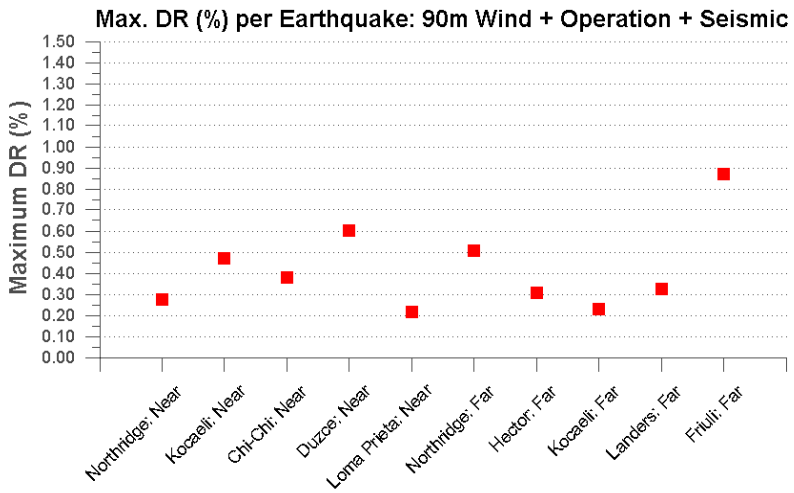

Figure 4-5: Maximum Drift Ratio (%): 90m Wind + Operation + Seismic Loading

For the 120-meter turbine under wind, operation and seismic loads, the maximum drift ratio is 0.6 for the Friuli: Far record, while the minimum drift ratio is 0.21 for the Loma Prieta: Near record. The average drift ratio is 0.38.

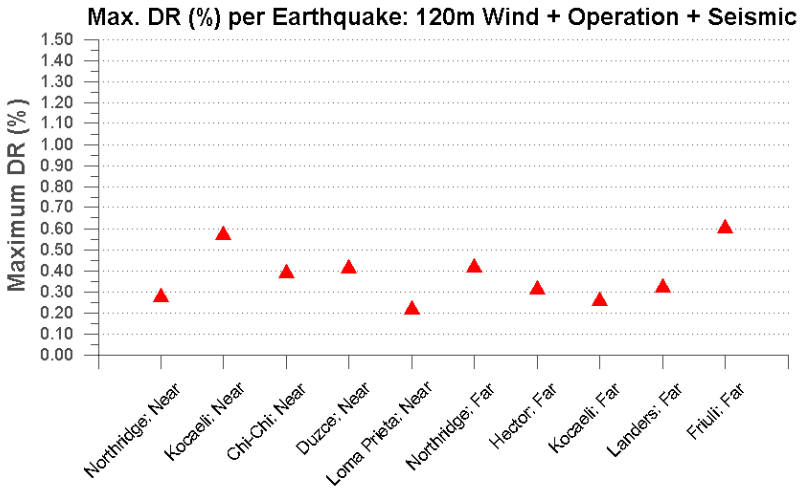

Figure 4-6: Maximum Drift Ratio (%): 120m Wind + Operation + Seismic Loading

4.2.2 Base Shear

The base shear determines the total lateral force that can be expected in each model from the two load combinations. For each model, the base shear is normalized by the total weight of the turbine model (V/W) in order to adequately provide comparison between the three turbine heights. In this case, V/W is plotted similarly to the drift ratio, where the maximum values from each analysis are plotted for the various turbine models and the corresponding loads. Figure 4-7, Figure 4-8 and Figure 4-9 represent the maximum V/W for the 60-meter, 90-meter and 120-meter models, respectively, under operation and seismic loading. Figure 4-10, Figure 4-11 and Figure 4-12 represent the maximum V/W for the three turbine models under wind, operation and seismic loading.

For the 60-meter turbine under operation and seismic loads, the maximum V/W is 0.35 for the Northridge: Far record, while the minimum drift ratio is almost zero for the Loma Prieta: Near record. The average V/W is 0.17.

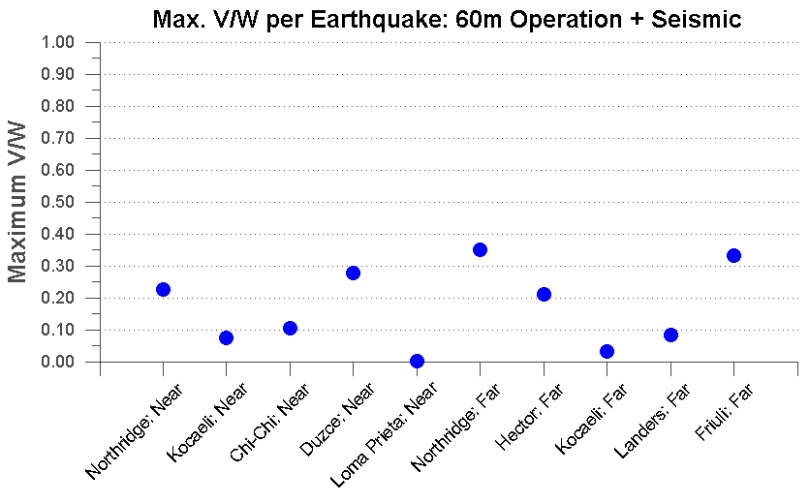

Figure 4-7: Maximum V/W: 60m Operation + Seismic Loading

For the 90-meter turbine under operation and seismic loads, the maximum V/W is 1.90 for the Northridge: Far record, while the minimum drift ratio is almost zero for the Loma Prieta: Near record. The average V/W is 0.38.

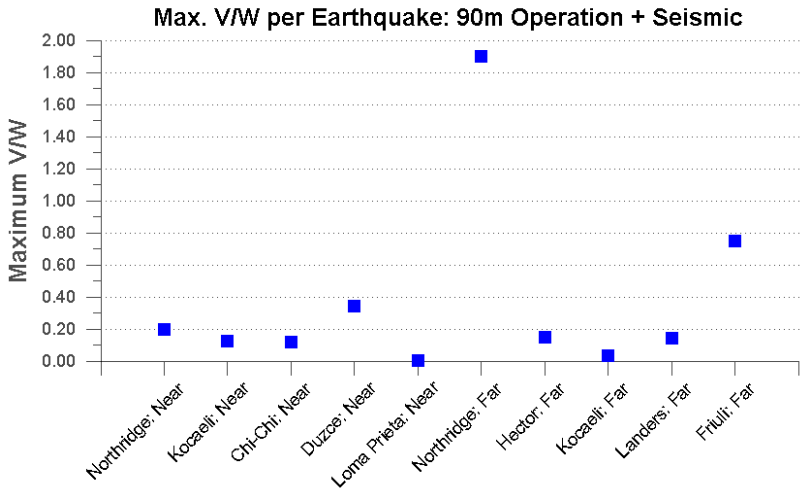

Figure 4-8: Maximum V/W: 90m Operation + Seismic Loading

For the 120-meter turbine under operation and seismic loads, the maximum V/W is 5.21 for the Northridge: Far record, while the minimum drift ratio is almost zero for the Loma Prieta: Near record. The average V/W is 0.70.

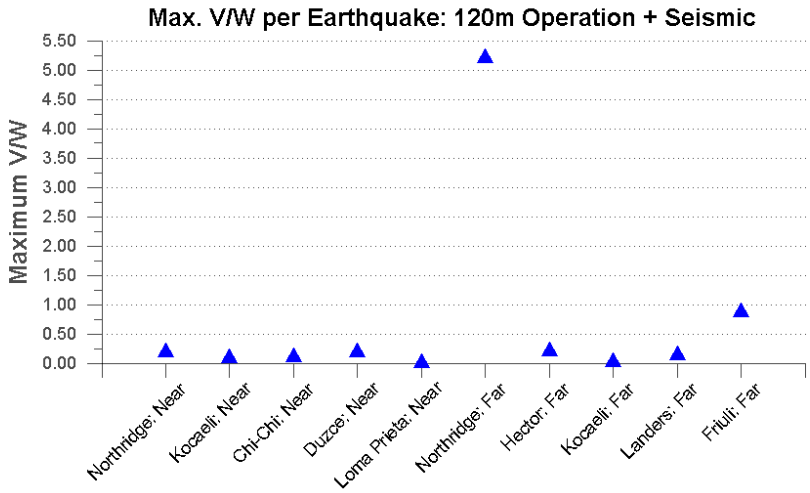

Figure 4-9: Maximum V/W: 120m Operation + Seismic Loading

For the 60-meter turbine under wind, operation and seismic loads, the maximum V/W is 0.44 for the Northridge: Far record, while the minimum drift ratio is 0.09 for the Loma Prieta: Near record. The average V/W is 0.24.

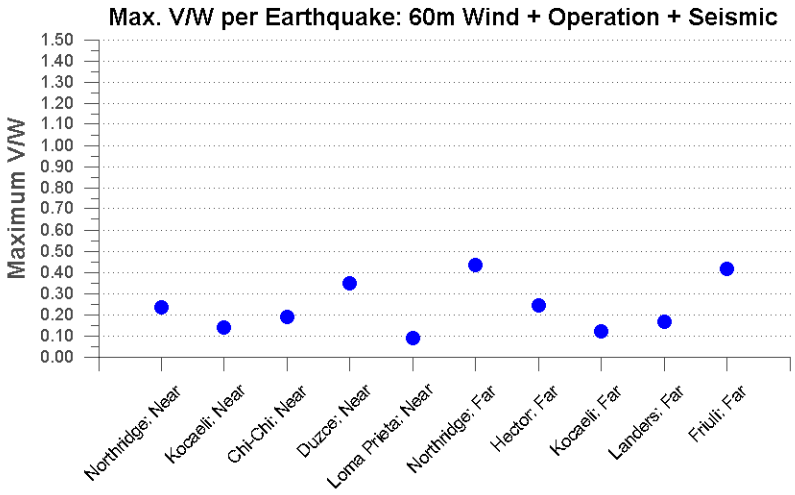

Figure 4-10: Maximum V/W: 60m Wind + Operation + Seismic Loading

For the 90-meter turbine under wind, operation and seismic loads, the maximum V/W is 0.90 for the Northridge: Near record, while the minimum drift ratio is 0.07 for the Loma Prieta: Near record. The average V/W is 0.37.

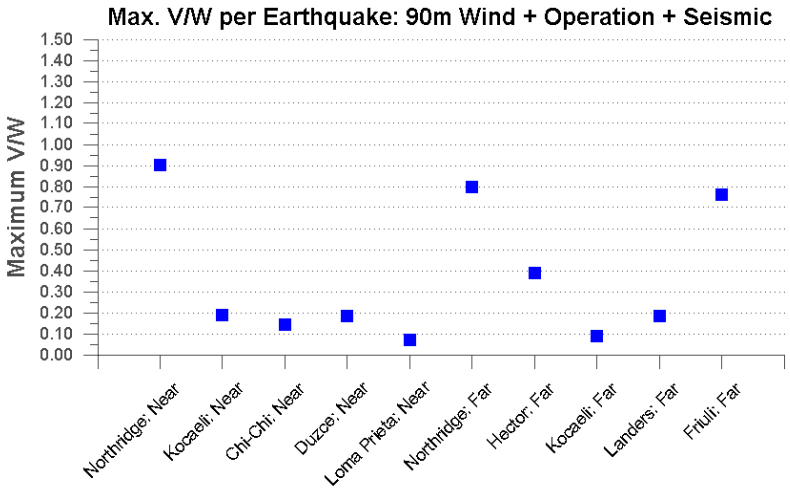

Figure 4-11: Maximum V/W: 90m Wind + Operation + Seismic Loading

For the 120-meter turbine under wind, operation and seismic loads, the maximum V/W is 1.28 for the Northridge: Far record, while the minimum drift ratio is 0.05 for the Loma Prieta: Near record. The average V/W is 0.32.

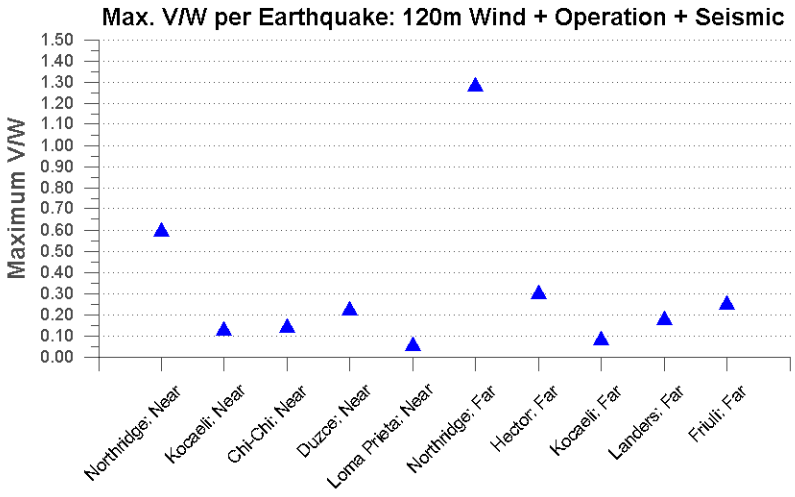

Figure 4-12: Maximum V/W: 120m Wind + Operation + Seismic Loading

4.2.3 Turbine Operational Stability (FFT Analyses)

The operational stability of the turbine is analyzed through the comparison of the ground motion frequencies to that of the modal and blade rotational frequencies. This is conducted through FFT analyses. These results are presented by depicting the frequency of the first three modes of vibration for the corresponding turbine height, the frequency of the rotational velocity of the blades and finally, the predominant frequency of the ground motion. Figure 4-13, Figure 4-14 and Figure 4-15 show the FFT results for the 60-meter, 90-meter and 120-meter turbine models, respectively. The ratio of the mode 1 frequency to the operational frequency is 3.41 for the 60-meter turbine, 2.31 for the 90-meter turbine and 1.79 for the 120-meter turbine. The following chapter will discuss the potential implications from these results.

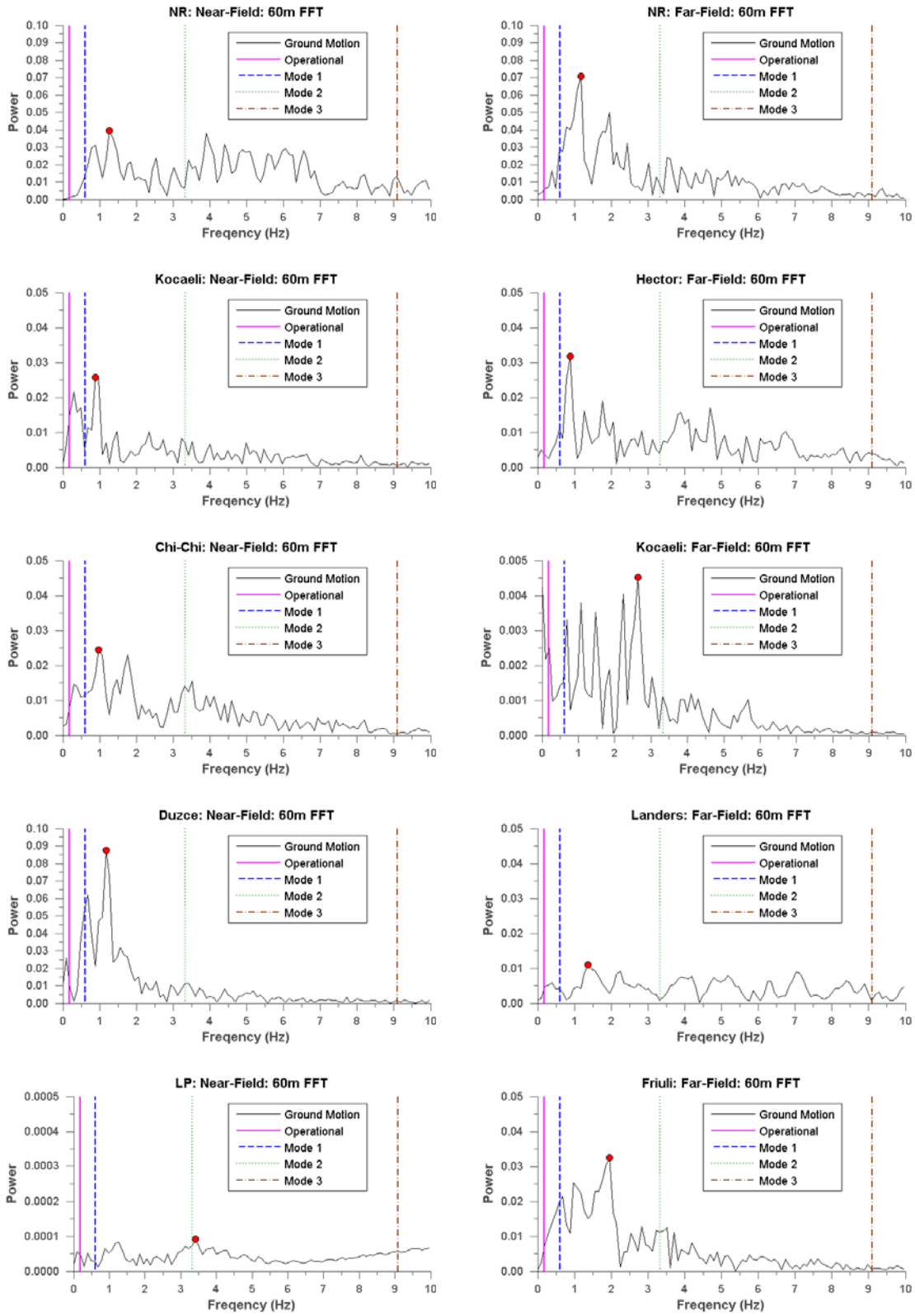

Figure 4-13: FFT Analyses for 60m Turbine for all Earthquake Records

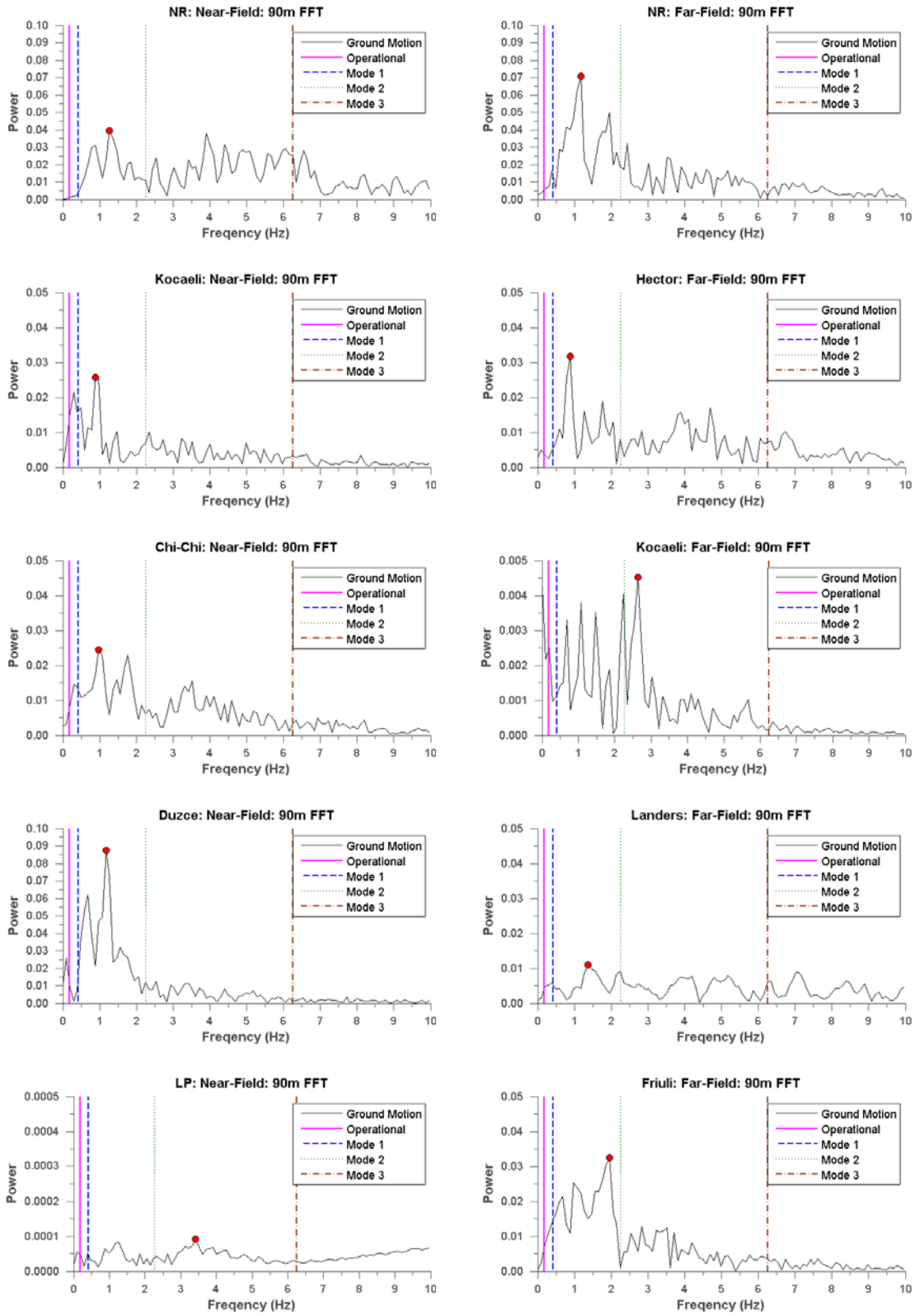

Figure 4-14: FFT Analyses for 90m Turbine for all Earthquake Records

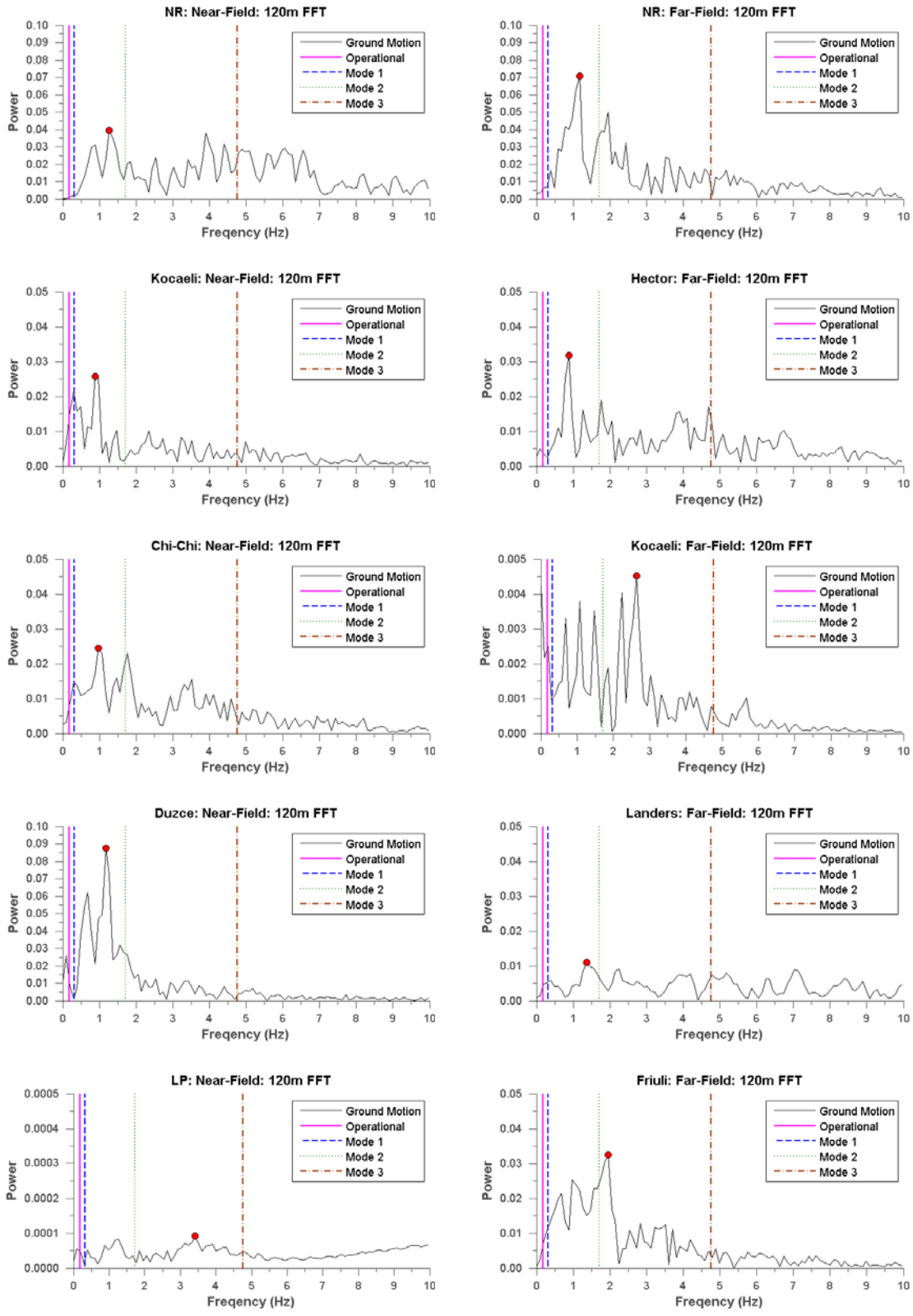

Figure 4-15: FFT Analyses for 120m Turbine for all Earthquake Records

4.3 Local Behavior

4.3.1 Von Mises Stress

The Von Mises stresses are presented for each analysis to demonstrate the stresses experienced by each model. These stresses indicate if the material has yielded during an analysis. The maximum Mises stress is plotted for each turbine model for the two load situations. Figure 4-16, Figure 4-17 and Figure 4-18 represent the stress experienced by the 60-meter, 90-meter and 120-meter turbines, respectively, during operation and seismic loading. Figure 4-19, Figure 4-20 and Figure 4-21 demonstrate the stress experienced for the three turbine models during wind, operation and seismic loading.

For the 60-meter turbine under operation and seismic loads, the maximum Mises stress is 350MPa for the Duzce: Near and Northridge: Far records, while the minimum is 48MPa for the Loma Prieta: Near record. The average Mises stress is 187MPa.

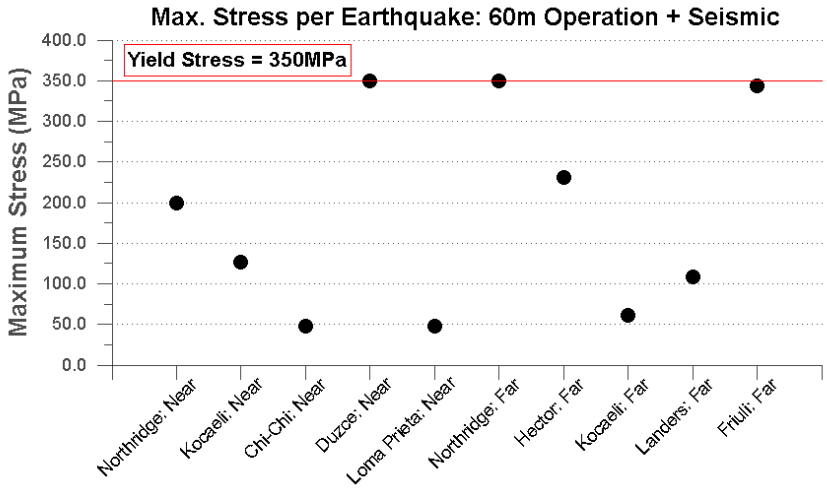

Figure 4-16: Maximum Stress: 60m Operation + Seismic Loading

For the 90-meter turbine under operation and seismic loads, the maximum Mises stress is 350MPa for the Northridge: Far and Friuli: Far records, while the minimum is 65MPa for the Loma Prieta: Near record. The average Mises stress is 197MPa.

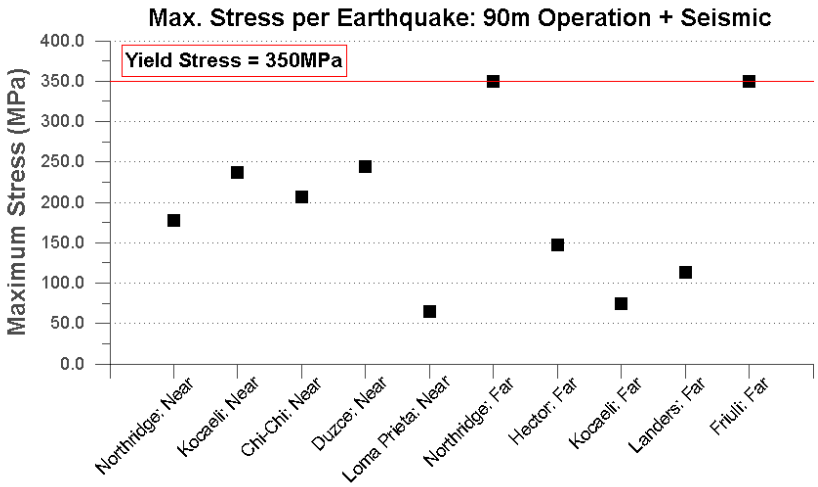

Figure 4-17: Maximum Stress: 90m Operation + Seismic Loading

For the 120-meter turbine under operation and seismic loads, the maximum Mises stress is 189MPa for the Friuli: Far record, while the minimum is 55MPa for the Loma Prieta: Near record. The average Mises stress is 124MPa.

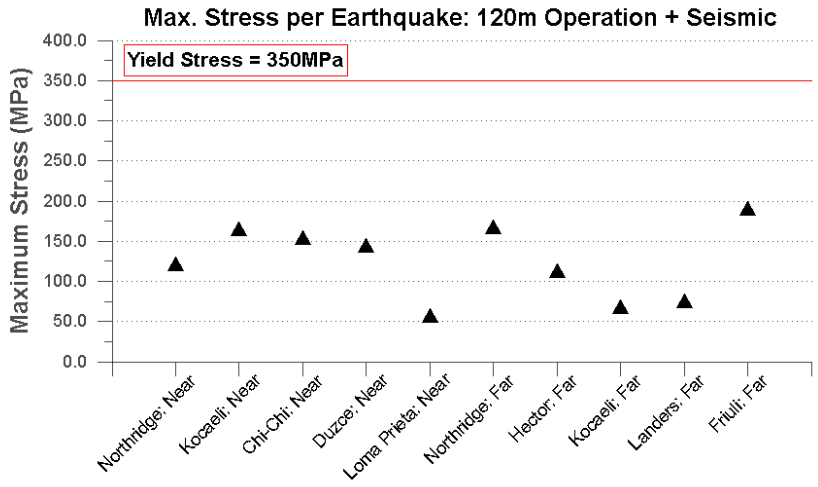

Figure 4-18: Maximum Stress: 120m Operation + Seismic Loading

For the 60-meter turbine under wind, operation and seismic loads, the maximum Mises stress is 350MPa for the Northridge: Far record, while the minimum is 83MPa for the Loma Prieta: Near record. The average Mises stress is 213MPa.

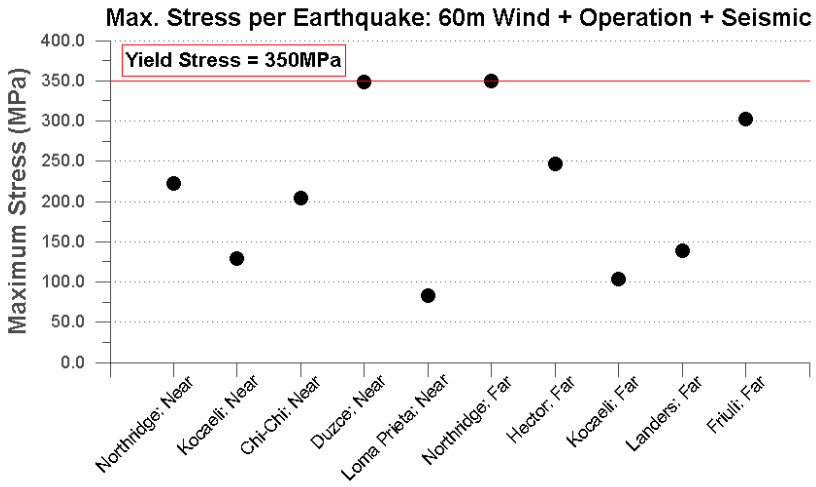

Figure 4-19: Maximum Stress: 60m Wind + Operation + Seismic Loading

For the 90-meter turbine under wind, operation and seismic loads, the maximum Mises stress is 350MPa for the Friuli: Far record, while the minimum is 87MPa for the Loma Prieta: Near record. The average Mises stress is 204MPa.

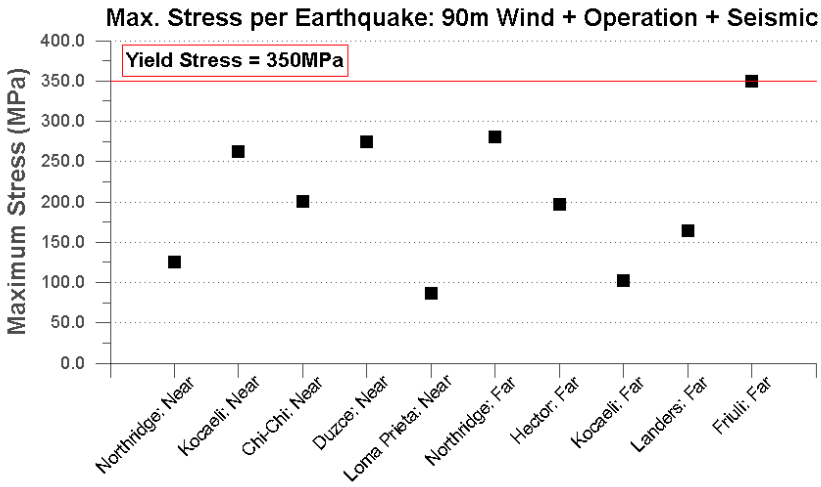

Figure 4-20: Maximum Stress: 90m Wind + Operation + Seismic Loading

For the 120-meter turbine under wind, operation and seismic loads, the maximum Mises stress is 187MPa for the Friuli: Far record, while the minimum is 53MPa for the Loma Prieta: Near record. The average Mises stress is 121MPa.

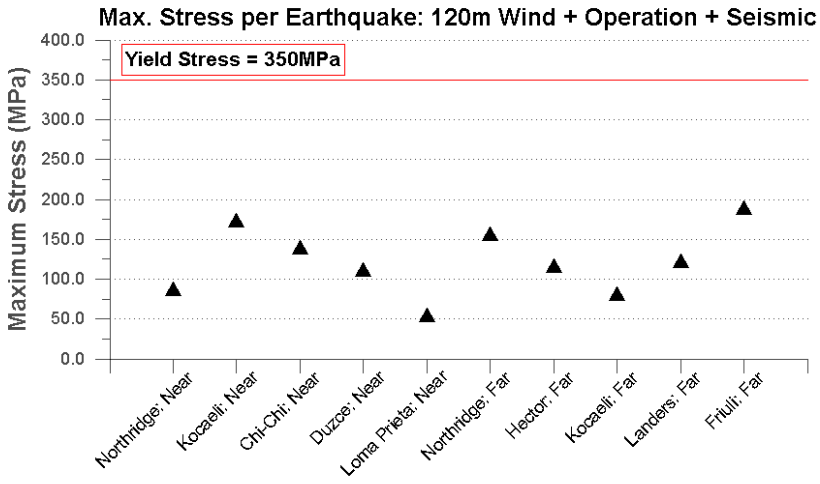

Figure 4-21: Maximum Stress: 120m Wind + Operation + Seismic Loading

4.3.2 Low-Cycle Fatigue

The low-cycle fatigue analysis shows the expected lifetime in terms of number of cycles to failure of each turbine under its respective earthquake against the total number of cycles for that earthquake. This demonstrates how many of the same earthquake each turbine could experience before damage would occur due to low-cycle fatigue. In this case, damage is defined as the initiation of a crack in the turbine at its welded connection with the base flange. In order to calculate the number of cycles to failure, the equivalent strain is first calculated by evaluating the six strain components ("Equivalent Von Mises Strain," 1999). This is represented by the following equation.

$$\varepsilon_{eq} = \frac{2}{3}\sqrt{\frac{3\left(\varepsilon_{xx}^2+\varepsilon_{yy}^2+\varepsilon_{zz}^2\right)}{2}+\frac{3\left(\gamma_{xy}^2+\gamma_{yz}^2+\gamma_{xz}^2\right)}{4}} \qquad \text{Equation 4-1}$$

The next step uses a rainflow counting method developed by the American Society for Testing and Materials (ASTM) before the effective strain could be calculated for the analysis in question (ASTM, 2005). This method divides the strain ranges into several bins for ease in analyzing the strain amplitude of the entire data set. Finally, the Coffin-Manson relationship, which is especially applicable for low-cycle fatigue analyses, is used for determining the number of cycles to failure (ASTM, 2008). This equation is given below.

$$\frac{\Delta\varepsilon_p}{2} = \varepsilon_f'(2N_f)^c \qquad \text{Equation 4-2}$$

Where, $\Delta\varepsilon_p$ is the plastic strain amplitude, ε'_f is the fatigue ductility coefficient, N_f is the number of cycles to failure and c is the fatigue ductility exponent. For the yield stress of 350MPa, ε'_f is 2.01 and c is -0.789 (ArcelorMittal, 2009). Using this equation, the number of cycles to failure for each analysis is found.

The results of the analysis are shown for the operation and seismic load case and the wind, operation and seismic load case. Figure 4-22, Figure 4-23 and Figure 4-24 show the low-cycle fatigue results under operation and seismic load for the 60-meter, 90-meter and 120-meter turbines, respectively. It is noted that for each of these figures, the number of cycles to failure for the Loma Prieta: Near analyses were much higher than the other records. Therefore, subplots are placed in each figure to represent the results for this data. Figure 4-25, Figure 4-26 and Figure 4-27 show the results under wind, operation and seismic load for the three models.

For the 60-meter turbine under operation and seismic loads, the maximum number of cycles to failure is 9,498,046 for the Loma Prieta: Near record, while the minimum is 11,641 for the Northridge: Far record. The average number of cycles to failure is

1,057,768. It is important to note that number of cycles to failure resulting from the Loma Prieta earthquake is significantly larger than those resulting from other earthquakes. The average number of cycles to failure excluding the Loma Prieta earthquake is 119,959.

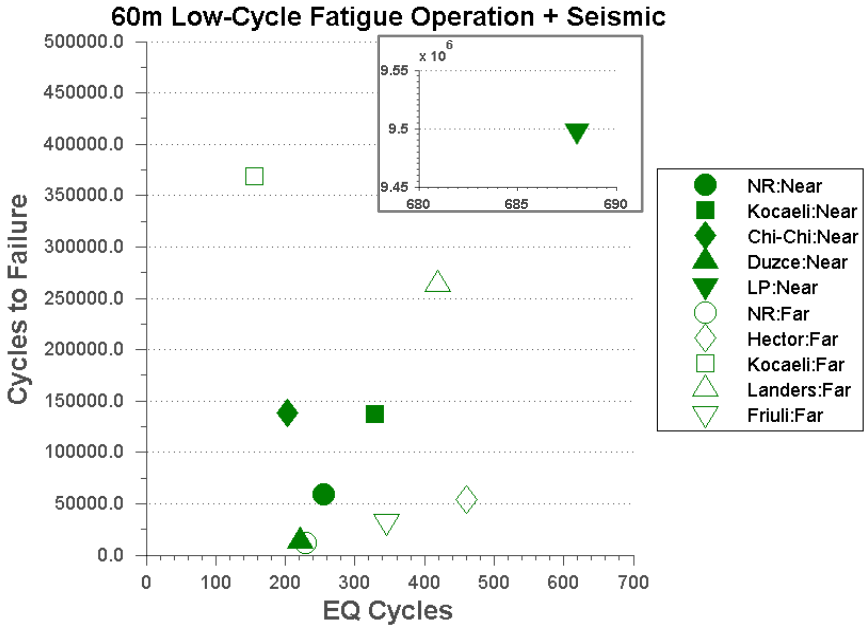

Figure 4-22: Low-Cycle Fatigue: 60m Turbine: Operation + Seismic

For the 90-meter turbine under operation and seismic loads, the maximum number of cycles to failure is 4,811,841 for the Loma Prieta: Near record, while the minimum is 19,503 for the Friuli: Far record. The average number of cycles to failure is 598,797. Similar to 60-meter tower, the number of cycles to failure resulting from the Loma Prieta earthquake is significantly larger than those resulting from other earthquakes. The average number of cycles to failure excluding the Loma Prieta earthquake is 130,681.

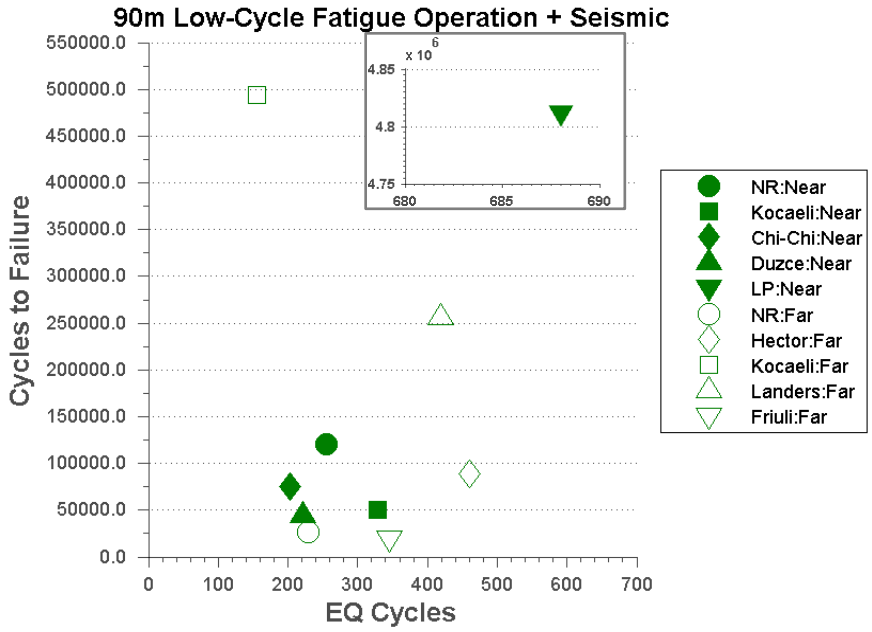

Figure 4-23: Low-Cycle Fatigue: 90m Turbine: Operation + Seismic

For the 120-meter turbine under operation and seismic loads, the maximum number of cycles to failure is 2,115,562 for the Loma Prieta: Near record, while the minimum is 69,018 for the Northridge: Far record. The average number of cycles to failure is 365,311. Similar to previous observations, the number of cycles to failure resulting from the Loma Prieta earthquake is an order of magnitude larger than those resulting from other earthquakes. The average number of cycles to failure excluding the Loma Prieta earthquake is 170,839.

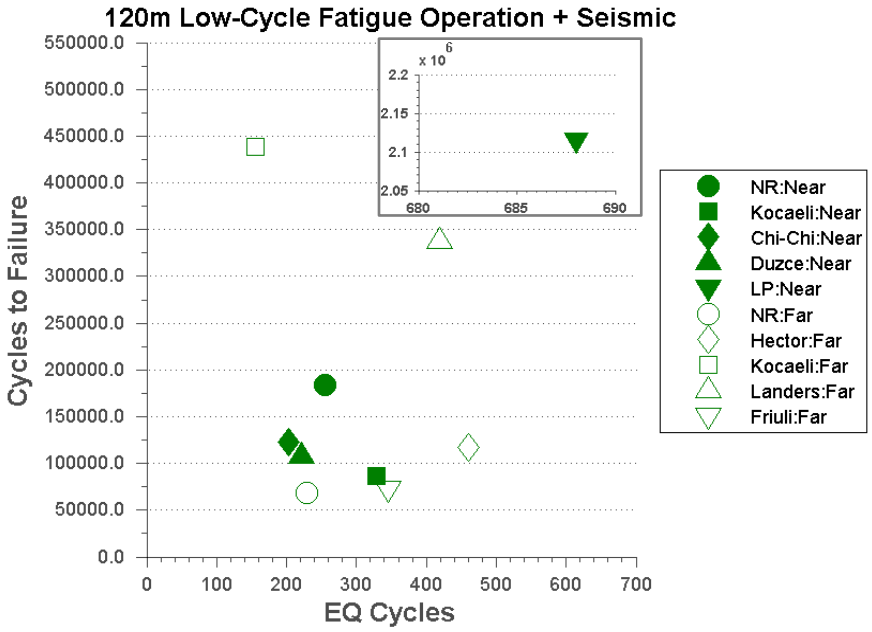

Figure 4-24: Low-Cycle Fatigue: 120m Turbine: Operation + Seismic

For the 60-meter turbine under wind, operation and seismic loads, the maximum number of cycles to failure is 285,303 for the Kocaeli: Far record, while the minimum is 7,378 for the Northridge: Far record. The average number of cycles to failure is 102,514.

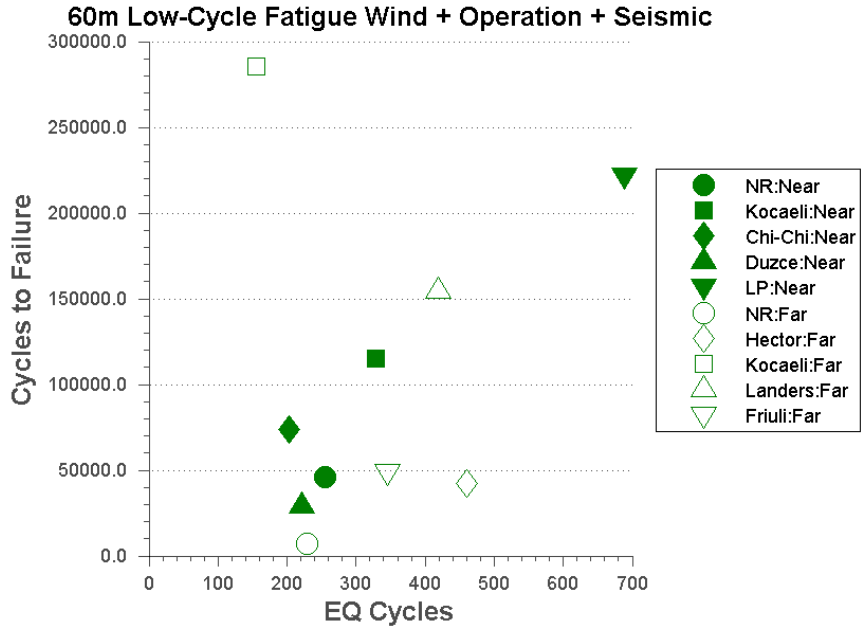

Figure 4-25: Low-Cycle Fatigue: 60m Turbine: Wind + Operation + Seismic

For the 90-meter turbine under wind, operation and seismic loads, the maximum cycles to failure is 185,062 for the Kocaeli: Far record, while the minimum is 14,988 for the Friuli: Far record. The average number of cycles to failure is 89,644.

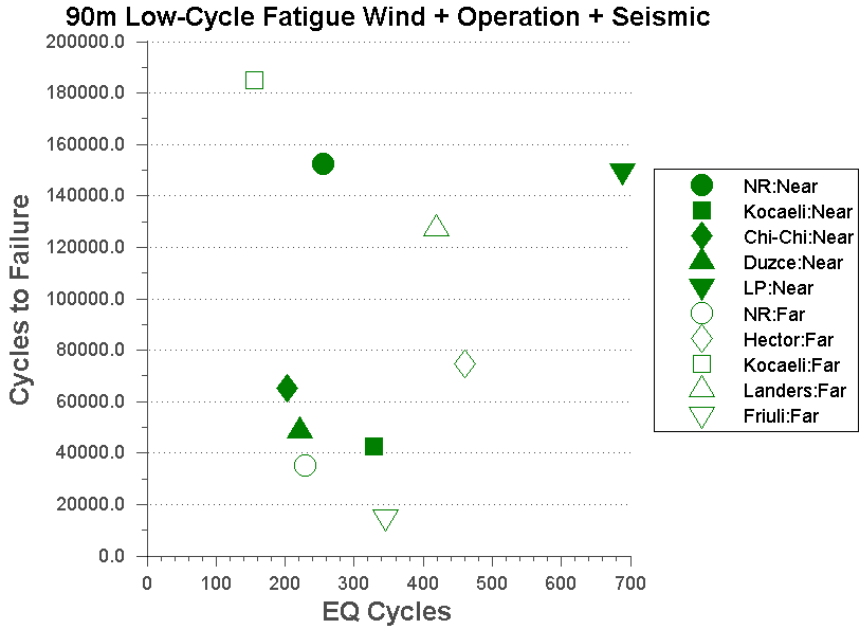

Figure 4-26: Low-Cycle Fatigue: 90m Turbine: Wind + Operation + Seismic

For the 120-meter turbine under wind, operation and seismic loads, the maximum number of cycles to failure is 291,099 for the Loma Prieta: Near record, while the minimum is 90,608 for the Friuli: Far record. The average number of cycles to failure is 169,733.

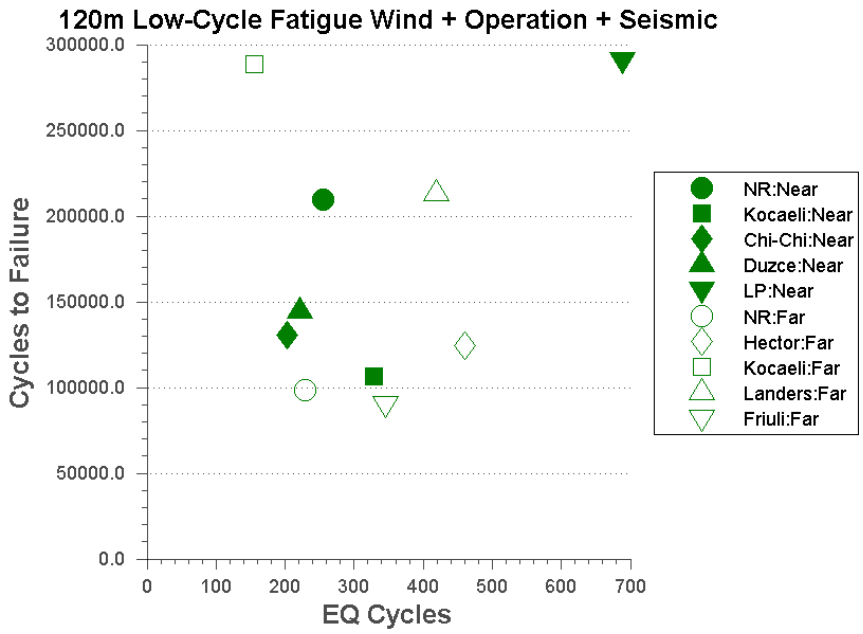

Figure 4-27: Low-Cycle Fatigue: 120m Turbine: Wind + Operation + Seismic

5 DISCUSSION OF RESULTS

5.1 Introduction

The results presented in the previous chapter provide valuable information for the response of each turbine model under different loading conditions. This chapter will both compare and discuss the various results throughout the three turbine models and the two types of loading used throughout the simulations. Maximum values will be compared both in tables and figures for ease in understanding the significance of the types of loads these turbines experienced. The ratio of maximum values for each turbine model will also be provided. This ratio indicates the change from the operation and seismic load case to the wind, operation and seismic load case. The maximum values from each of these tables are also highlighted. The potential implications of the FFT analyses will also be discussed.

5.2 Comparison of Drift Ratio

In order to provide a comparison between the three turbine models and the two load cases, several figures are provided. Figure 5-1 shows the difference in maximum drift ratio for each turbine model for the operation and seismic load case, while Figure 5-2 shows the difference in drift ratio for the wind, operation and seismic load case. The results indicate that the drift ratio varied significantly under certain earthquakes and very slightly for others. It is also observed that the difference in drift ratios between the two load cases is significant under certain earthquake records for different turbine heights. Table 5-1 provides the maximum drift ratio percentages for each of these analyses and Table 5-2 shows the ratio between the operation and seismic load case and the wind, operation and seismic load case for each turbine model and the corresponding earthquake record.

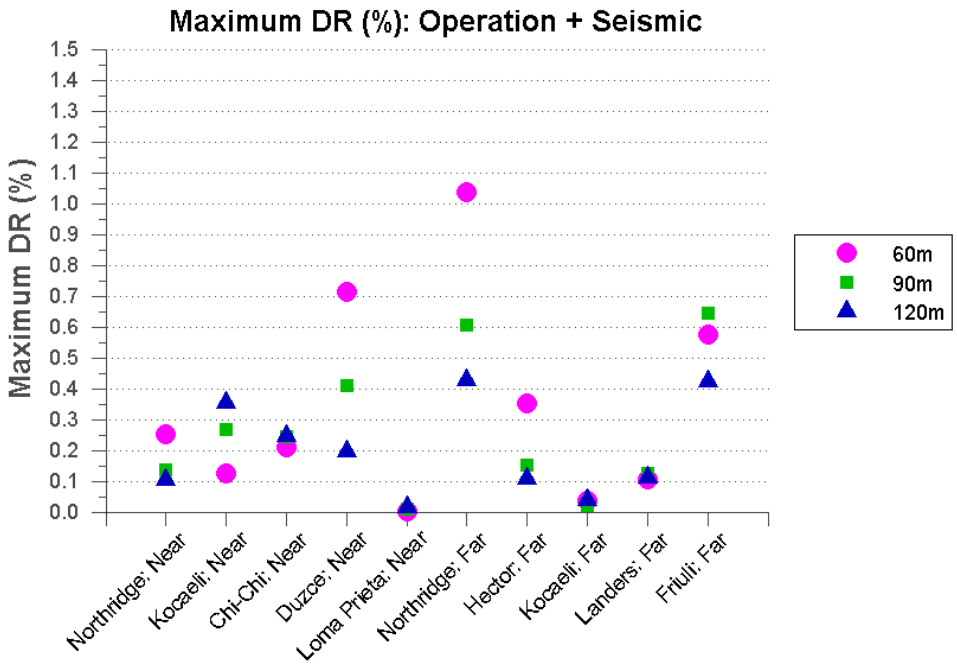

Figure 5-1: Maximum Drift Ratio (%) for Operation and Seismic Loading

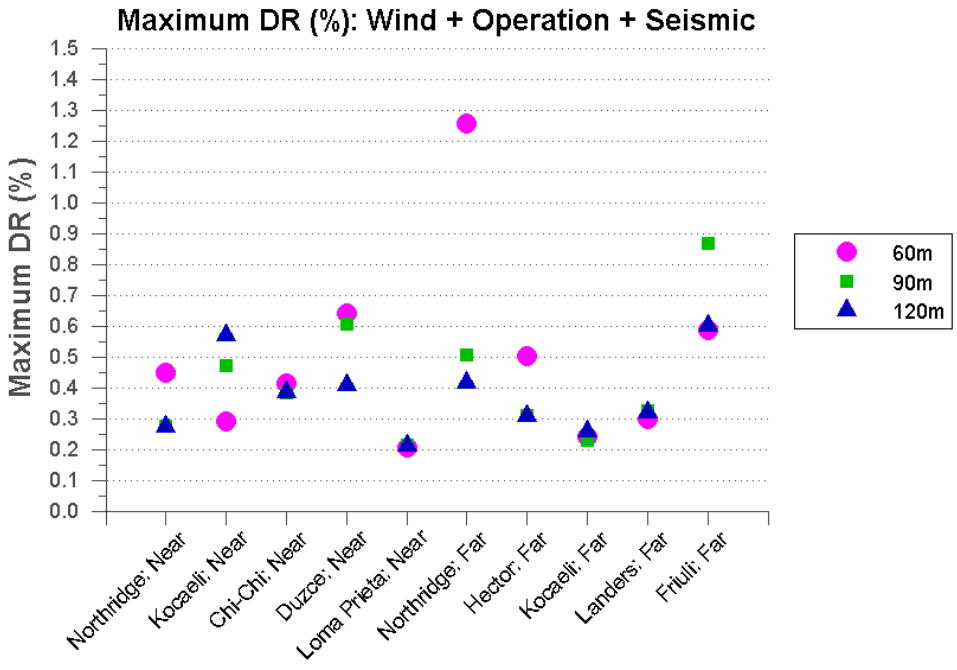

Figure 5-2: Maximum Drift Ratio (%) for Wind, Operation and Seismic Loading

Table 5-1: Maximum Drift Ratio Percentage for All Analyses

Maximum DR (%)						
Earthquake Record	**Operation + Seismic**			**Wind + Operation + Seismic**		
	60m	**90m**	**120m**	**60m**	**90m**	**120m**
Northridge: Near	0.25	0.14	0.11	0.45	0.27	0.27
Kocaeli: Near	0.13	0.27	0.35	0.29	0.47	0.57
Chi-Chi: Near	0.21	0.24	0.25	0.41	0.38	0.39
Duzce: Near	0.72	0.41	0.20	0.64	0.60	0.41
Loma Prieta: Near	0.00	0.01	0.02	0.21	0.21	0.21
Northridge: Far	1.04	0.61	0.43	1.25	0.50	0.42
Hector: Far	0.35	0.15	0.11	0.50	0.31	0.31
Kocaeli: Far	0.04	0.02	0.04	0.24	0.23	0.26
Landers: Far	0.10	0.12	0.11	0.30	0.32	0.32
Friuli: Far	0.58	0.65	0.42	0.59	0.87	0.60

Table 5-2: Ratio of Drift Ratio between Load Cases

Ratio of DR (%) Between Load Cases			
Earthquake Record	**60m**	**90m**	**120m**
Northridge: Near	0.56	0.50	0.39
Kocaeli: Near	0.44	0.57	0.62
Chi-Chi: Near	0.51	0.64	0.64
Duzce: Near	1.12	0.68	0.48
Loma Prieta: Near	0.02	0.05	0.08
Northridge: Far	0.83	1.20	1.03
Hector: Far	0.70	0.49	0.35
Kocaeli: Far	0.15	0.10	0.16
Landers: Far	0.35	0.39	0.35
Friuli: Far	0.98	0.74	0.71

Some of the results from these analyses are as expected. For example, the drift ratio percentage increases between the two load cases for most of the individual turbine models. For several cases, the drift ratio is higher for the operation and seismic load case. The 60-meter Duzce: Near, 90-meter Northridge: Far and 120-meter Northridge: Far analyses all experience a decrease from this load case to the wind, operation and seismic load case. It is also interesting to

note that there are several instances where the drift ratio is higher for the 60-meter turbine than it is for the 90-meter or 120-meter turbines. For the Northridge: Near, Duzce: Near, Northridge: Far and Hector: Far earthquake records, the 60-meter turbine has the largest drift ratio for both load cases at 0.25%, 0.72%, 1.04% and 0.35%, respectively, for the operation and seismic case and 0.45%, 0.64%, 1.25% and 0.50%, respectively, for the wind, operation and seismic load case. The Chi-Chi: Near analysis provides the largest drift ratio for the wind, operation and seismic load case at 0.41%.

There is also a clear difference between how close or far values are between the three turbine heights. Specifically, it is noted that for the Chi-Chi: Near, Loma Prieta: Near, Kocaeli: Far and Landers: Far earthquake records, there is almost no change in drift ratio between the three turbine heights for this load case. Much greater differences are seen for the Duzce: Near and Northridge: Far earthquake records.

In general, it appears that the drift ratio values are larger for the 60-meter and 90-meter turbines and that the 120-meter turbine experiences less drift ratio throughout the analyses. The maximum observed value for the operation and seismic load case is 1.04% for the Northridge: Far 60-meter analysis. The maximum observed value for the wind, operation and seismic load case is 1.25%, which also occurred for the Northridge: Far 60-meter analysis.

5.3 Comparison of V/W

The normalized base shear values varied greatly between the two load cases and the corresponding turbine models. For certain earthquake records, the values for V/W change significantly between the two load cases. Figure 5-3 shows the maximum V/W for the operation and seismic load case for the three models and Figure 5-4 shows the maximum V/W for the wind, operation and seismic load case for the three models.

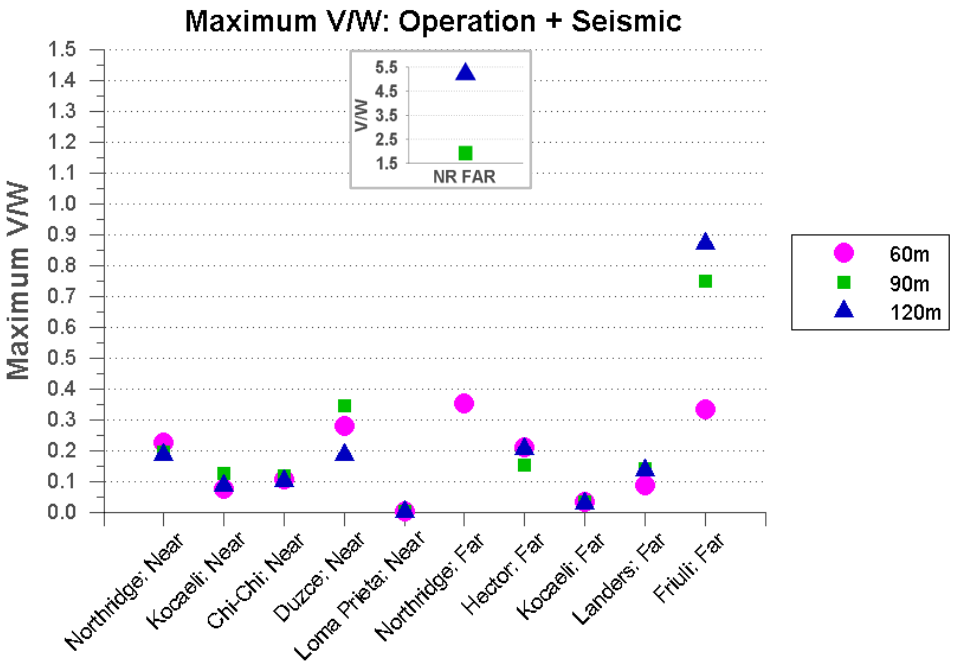

Figure 5-3: Maximum V/W for Operation and Seismic Loading

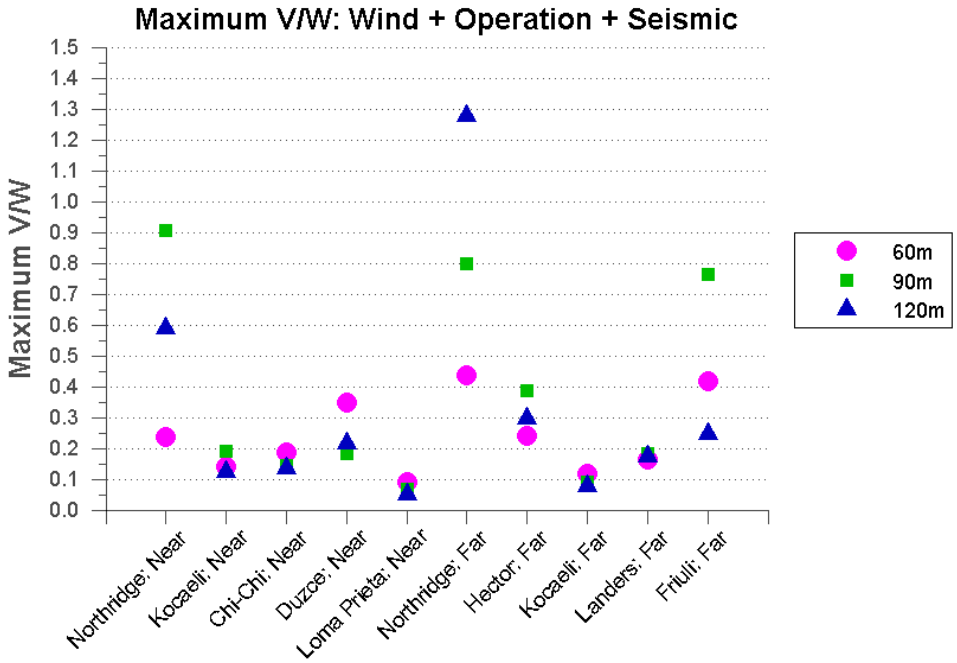

Figure 5-4: Maximum V/W for Wind, Operation and Seismic Loading

It is noted that the maximum V/W values for the 90-meter and 120-meter models under the Northridge: Far earthquake record for the operation and seismic load case are shown as an subplot within this figure. These values are much higher than the values for all other records for this load case. All values for each analysis can be seen in Table 5-3 below and the ratio between the two load cases can be seen in Table 5-4.

Table 5-3: Maximum V/W for All Analyses

Maximum V/W						
Earthquake Record	**Operation + Seismic**			**Wind + Operation + Seismic**		
	60m	**90m**	**120m**	**60m**	**90m**	**120m**
Northridge: Near	0.23	0.20	0.19	0.24	0.90	0.59
Kocaeli: Near	0.07	0.13	0.09	0.14	0.19	0.12
Chi-Chi: Near	0.10	0.12	0.10	0.19	0.14	0.14
Duzce: Near	0.28	0.34	0.19	0.35	0.18	0.22
Loma Prieta: Near	0.00	0.00	0.00	0.09	0.07	0.05
Northridge: Far	0.35	1.90	5.21	0.44	0.80	1.28
Hector: Far	0.21	0.15	0.21	0.24	0.39	0.30
Kocaeli: Far	0.03	0.03	0.03	0.12	0.09	0.08
Landers: Far	0.08	0.14	0.14	0.16	0.18	0.18
Friuli: Far	0.33	0.75	0.87	0.42	0.76	0.25

Table 5-4: Ratio of V/W between Load Cases

Ratio of V/W Between Load Cases			
Earthquake Record	**60m**	**90m**	**120m**
Northridge: Near	0.96	0.22	0.31
Kocaeli: Near	0.54	0.66	0.69
Chi-Chi: Near	0.55	0.84	0.74
Duzce: Near	0.80	1.87	0.86
Loma Prieta: Near	0.00	0.02	0.03
Northridge: Far	0.81	2.39	4.07
Hector: Far	0.87	0.39	0.70
Kocaeli: Far	0.27	0.36	0.38
Landers: Far	0.51	0.77	0.78
Friuli: Far	0.80	0.98	3.53

These results indicate that the 120-meter turbine is generally less affected by the loading than the 60-meter and/or 90-meter turbine. For the operation and seismic load case, only the Northridge: Far and Friuli: Far analyses has a higher V/W for the 120-meter turbine than for the 60- or 90-meter turbines. These values are 5.21 and 0.87, respectively. The wind, operation and seismic load case has a higher V/W for the 120-meter turbine under the Northridge: Far earthquake record at 1.28.

Between the two load cases, there are significant V/W differences for several turbine models. More specifically, the 90-meter and 120-meter turbines experience a large increase for the Northridge: Near earthquake record from the operation and seismic load case to the wind, operation and seismic load case. For this analysis, the 60-meter V/W remains unchanged between the two load cases. The 90-meter analysis increased from 0.20 to 0.90 and the 120-meter analysis increased from 0.19 to 0.59. The values for V/W change for all three models between the two load cases under the Northridge: Far earthquake as well. In this case, V/W increases for the 60-meter turbine from the operation and seismic load case to the wind, operation and seismic load case while V/W for the 90-meter and the 120-meter turbines decreases. The 60-meter V/W changed from 0.35 to 0.44. The 90-meter and 120-meter analyses decrease from 1.90 to 0.80 and 5.21 to 1.28, respectively.

Another notable result is the changes seen for the Friuli: Far earthquake record. These results are different from any other analysis. In this case, V/W slightly increases for the 60-meter turbine (0.33 to 0.42), stays relatively unchanged for the 90-meter turbine (0.75 to 0.76) and decreases significantly for the 120-meter turbine (0.87 to 0.25) from the operation and seismic load case to the wind, operation and seismic load case.

The results from each of these analyses indicate that various earthquake records had a larger impact on the overall V/W for each turbine model. When evaluating the differences in load cases, it can also be seen that the operation and seismic load case had a larger impact on various turbine models. Similarly to the drift ratio results, however, the wind, operation and seismic load combination produces higher V/W for most models.

5.4 Comparison of FFT Analyses

Because the FFT analyses evaluated the frequencies of the first three modes, the blade rotational frequency and the frequency of the ground motion, no comparison is necessary between the two load cases. This analysis allows for a better understanding of the overall response of various models during certain earthquakes within the two load cases. Table 5-5 shows the values for the predominant ground motion frequency for each earthquake record, the frequencies for the first three modes of vibration for each turbine model and the blade rotational frequency. All frequencies are in units of Hertz (Hz).

Table 5-5: Turbine, Operational and Ground Motion Frequencies for FFT Analyses

Earthquake Record	Earthquake Frequency	Mode 1	Mode 2	Mode 3	Turbine Model	Operational Frequency
Northridge: Near	1.27	0.64	3.33	9.09	60m	0.18
Kocaeli: Near	0.88					
Chi-Chi: Near	0.98					
Duzce: Near	1.17	0.43	2.27	6.25	90m	
Loma Prieta: Near	3.42					
Northridge: Far	1.17					
Hector: Far	0.88	0.33	1.72	4.76	120m	
Kocaeli: Far	2.64					
Landers: Far	1.37					
Friuli: Far	1.95					

From this table, several analyses that have similar frequencies are identified. In the case of the 60-meter model, the predominant frequency of the ground motion is similar to the mode 1 frequency for the Kocaeli: Near and Hector: Far analyses. These analyses show a mode 1 frequency of 0.64Hz with predominant ground motion frequencies of 0.88Hz for both earthquake records. Most of the earthquake frequencies fall between the frequencies for the first and second modes. It can also be noted that several earthquake records had ground motion frequencies that occurred often, but were not necessarily the predominant frequency. Several of these can be seen in Figure 5-5 below. These include the 60-meter Duzce: Near and Friuli: Far, the 90-meter Kocaeli: Near and Kocaeli: Far and the 120-meter Kocaeli: Near analyses.

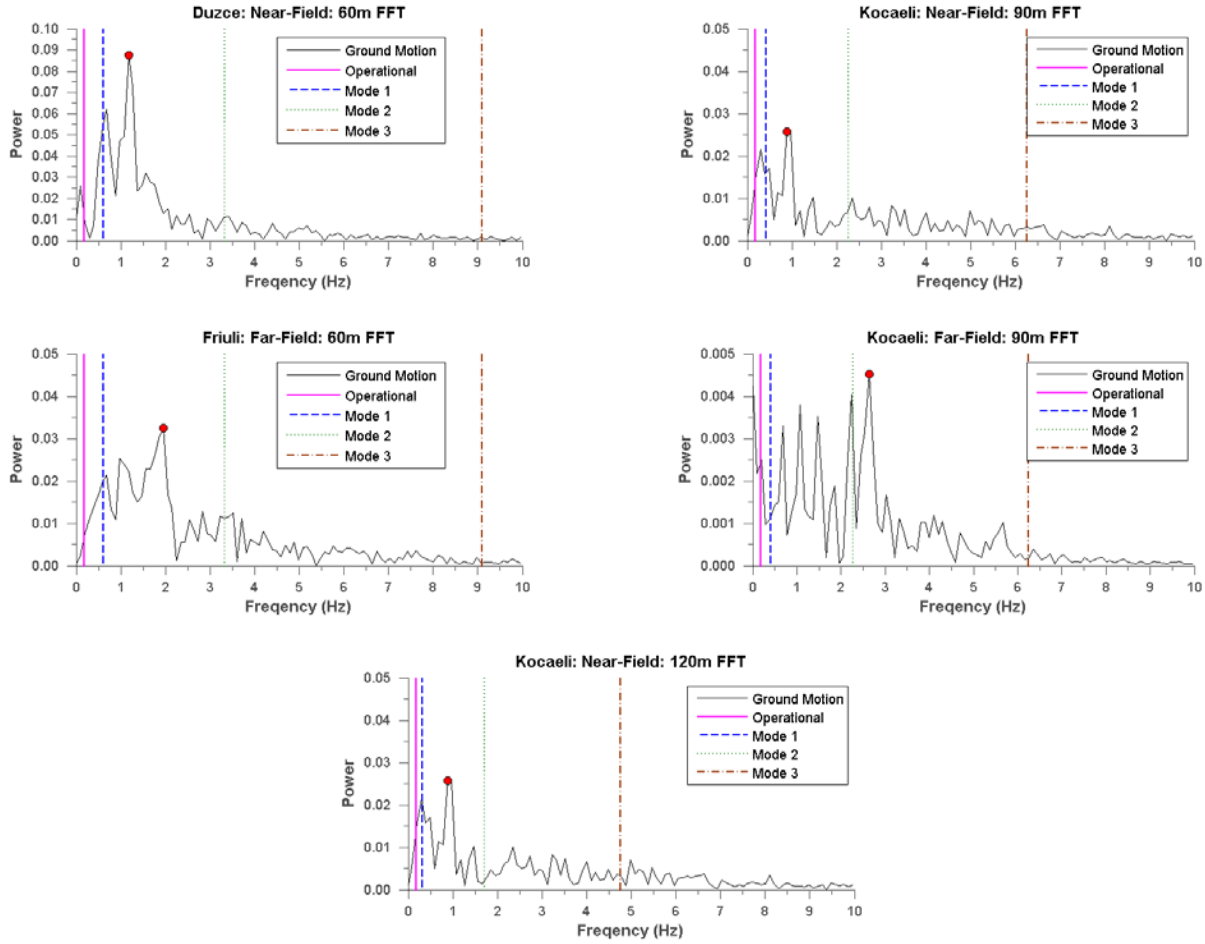

Figure 5-5: Critical FFT Analyses

For the 60-meter model, the second most predominant ground motion frequency is similar to the mode 1 frequency of 0.64Hz for the Duzce: Near analysis while the third most predominant ground motion frequency is similar to the mode 1 frequency for the Friuli: Far analysis. The 90-meter analyses indicate that the mode 1 and operational frequencies of 0.43Hz and 0.18Hz, respectively, closely match the second most predominant ground motion frequency for the Kocaeli: Near analysis while the mode 2 frequency of 2.27Hz is similar to the second most predominant ground motion frequency for the Kocaeli: Far analysis. Finally, the mode 1 and operational frequencies of 0.33Hz and 0.18Hz, respectively, are similar to the second most predominant ground motion frequency in the case of the 120-meter Kocaeli: Near analysis.

It is clear that in several simulations, having a similarity between the ground motion frequency, modal frequency and operational frequency had an effect on the stability of the model and overall convergence during an analysis. For example, the 60-meter Duzce: Near analysis did not fully converge and therefore only completed approximately 13.5 out of 15 total seconds for the wind, operation and seismic load combination. This indicates that a near-resonance state may have occurred during the analysis. This information is helpful in understanding the interaction between these frequencies during a seismic event.

5.5 Comparison of Von Mises Stresses

As previously discussed, the maximum values for the Von Mises stress were found for critical elements within each turbine model. Some of the results indicate that some analyses reached yield stress during an analysis. Figure 5-6 shows the results for each turbine model for operation and seismic loading and Figure 5-7 shows the results for the wind, operation and seismic loading.

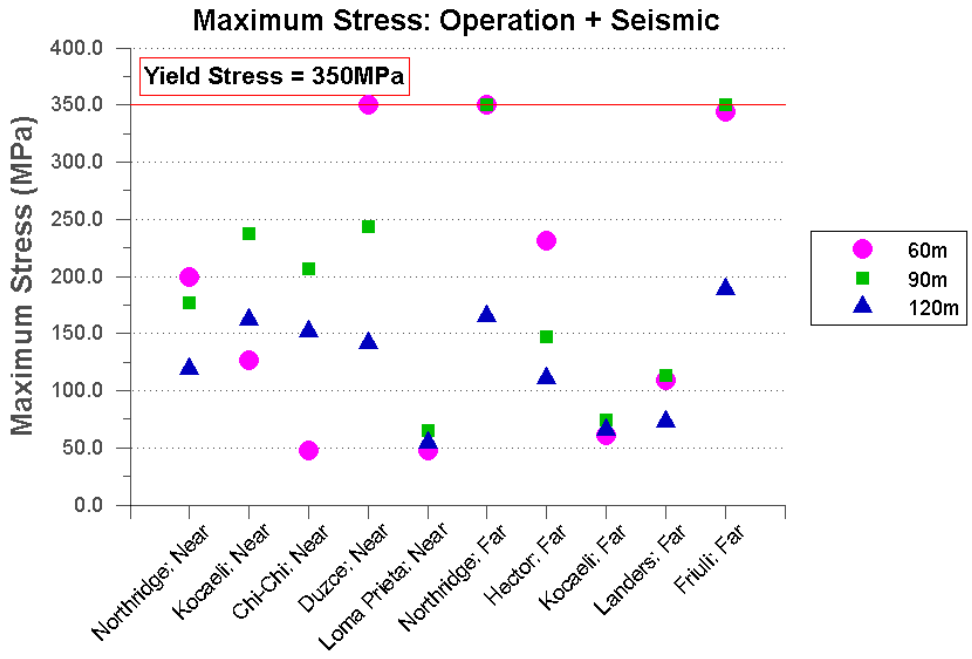

Figure 5-6: Maximum Stress for Operation and Seismic Loading

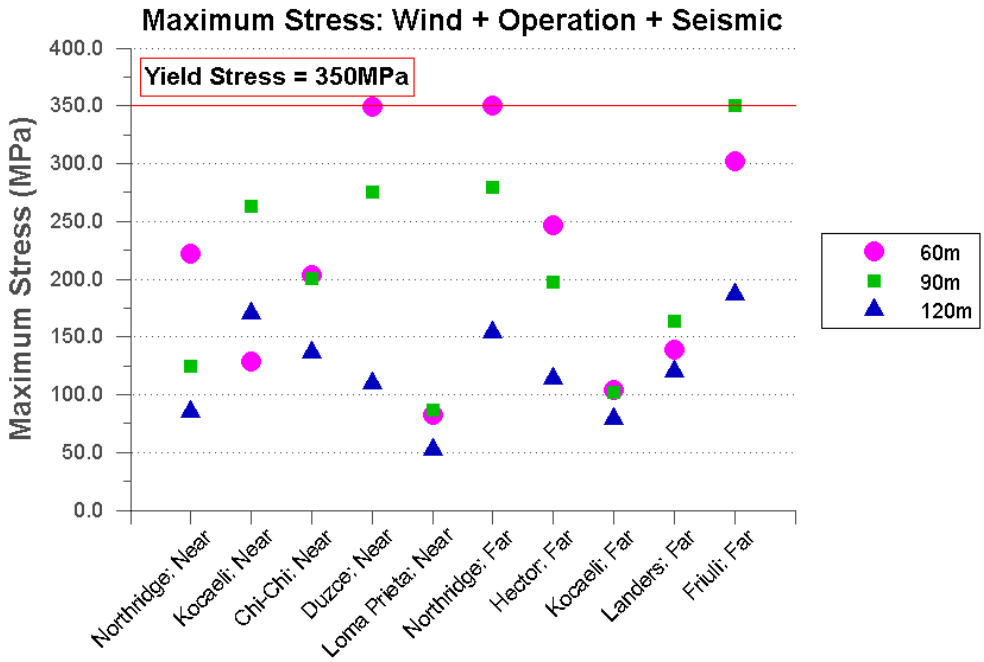

Figure 5-7: Maximum Stress for Wind, Operation and Seismic Loading

These figures indicate that four of the analyses for the operation and seismic load case reached yield stress, while two reached yield stress for the wind, operation and seismic load case.

In general, it appears that the maximum Von Mises stress seen in each of the turbine models is less for the wind, operation and seismic load case. Table 5-6 verifies some of these observations. Table 5-7 provides a ratio of maximum stress between the two load cases for each model.

Table 5-6: Maximum Stress (MPa) for All Analyses

Maximum Stress (MPa)						
Earthquake Record	**Operation + Seismic**			**Wind + Operation + Seismic**		
	60m	**90m**	**120m**	**60m**	**90m**	**120m**
Northridge: Near	199.0	177.0	120.0	222.0	125.0	86.0
Kocaeli: Near	127.0	237.0	163.0	129.0	263.0	171.0
Chi-Chi: Near	47.6	207.0	152.0	204.0	201.0	137.0
Duzce: Near	350.0	244.0	142.0	349.0	275.0	110.0
Loma Prieta: Near	47.7	65.4	55.0	82.8	86.8	53.0
Northridge: Far	350.0	350.0	166.0	350.0	280.0	154.0
Hector: Far	231.0	147.0	111.0	247.0	197.0	114.0
Kocaeli: Far	61.1	74.5	65.7	104.0	102.0	79.4
Landers: Far	109.0	113.0	73.7	139.0	164.0	121.0
Friuli: Far	344.0	350.0	189.0	302.0	350.0	187.0

Table 5-7: Ratio of Stresses between Load Cases

Ratio of Stress Between Load Cases			
Earthquake Record	**60m**	**90m**	**120m**
Northridge: Near	0.90	1.42	1.40
Kocaeli: Near	0.98	0.90	0.95
Chi-Chi: Near	0.23	1.03	1.11
Duzce: Near	1.00	0.89	1.29
Loma Prieta: Near	0.58	0.75	1.04
Northridge: Far	1.00	1.25	1.08
Hector: Far	0.94	0.75	0.97
Kocaeli: Far	0.59	0.73	0.83
Landers: Far	0.78	0.69	0.61
Friuli: Far	1.14	1.00	1.01

It is also important to note that for several analyses, the stress is very close to yield stress. These cases include the 60-meter Friuli: Far for the operation and seismic load case where the

maximum observed stress is 344MPa as well as the 60-meter Duzce: Near for the wind, operation and seismic load case where the maximum observed stress is 349MPa. Another important observation is that the 60-meter and 90-meter stresses dominate each load case. No analyses has a maximum stress for the 120-meter turbine whereas the 90-meter turbine has the highest stresses for the operation and seismic load case and the 60-meter turbine has the highest stresses for the wind, operation and seismic load case. The maximum observed stress for any of the 120-meter analyses occurs for the Friuli: Far record at 189MPa for the operation and seismic load case and 187MPa for the wind, operation and seismic load case.

Again, it seems that the 120-meter tower is less affected by both load cases and that higher stresses are seen in the 60-meter and 90-meter turbines. Between the two load cases, it is noted that higher stresses occur within the 90-meter turbine for the operation and seismic case and higher stresses occur within the 60-meter turbine for the wind, operation and seismic load case. Yield stress is reached in several 60-meter and 90-meter analyses, but the highest observed stress in any 120-meter analysis is well below the yield stress for these analyses.

5.6 Comparison of Low-Cycle Fatigue

For each analysis, the number of cycles to failure is determined and then compared against the number of cycles for the earthquake record used in that analysis. This is significant because it indicates how many times the wind turbine model can withstand the same earthquake before a crack develops at the base of the tower near the tower-to-base flange weld. The results for the 60-meter, 90-meter and 120-meter turbines are presented for the operation and seismic load case as well as the wind, operation and seismic load case. These results can be seen in Figure 5-8 and Figure 5-9 below.

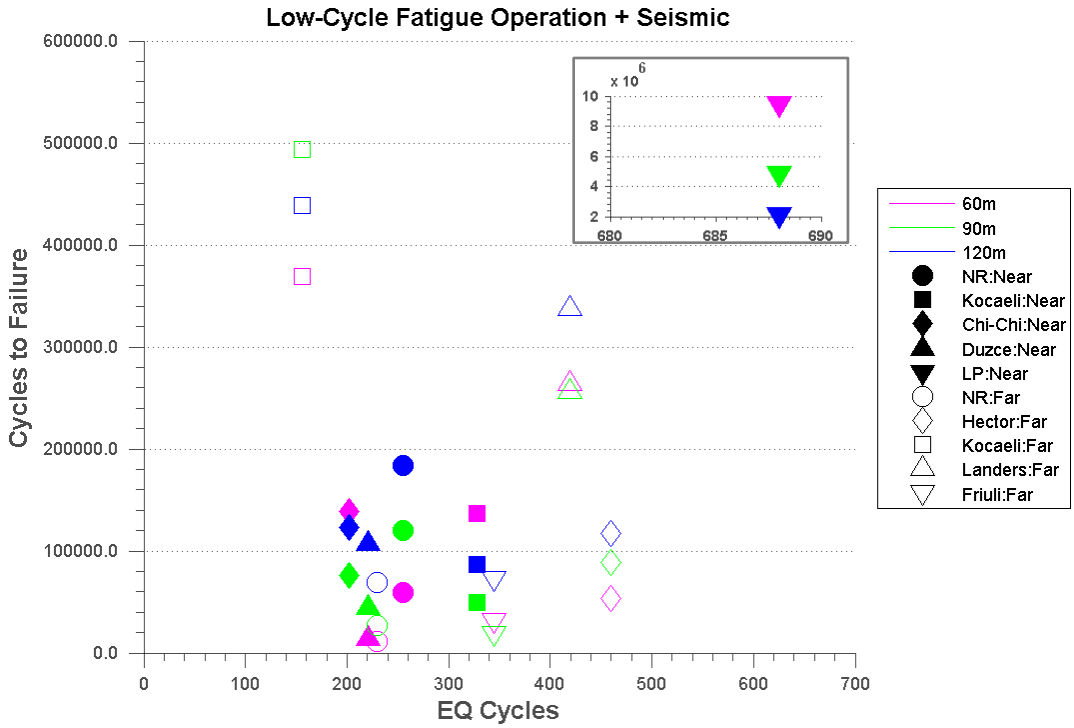

Figure 5-8: Low-Cycle Fatgue for Operation and Seismic Loading

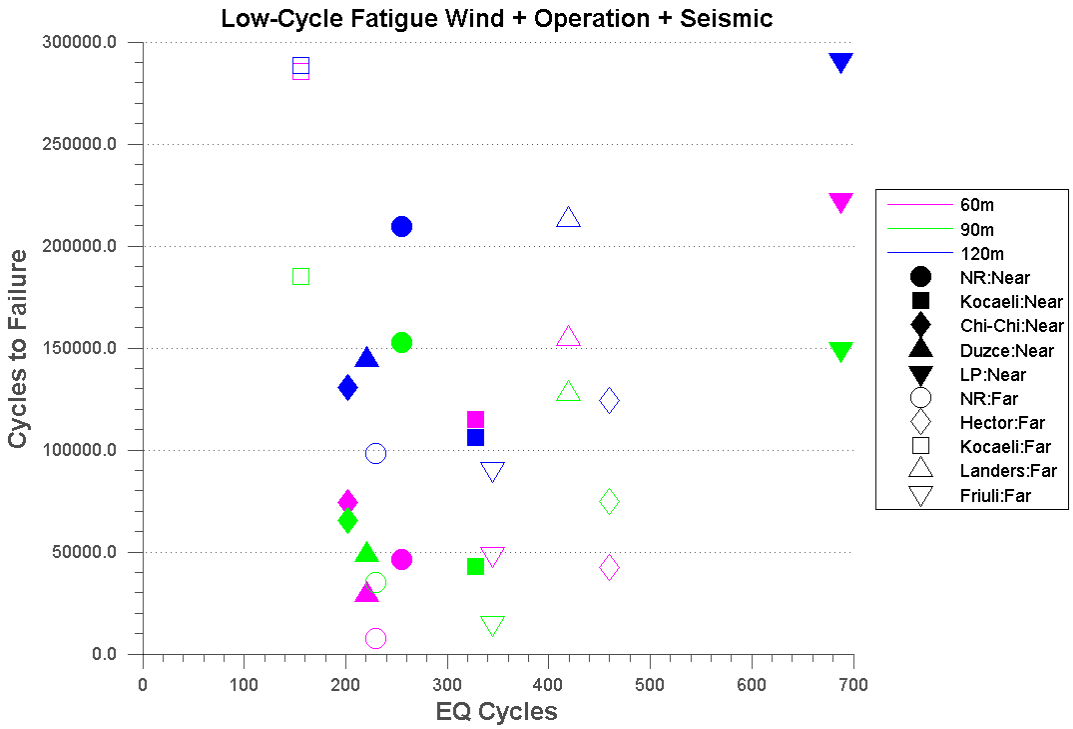

Figure 5-9: Low-Cycle Fatigue for Wind, Operation and Seismic Loading

When comparing these two figures, it is clear that none of the models develops a through-thickness crack under either load combination. The maximum number of earthquake cycles for any of the seismic records is 688, while the minimum number of cycles to failure for any of the analyses is 7,378, which indicates that these models are not as impacted by low-cycle fatigue as they are for drift ratio, base shear or stress. To clearly identify which models are more impacted by low-cycle fatigue, Table 5-8 provides the number of cycles to failure for all analyses and Table 5-9 shows a ratio between the number of cycles to failure versus the number of earthquake cycles for both load cases. This ratio demonstrates the number of times that specific earthquake could occur for that given model before any damage due to low-cycle fatigue would occur. The maximum values in both tables are highlighted in light grey, and the minimum values are highlighted in darker grey. For these results, it is important to demonstrate the minimum values along with the maximum values because they show which analyses would be more susceptible to low-cycle fatigue damage.

Table 5-8: Number of Cycles to Failure for All Analyses

Number of Cycles to Failure						
Earthquake Record	**Operation + Seismic**			**Wind + Operation + Seismic**		
	60m	**90m**	**120m**	**60m**	**90m**	**120m**
Northridge: Near	59,414	120,138	183,869	46,213	152,617	209,779
Kocaeli: Near	137,103	49,913	86,732	114,989	42,700	106,236
Chi-Chi: Near	138,552	75,734	123,273	74,044	65,316	130,841
Duzce: Near	14,161	44,158	107,619	29,270	48,769	144,562
Loma Prieta: Near	9,498,046	4,811,841	2,115,562	222,199	149,509	291,099
Northridge: Far	11,641	27,068	69,018	7,378	35,192	98,507
Hector: Far	53,677	88,845	117,639	42,255	74,816	124,085
Kocaeli: Far	368,862	494,107	438,851	285,303	185,062	288,459
Landers: Far	264,178	256,662	337,868	154,637	127,474	213,156
Friuli: Far	32,041	19,503	72,678	48,854	14,988	90,608

Table 5-9: Ratio of Number of Cycles to Failure versus EQ Cycles

Ratio Between Cycles to Failure and Earthquake Cycles							
Earthquake Record	**EQ Cycles**	**Operation + Seismic**			**Wind + Operation + Seismic**		
		60m	**90m**	**120m**	**60m**	**90m**	**120m**
Northridge: Near	202.5	293	593	908	228	754	1,036
Kocaeli: Near	221	620	226	392	520	193	481
Chi-Chi: Near	345	402	220	357	215	189	379
Duzce: Near	460	31	96	234	64	106	314
Loma Prieta: Near	155.5	61,081	30,944	13,605	1,429	961	1,872
Northridge: Far	328	35	83	210	22	107	300
Hector: Far	419	128	212	281	101	179	296
Kocaeli: Far	688	536	718	638	415	269	419
Landers: Far	229.5	1,151	1,118	1,472	674	555	929
Friuli: Far	255.5	125	76	284	191	59	355

For most of the models, the results are similar to those seen for the other global results and local behavior in that no clear trend exists between each model and the two load cases. Overall, the 90-meter turbine has the highest occurrence of analyses with the lowest number of cycles to failure, while the 60-meter turbine has the next highest and the 120-meter turbine has two occurrences of the lowest cycles to failure.

Between the two load cases, most of the models follow the same trend. For example, when evaluating the Northridge: Near analyses, it is observed that the number of cycles to failure increases with turbine size for both load cases. For the Loma Prieta: Near and Kocaeli: Far earthquake records, no trend exists between the two load cases. For the Loma Prieta record, the number of cycles to failure decreased as the turbine size increased for the operation and seismic load case. Under the wind, operation and seismic load case, the number of cycles to failure decreases from the 60-meter to the 90-meter and then increases from the 90-meter to the 120-meter. The Kocaeli: Far record has an increase from the 60- to 90-meter turbine and then a decrease from the 90- to the 120-meter turbine for the operation and seismic load case, while the

wind, operation and seismic load case has a decrease from 60- to 90-meter turbine and an increase from the 90- to 120-meter turbine.

For the operation and seismic load case, the lowest observed ratio occurs for the 60-meter Duzce: Near analysis. In this case, the same earthquake could occur 35 times before any through-thickness crack would begin to develop. The 60-meter Northridge: Far analysis has the lowest ratio for the wind, operation and seismic load case. This earthquake could occur 22 times with before any through-thickness cracks would begin to develop.

These results indicate that the wind turbine tower and base configurations may already be adequately designed for low-cycle fatigue since these models can withstand many earthquakes before developing any cracks and thus last their 20-year service life.

5.7 Comparison of Near-Field and Far-Field Earthquake Records

Within the 10 earthquake records used for the various simulations, there were two earthquakes that had both a near-field and far-field record set. These include the Northridge and Kocaeli seismic events. The results that include these two records for both the near-field and far-field simulations will be used for comparison. Both the global results and localized behavior are presented for the two near-field and two far-field records.

Beginning with the global results, the maximum values for drift ratio and base shear are provided as well as a ratio between the two load combinations for the Northridge and Kocaeli earthquake records. A comparison of the FFT analyses for these four records is also discussed. Table 5-10 and Table 5-11 show the maximum drift ratio percentages for these records and the ratio between the two load cases.

Table 5-10: Maximum Drift Ratio Percentages for Northridge and Kocaeli Records

Maximum DR (%) for Northridge and Kocaeli Records						
Earthquake Record	**Operation + Seismic**			**Wind + Operation + Seismic**		
	60m	**90m**	**120m**	**60m**	**90m**	**120m**
Northridge: Near	0.25	0.14	0.11	0.45	0.27	0.27
Kocaeli: Near	0.13	0.27	0.35	0.29	0.47	0.57
Northridge: Far	1.04	0.61	0.43	1.25	0.50	0.42
Kocaeli: Far	0.04	0.02	0.04	0.24	0.23	0.26

Table 5-11: Ratio of Drift Ratio Percentages for Northridge and Kocaeli Records

Ratio of DR (%) Between Load Cases			
Earthquake Record	**60m**	**90m**	**120m**
Northridge: Near	0.56	0.50	0.39
Kocaeli: Near	0.44	0.57	0.62
Northridge: Far	0.83	1.20	1.03
Kocaeli: Far	0.15	0.10	0.16

The drift ratio results between the near- and far-field records indicate that there were larger drift ratios for the Northridge: Far record than for the Northridge: Near record, but less for the Kocaeli: Far than for the Kocaeli: Near. However, a similar trend occurs for each model under the Northridge records through both load cases. The maximum drift ratio percentages decrease for both load combinations as the turbine size increases. This trend does not exist within the Kocaeli records. In the case of the near-field record, the maximum drift ratio percentages increase for both load cases as the turbine size increases, but has no real trend for the far-field record. In both load combinations, the 60-meter and 120-meter turbines have larger drift ratio percentages than the 90-meter turbine.

The maximum V/W for the four records as well as the ratio between load combinations is represented in Table 5-12 and Table 5-13 below.

Table 5-12: Maximum V/W for Northridge and Kocaeli Records

Maximum V/W for Northridge and Kocaeli Records						
Earthquake Record	**Operation + Seismic**			**Wind + Operation + Seismic**		
	60m	**90m**	**120m**	**60m**	**90m**	**120m**
Northridge: Near	0.23	0.20	0.19	0.24	0.90	0.59
Kocaeli: Near	0.07	0.13	0.09	0.14	0.19	0.12
Northridge: Far	0.35	1.90	5.21	0.44	0.80	1.28
Kocaeli: Far	0.03	0.03	0.03	0.12	0.09	0.08

Table 5-13: Ratio of V/W for Northridge and Kocaeli Records

Ratio of V/W Between Load Cases			
Earthquake Record	**60m**	**90m**	**120m**
Northridge: Near	0.96	0.22	0.31
Kocaeli: Near	0.54	0.66	0.69
Northridge: Far	0.81	2.39	4.07
Kocaeli: Far	0.27	0.36	0.38

From these results, it is clear that the trend that exists for the drift ratio between the near- and far-field Northridge records does not exist for V/W. In the near-field record, the operation and seismic case shows a decrease throughout turbine sizes, and shows smaller 60- and 120-meter values, with the largest V/W occurring for the 90-meter turbine for the wind, operation and seismic load case. For the far-field record, both load combinations show an increase in V/W throughout the turbine models.

The Kocaeli records also show no trend between the near-field and far-field records. The near-field record has a larger V/W for the 90-meter turbine with smaller values for both the 60-meter and 120-meter turbines for both load combinations. The far-field record has identical results for all three turbines under operation and seismic loads, and a decrease in values as the turbine height increases for the wind, operation and seismic loads. These results do not provide a

clear indication of how the V/W results may change between near-field and far-field earthquakes.

The results from the FFT analyses for each earthquake record are presented in Table 5-14.

Table 5-14: FFT Analyses for Northridge and Kocaeli Records

Earthquake Record	Earthquake Frequency	Mode 1	Mode 2	Mode 3	Turbine Model	Operational Frequency
Northridge: Near	1.27	0.61	3.33	9.09	60m	1.15
Kocaeli: Near	0.88	0.42	2.27	6.25	90m	
Northridge: Far	1.17	0.32	1.72	4.76	120m	
Kocaeli: Far	2.64					

These results indicate that the predominant frequency of the ground motion is similar for the Northridge records, but very different for the Kocaeli records. As in the case of the drift ratio and V/W results, there is no indication of a general trend for predominant ground motion frequencies between near-field and far-field records.

For the localized behavior, both the maximum Von Mises stresses and fatigue results are presented for the Northridge and Kocaeli earthquake records. Table 5-15 and Table 5-16 provide the maximum stresses and ratio of stress between the two load cases for these records.

Table 5-15: Maximum Stress (MPa) for Northridge and Kocaeli Records

Maximum Stress (MPa) for Northridge and Kocaeli Records						
Earthquake Record	Operation + Seismic			Wind + Operation + Seismic		
	60m	90m	120m	60m	90m	120m
Northridge: Near	199.0	177.0	120.0	222.0	125.0	86.0
Kocaeli: Near	127.0	237.0	163.0	129.0	263.0	171.0
Northridge: Far	350.0	350.0	166.0	350.0	280.0	154.0
Kocaeli: Far	61.1	74.5	65.7	104.0	102.0	79.4

Table 5-16: Ratio of Stress for Northridge and Kocaeli Records

Ratio of Stress Between Load Cases			
Earthquake Record	**60m**	**90m**	**120m**
Northridge: Near	0.90	1.42	1.40
Kocaeli: Near	0.98	0.90	0.95
Northridge: Far	1.00	1.25	1.08
Kocaeli: Far	0.59	0.73	0.83

The Northridge: Near field results indicate a decrease in maximum stress as the turbine size increases for both load cases. This trend continues for the wind, operation and seismic load case for the far-field record, but identical stresses are seen for both the 60-meter and 90-meter turbines under the operation and seismic load case.

The Kocaeli: Near field results show that the 90-meter turbine has the largest stresses for both load cases at 237MPa and 263MPa, respectively. This holds for the operation and seismic load case for the far-field record, but a decrease in maximum stress occurs as the turbine size increases for the wind, operation and seismic load case.

These results are similar to the drift ratio and V/W results in that they do not indicate a clear pattern in how near-field and far-field records would impact a turbine under various load combinations.

Finally, the low-cycle fatigue results are provided for both the Northridge and Kocaeli earthquake records. This information can be seen in Table 5-17 and Table 5-18 below.

The Northridge analysis results show that for both the near and far records, the number of cycles to failure increases as the turbine size increases for both load cases. For both records, the 60-meter turbine has a higher number of cycles to failure for the operation and seismic load case whereas the number of cycles to failure for the 90-meter and 120-meter turbines is lower for this load case.

Table 5-17: Number of Cycles to Failure for Northridge and Kocaeli Records

Number of Cycles to Failure for Northridge and Kocaeli Records						
Earthquake Record	**Operation + Seismic**			**Wind + Operation + Seismic**		
	60m	**90m**	**120m**	**60m**	**90m**	**120m**
Northridge: Near	59,414	120,138	183,869	46,213	152,617	209,779
Kocaeli: Near	137,103	49,913	86,732	114,989	42,700	106,236
Northridge: Far	11,641	27,068	69,018	7,378	35,192	98,507
Kocaeli: Far	368,862	494,107	438,851	285,303	185,062	288,459

Table 5-18: Ratios for Low-Cycle Fatigue Results Northridge and Kocaeli Records

Ratio Between Cycles to Failure and Earthquake Cycles							
Earthquake Record	**EQ Cycles**	**Operation + Seismic**			**Wind + Operation + Seismic**		
		60m	**90m**	**120m**	**60m**	**90m**	**120m**
Northridge: Near	202.5	293	593	908	228	754	1,036
Kocaeli: Near	221	620	226	392	520	193	481
Northridge: Far	328	35	83	210	22	107	300
Kocaeli: Far	688	536	718	638	415	269	419

The Kocaeli analyses indicate that the number of cycles to failure increases as the turbine size increases for the near-field record under both load cases. For the far-field record, the 90-meter turbine has the highest number of cycles to failure for the operation and seismic load case and the lowest number of cycles to failure for the wind, operation and seismic load case.

5.8 Conclusion

By comparing the global results and local behavior between the three models and two load cases, several conclusions can be drawn. For each result, it is apparent that the operation and seismic load combination has a larger impact on each turbine model than the wind, operation and seismic load combination. It is also evident that the 60-meter and 90-meter turbines are at a higher risk for global and local deformation. Throughout each analysis, the 120-meter turbine performed much better than the other two models.

Several seismic records created significantly higher drift ratios and base shear values for several models. The occurrence of resonance is also seen in several turbine models, which indicates the need to understand the response of these turbines under various types of loading. Yield stress is reached in multiple 60-meter and 90-meter turbines, whereas the 120-meter turbine never yields. This indicates that the design of the 60- and 90-meter turbines must be improved if they are expected to withstand an earthquake. The fatigue analyses demonstrate that none of the models developed any cracks near the base of the turbine due to the seismic loading on the system. These results demonstrate the importance in understanding the response of different turbine sizes to seismic loads in combination with other types of loads.

6 CONCLUSIONS AND FUTURE RESEARCH

6.1 Summary of Current Work

In this study, the evaluation of wind turbine structural performance is investigated for two load cases. This methodology includes finite element analyses to conduct simulations for operation and seismic loads as well as operation, seismic and wind loads. Global responses and local behavior are obtained, which identify critical load cases, wind turbine sizes and areas of necessary improvement within the turbine models.

The investigated models comprise of 60-meter, 90-meter and 120-meter turbines. The simulations consist of 10 analyses per model per load case for a total of 60 analyses. Two load cases are used for the two load combinations, which include operation and seismic loads and wind, operation and seismic loads. The operation load is representative of a constant average rotational speed for the wind turbine blades. Wind loading is applied as a constant force that represents the necessary wind velocity in order for the wind turbine to be operational. Seismic load is applied as an acceleration time-history to the base of the wind turbine. For these analyses, 10 seismic records are used including five near-field and five far-field records. Each analysis includes 10 seconds of the earthquake record to adequately compare the differences in results between the two load cases. The reason for applying the wind turbine as a constant load is because in the 10 second time, which is typical of the earthquakes used in this study, it is assumed that the wind velocity does not change in magnitude or direction.

The global results captured in each analysis include the drift ratio, normalized base shear and turbine operational stability analyses. Local behavior includes the Von Mises stresses and low-cycle fatigue. These results aid in understanding the overall response of each wind turbine system. Certain results, such as the FFT analyses, also aid in understanding why some analyses

were computationally demanding and were therefore unable to converge. Overall, the results aid in identifying high stress areas, resonance within the model and large deformations in various turbines.

6.2 Summary of Results

6.2.1 Finite Element Simulations

The simulations for the operation and seismic load case were completed for a period of 10 seconds, while the wind, operation and seismic load case analyses were completed for a period of 15 seconds (the wind load is ramped linearly for five seconds then kept constant as the earthquake load is applied). In general, the maximum drift ratio and normalized base shear cover a wide range of values. FFT analyses indicate resonance may have occurred throughout some analyses, which can cause instability in the blades. Several turbine models reach yield stress throughout various analyses, but no damage due to low-cycle fatigue is observed.

When evaluating the global behavior for each turbine model, three types of results are generated. The maximum drift ratio, maximum base shear and FFT analyses characterize the global response of each turbine.

For the operation and seismic load case, the drift ratio is below 0.45% for most analyses. For several analyses, these values are significantly higher. The Duzce: Near analyses has a maximum of 0.72% for the 60-meter turbine. The Northridge: Far analyses have maximum values of 1.04% and 0.61% for the 60-meter and 90-meter turbines, respectively. The Friuli: Far analyses have maximum values of 0.58% and 0.65% for the 60-meter and 90-meter turbines, respectively. Under operation, seismic and wind loads, most drift ratios are below 0.6%, with several exceptions. Maximum

values of 0.64% and 1.25% are observed for the 60-meter tower for the Duzce: Near and Northridge: Far analyses, respectively. The Friuli: Far analyses indicate a maximum value of 0.87% for the 90-meter turbine.

Overall, the maximum drift ratio values are higher for the wind, operation and seismic load case. This is as expected because of the addition of the wind load to the system. It is also noted that the drift ratio values are higher for the 60-meter and 90-meter turbines than for the 120-meter turbine in most cases. More specifically, in the case of the Duzce: Near, Northridge: Far and Friuli: Far analyses, the drift ratios are significantly higher when compared to the other analyses and also when comparing the 60- and 90-meter turbines to the 120-meter turbine. It could be concluded that as these 60- and 90-meter turbines neared or reached yield stress under these earthquake records, the overall stiffness of the turbine decreased thereby increasing the period of the structure. The increase in the period implies that the system is more sensitive to displacement.

Most of the maximum V/W values observed are fairly small. For the operation and seismic load case, most occur below 0.3. The three earthquakes that generated larger drift ratio percentages, however, generated larger V/W values as well. The Duzce: Near analyses has a 90-meter maximum V/W of 0.34. The Northridge: Far record has maximum V/W of 0.35, 1.9 and 5.21 for the 60-, 90- and 120-meter turbines, respectively. The Friuli: Far record also generated larger V/W for all three models. V/W of 0.33, 0.75 and 0.87 occur for the 60-, 90- and 120-meter turbines, respectively.

The wind, operation and seismic load case also has maximum V/W values below 0.3 for most analyses. However, the three earthquakes mentioned for the operation and

seismic load case have higher observed V/W values for this load case. The Duzce: Near earthquake produces V/W of 0.35 for the 60-meter turbine. The Northridge: Far earthquake has V/W of 0.44, 0.8 and 1.28 for the 60-, 90- and 120-meter turbines, respectively. The Friuli: Far record also produces V/W values of 0.42 and 0.76 for the 60- and 90-meter turbines, respectively. For this load case, the Northridge: Near record produced values significantly higher than the values observed for this earthquake under operation and seismic loading. The 90-meter analysis has a V/W of 0.9, and the 120-meter analysis has a V/W of 0.59 as compared to values of 0.2 and 0.19. For this earthquake, the V/W for the 60-meter analysis remains nearly identical between the two load cases.

In general, the largest V/W values are observed for the wind, operation and seismic load case. The V/W values are also higher for the 60-meter and 90-meter turbines in 54 of the 60 analyses. This again indicates that the 120-meter turbine is less affected by the applied loading than the other two models. It can be concluded that because the 120-meter turbine has a longer period, it attracts less acceleration, therefore producing smaller V/W values.

The final global result is the FFT analysis, which was conducted for all three turbine models and each earthquake record. Most of the turbines exhibit modal and operational frequencies that are not in close proximity to the predominant frequency of the ground motion. Several models have frequencies that are close, however. Specifically, the 60-meter Duzce: Near analysis has a mode 1 frequency that is nearly identical to the second most predominant ground motion frequency. It is possible that resonance occurred for the wind, operation and seismic analysis for this model because it was unable to

converge. Other analyses that may have been close to operating in resonant conditions include the 60-meter Friuli: Far, 90- and 120-meter Kocaeli: Near and the 90-meter: Kocaeli: Far simulations. For each of these, the second or third most predominant ground motion frequency is similar to the mode 1 and/or operational frequencies of the wind turbine model.

Understanding the possible implications of these FFT analyses for these wind turbines is critical because resonance can cause severe damage for these structures. As each of these earthquake records are only 10 seconds long, it is important to understand the impact the seismic load has on several of the turbine models in such a short period of time. From these observations, it can be concluded that emergency shutdown of operating wind turbines is necessary for the safety of these structures during an earthquake. In some cases, if emergency shutdown were to take longer than 10 seconds, severe damage may occur within a wind turbine because resonance is reached shortly after the earthquake begins. While emergency shutdown would lower the damping of the entire system, it would be necessary for maintaining the stability of the blades and nacelle at the top of the turbine.

To evaluate the local behavior of the wind turbine models, Von Mises stresses and the number of cycles to failure (through low-cycle fatigue analyses) are found.

By evaluating the Von Mises stresses for the operation and seismic load case, it can be observed that four of the analyses reach yield stress of 350MPa, with one nearly reaching yield. These include the 60-meter Duzce: Near, 60-meter and 90-meter Northridge: Far and 90-meter Friuli: Far analyses. The 60-meter Friuli: Far analysis reaches 344MPa. The wind, operation and seismic load case has two analyses that reach

yield stress, with one nearly reaching yield. The two that reach yield include the 60-meter Northridge: Far and 90-meter Friuli: Far. The 60-meter Duzce: Near has a maximum stress of 349MPa.

In general, the operation and seismic load case creates larger stresses for each analysis. The 120-meter turbine never reaches yield stress throughout either load case. Maximum stresses for the 120-meter turbine are 189MPa and 187MPa for the Friuli: Far earthquake under operation and seismic loads, and wind, operation and seismic loads, respectively. These results indicate that while the turbine may not have a critical global response, the base of the turbine experiences yielding. The yielding that occurs at the base of the turbine would compromise the integrity of the entire system during an earthquake, and could ultimately lead to significant damage to the turbine. The yielding would become most problematic if a turbine were to experience several earthquakes without any repairs being made to the turbine base region.

Low-cycle fatigue analyses were conducted for all of the turbine models under both load cases. To best represent this data, the number of cycles to failure were determined for each model and subsequently compared to the number of cycles per earthquake. For all analyses, no through-thickness cracks developed as a result of the loading on the turbine. For the operation and seismic load case, most of the analyses have cycles to failure under 200,000, whereas the wind, operation and seismic load case has cycles to failure under 150,000. Several analyses have significantly higher numbers, including the Loma Prieta: Near, Kocaeli: Far and Landers: Far analyses for the operation and seismic load case. The wind, operation and seismic load case has higher numbers for the 90- and 120-meter Northridge: Near, Loma Prieta: Near, Kocaeli: Far and the 60- and

120-meter Landers: Far analyses. The Duzce: Near, Northridge: Far and Friuli: Far records produce the lowest number of cycles to failure throughout the three turbine models. These three records coincide with the records that produce the highest drift ratios, V/W and stresses for these analyses.

It can be concluded from the low-cycle fatigue analyses that current wind turbine designs may be sufficient to prevent any through-thickness crack development under any loading. It is important to note, however, that several of these models reached yield stress under the two load cases. While damage caused by fatigue does not occur, significant damage caused by yielding under multiple earthquakes may occur, which could be catastrophic for the stability of an operating wind turbine. It is therefore important that these designs are improved so that they can withstand various combinations of loads without experiencing significant damage.

6.2.2 Critical Design and Operation Protocol Issues

After evaluating the response of the wind turbine models to two load cases, several design and operating protocol issues can be identified. These include potential modifications and updated requirements to existing wind turbine design and operation protocol; namely design modifications to the wind turbine base region, which includes the base flange, welds and tower as well as the emergency shutdown of wind turbines.

To improve the global behavior of the wind turbine system, it is important that emergency shutdown procedures are optimized so that operating wind turbines can shut down as quickly as possible at the onset of seismic activity. These emergency shutdown procedures should be implemented such that they effectively stop the rotation of the wind turbine blades as soon as any ground motion is detected. This would enable the blades

and other mechanical equipment at the top of the turbine to remain stable throughout a seismic event. By ensuring the stability of these components, the overall structural integrity of the tower is also maintained.

Modifications could also be made to the design of the base of wind turbines. Because yield stress was detected in several models, it is important that any wind turbine design address this area of concern. Modifications can be made to the geometry of these sections. Developing a larger tower bottom section, for instance, may aid in relieving some of the high stresses seen under combined loading. Additional areas of improvement could also include the welds and base flange. Yielding may not cause significant damage to the turbine under one earthquake, but if yielding occurs under several earthquakes, the turbine could be at risk of failure.

By making these modifications to wind turbine design and operation protocol, the safety and reliability of these systems can be greatly increased. Wind turbines could withstand the impact of seismic loads in combination with other loads because they would not experience significant damage due to yielding or resonant conditions. These changes would ensure that wind turbines would meet the 20-year service life they are designed for.

6.3 Summary of Future Research Requirements

In this study, finite element simulations are carried out to evaluate the performance of wind turbine designs under combined loading. This method focuses on developing an accurate finite element model for the analysis of these structures under seismic loading in combination with operation and/or wind loads. The results indicate that several changes could be made to current wind turbine designs so that these structures remain safe and reliable under various loads.

Additional studies are necessary for further understanding the impact of seismic and combined loads on wind turbines. Future research in this field can include:

- The finite element simulations utilized line elements to represent the wind turbine blades and nacelle. The effect of the realistic blade and nacelle geometry on the overall performance of the wind turbine should be investigated because it could change both global results and local behavior. These changes could impact the displacements experienced at the top of the turbine and also impact the stresses seen at the base of the turbine.
- The operational speed of the rotor used for these analyses remained constant at an average operating speed of 1.15 rad/s. By increasing this to the maximum value for each wind turbine height, the global and local response of the system could change significantly. These results could also show potential cases of resonance for different wind turbine heights depending on the frequency of operation and the predominant ground motion frequency.
- For all of the wind, operation and seismic analyses, a constant wind profile was used and idealized as forces on the wind turbine tower and blades. The creation in an actual wind profile applied to the entire tower and blade assembly would allow for changes in the response of the system. This change would more accurately represent what an actual wind turbine experiences. This would likely impact the drift ratio and V/W values seen within each model.
- The analyses conducted for this research used 10 seconds of each earthquake record. By performing longer analyses, the overall wind turbine response and performance throughout an entire earthquake could be captured. Several models that did not yield

within the first 10 or 15 seconds may yield at some point later in the earthquake. These results would aid in future wind turbine seismic design requirements.

- The research conducted focused on two load cases including operation and seismic loads and wind, operation and seismic loads. By evaluating the performance of wind turbines under a larger variety of load combinations, more results can be gathered on how the system responds under different conditions. Some of these additional loads could include various operational speeds and wind velocities.
- Finally, this study focused on three turbine models. Through the results, it became clear that the smaller wind turbine sizes were more impacted by the two load cases used than the largest wind turbine model. The investigation of the response of smaller wind turbines may also be critical in understanding how to best design these structures for seismic loads and combined loads.

In general, the results from the finite element simulations presented in this thesis highlight the potential damage to wind turbines caused by seismic loads in combination with other types of loads. These results also highlight the significant differences that may exist between the global and local performance of various turbine models under these load cases.

REFERENCES

Agbayani, N. A. (2010). The Lack of US Structural Design Guidelines for Wind Farm Towers: Basic Code Compliance Issues at the High-Tech Frontier. *2010 Structures Congress*. Orlando, FL: American Society of Civil Engineers.

AISC. (2005). *Steel Construction Manual*. (American Institute of Steel Construction (AISC), Ed.) (13th ed.). Chicago, IL.

Applied Technology Council. (2008). *ATC-63 (FEMA P695): Quantification of Building Seismic Performance Factors*. Redwood City, CA.

ArcelorMittal. (2009). High Strength Steels.

ASCE. (2005). *ASCE/SEI 7-05 Minimum Design Loads for Buildings and Other Structures*. Reston, VA: American Society of Civil Engineers.

ASTM. (2005). *ASTM E 1049-85 Standard Practices for Cycle Counting in Fatigue Analysis*. West Conshohocken, PA.

ASTM. (2008). *Chapter 14: Fatigue*. Materials Park, OH: ASM International.

Bazeos, N., Hatzigeorgiou, G. D., Hondros, I. D., Karamaneas, H., Karabalis, D. L., & Beskos, D. E. (2002). Static, seismic and stability analyses of a prototype wind turbine steel tower. *Engineering Structures*, *24*(8), 1015–1025.

Brome, T. (2010). Wyoming Turbine Collapse. *Industrial Wind Action Group*. Retrieved February 20, 2013, from http://www.windaction.org/pictures/30961

Chowdhury, I., & Dasgupta, S. P. (2003). Computation of Rayleigh Damping Coefficients for Large Systems. *Electronic Journal of Geotechnical Engineering*, *8*.

Earth Systems Southwest. (2006). *Geotechnical Engineering Report for Mountain View IV Wind Project* (pp. 1–68). Indio, CA.

Equivalent Von Mises Strain. (1999).*DIANA Finite Element Analysis User's Manual Analysis Procedures*.

Fitzwater, L. M. (2004). *Estimation Of Fatigue And Extreme Load Distributions From Limited Data With Application To Wind Energy Systems*. Albuquerque, NM.

GL. (2010). *Guideline for the Certification of Wind Turbines*. Hamburg, Germany: Germanischer LLoyd.

GL Garrad Hassan. (2013). Onshore Wind. *GL Garrad Hassan*. Retrieved March 19, 2013, from http://www.gl-garradhassan.com/en/OnshoreWind.php

Goode, J. S., & Van de Lindt, J. W. (2006). Development of a Reliability-Based Design Procedure for High-Mast Lighting Structural Supports in Colorado. *Structures Congress*. ASCE.

Griffin, D. A. (2001). *WindPACT Turbine Design Scaling Studies Technical Area 1 – Composite Blades for 80- to 120-Meter Rotor*. Kirkland, WA.

Holmes, J. D. (2002). Fatigue life under along-wind loading — closed-form solutions. *Engineering Structures*, *24*(1), 109–114.

Huskey, A., & Prascher, D. (2005). *Tower Design Load Verification on a 1-kW Wind Turbine*. Golden, CO: National Renewable Energy Laboratory.

ICC. (2006). *International Building Code 2006*. Country Club Hills, IL: International Code Council.

IEC. (2009). *Amendment to IEC 61400-1 Ed. 3: Wind Turbines - Part 1: Design Requirements*. Geneva, Switzerland: International Electrotechnical Commission.

Lynch, D. K. (2006). The San Andreas Fault. *geology.com*. Retrieved March 4, 2013, from http://geology.com/articles/san-andreas-fault.shtml

Madsen, P. H., Pierce, K., & Buhl, M. (1999). Predicting Ultimate Loads for Wind Turbine Design. *AIAA/ASME Wind Energy Symposium*. Golden, CO: National Renewable Energy Laboratory.

Malcolm, D. J., & Hansen, A. C. (2006). *WindPACT Turbine Rotor Design Study*. Golden, CO.

Nijssen, L. (2006). *Fatigue Life Prediction and Strength Degradation of Wind Turbine Rotor Blade Composites*. Delft University.

NREL. (2009). United States - Wind Resource Map. *National Renewable Energy Laboratory*. Retrieved April 9, 2013, from http://www.nrel.gov/gis/pdfs/windsmodel4pub1-1-9base200904enh.pdf

Ntambakwa, E., & Rogers, M. (2009). Seismic Forces for Wind Turbine Foundations Wind Turbine Structures, Dynamics, Loads and Control. *AWEA Windpower Conference* (Vol. 05). Chicago, IL.

Overview of Wind Energy in California. (2013).*California Energy Commission*. Retrieved March 29, 2013, from http://www.energy.ca.gov/wind/overview.html

Prowell, I, Elgamal, A., & Jonkman, J. (2009). FAST Simulation of Wind Turbine Seismic Response. *2009 Asian-Pacific Network of Centers for Earthquake Engineering Research (ANCER) Workshop*. Golden, CO: National Renewable Energy Laboratory.

Prowell, I, Elgamal, A., Romanowitz, H., Duggan, H. E., & Jonkman, J. (2010). *Earthquake Response Modeling for a Parked and Operating Megawatt-Scale Wind Turbine*. Golden, CO.

Prowell, I, Elgamal, A., & Uang, C. (2010). Estimation of Seismic Load Demand for a Wind Turbine in the Time Domain Preprint. *European Wind Energy Conference and Exhibition 2010*. Golden, CO: National Renewable Energy Laboratory.

Prowell, I, Veletzos, M., Elgamal, A., & Restrepo, J. (2008). Shake Table Test of a 65kW Wind Turbine and Computational Simulation. *14th World Conference on Earthquake Engineering*. Beijing, China.

Prowell, Ian, Elgamal, A., Jonkman, J., & Uang, C. (2010). Estimation of Seismic Load Demand for a Wind Turbine in the Time Domain. *European Wind Energy Conference and Exhibition 2010* (Vol. 11). Warsaw, Poland.

Prowell, Ian, Veletzos, M., & Elgamal, A. (2008). Full Scale Testing for Investigation of Wind Turbine Seismic Response. *7th World Wind Energy Conference*. Kingston, Ontario, Canada.

Riso National Laboratory. (2001). *Guidelines for Design of Wind Turbines, Second Edition*. (W. E. Department, Ed.). Copenhagen, Denmark: Riso National Laboratory.

Ritschel, U., Warnke, I., & Haenler, M. (2006). Systematic modelling of wind turbine dynamics and earthquake loads on wind turbines. *European Wind Energy Conference and Exhibition 2006*. Athens, Greece.

Ritschel, U., Warnke, I., Kirchner, J., & Meussen, B. (2003). Wind Turbines and Earthquakes. *2nd World Wind Energy Conference*. Cape Town, South Africa.

Schreck, S., & Robinson, M. (2007). Wind Turbine Blade Flow Fields and Prospects for Active Aerodynamic Control. *ASME 2007 Fluids Engineering Division Summer Meeting*. Golden, CO: National Renewable Energy Laboratory.

Sutherland, H. J. (1999). *On the Fatigue Analysis of Wind Turbines*. Albuquerque, NM.

Sutherland, H. J., & Veers, P. S. (1995). Fatigue Case Study and Reliability Analyses for Wind Turbines. *1995 ASME/JSME/JSES International Solar Energy Conference*. Albuquerque, NM: Sandia National Laboratory.

True Wind Solutions, L. (2007). California Wind Resource Maps. *California Energy Commission*. Retrieved April 23, 2013, from http://www.energy.ca.gov/maps/renewable/wind.html

USGS. (2008). 2008 NSHM Figures. *U.S. Geological Survey*. Retrieved March 29, 2013, from http://earthquake.usgs.gov/hazards/products/conterminous/2008/maps/

Verrengia, J. B. (2009). Bigger and Better: Lab Aims to Improve Giant Wind Turbines. *National Renewable Energy Laboratory2*. Retrieved April 12, 2013, from http://www.nrel.gov/news/features/feature_detail.cfm/feature_id=1927